628669

KELLETT Aircraft

KELLETT Aircraft CORPORATION

DOWNWASH TESTS OF THE DUAL TANDEM DUCTED PROPELLER VTOL RESEARCH AIRCRAFT CONFIGURATIONS TO EVALUATE ENGINE INLETS, PROTECTION DEVICES AND STUDY AERODYNAMIC INTERFERENCE

DATE 11/1/65 REPORT NO. 179T80-12

Distribution of This Report is Unlimited

PREPARED H. C. Curtiss, Jr.
Dr. H.C. Curtiss, Jr.
Consultant Aerodynamics

R. W. Struble
R. W. Struble
Project Engineer

APPROVED R C Winter
R. C. Winter
Manager of Engineering

NO. OF PAGES

FOREWORD

This report was prepared by the Kellett Aircraft Corporation, Willow Grove, Pennsylvania for the Bureau of Naval Weapons of the U.S. Navy and fulfills the requirements of Phase I, Item 4 of Contract NOw64-0439-f.

Testing for this program started in March 1964 and was completed in August 1965. The testing was supervised by Mr. James B. Jones, the Kellett Project Engineer and Mr. Ben Stein RAAD-3221, U.S. Navy, Bureau of Naval Weapons, who administered the project.

The cooperation of the Bell Aerosystems Company is gratefully acknowledged. Their drawings and suggestions significantly guided the design of the inlet protection devices tested. Mr. E. Sherman of Bell witnessed some of the tests and his aid and suggestions in the analysis of the test results are appreciated. The cooperation of the Hamilton Standard personnel in their phase of the test program is also greatly appreciated, as was the aid and suggestions of Mr. W. Koven and Mr. B. Stein of the Bureau of Naval Weapons. The assistance and supervision of these men has significantly contributed to the success of this program.

Dr. Howard C. Curtiss Jr. has interpreted, analyzed and supervised the collection and documentation of the aerodynamic data. Professor Curtiss prepared the aerodynamic interference sections of this report.

Mr. William P. Ryan, Installation Engineer of Hamilton Standard supervised the propeller blade stresses, instrumentation and the compilation thereof. Mr. Ryan also supervised the preparation of the propeller blade stress sections of the report.

Mr. R. Struble has integrated the entire test program into a published report.

A motion picture film (16mm color) supplements this report and can be obtained from the Bureau of Naval Weapons. This film will be a valuable addition to the understanding of downwash problems.

ABSTRACT

A full scale half-model simulation of a dual tandem ducted propeller VTOL aircraft has been tested under the severe environment caused by operation simulating vertical flight in close proximity to sand and crushed stone covered terrain. The model was the same as used in similar previous downwash effects programs, except that various propeller positions and inlet configurations were investigated. Four engine inlet protection devices were evaluated in this series of tests. Based on previous promising results, a wing-like deflector device was tested in two configurations of different chord lengths. A full inlet screen and a blocked half-screen inlet protection device were also tested. It was found that due to its location in the upflow region, the full screen tended to collect particles and thereby aggravated inlet ingestion. The blocked half-screen and the deflector devices significantly reduced ingestion, but were not sufficiently effective to positively prevent engine damage. Tests over crushed stone caused significantly worse inlet ingestion and airframe damage problems than those experienced over sand. Aerodynamic interference tests were also conducted. Single (Isolated duct) as well as tandem propeller configurations were investigated at various propeller blade settings, propeller duct heights, distances between ducts and power settings. Propeller blade stress investigations were

made during the aerodynamic interference tests. Recirculation was evident in the tandem aerodynamic tests, causing a reduction in thrust at a given blade angle and RPM. Also, as a result of the recirculation, thrust variations ranging from five to ten percent of the average thrust were measured.

TABLE OF CONTENTS

TABLE OF CONTENTS (Cont'd.)

TABLE OF CONTENTS (Cont'd.)

LIST OF ILLUSTRATIONS

LIST OF ILLUSTRATIONS (Cont'd.)

LIST OF ILLUSTRATIONS (Cont'd.)

LIST OF TABLES

LIST OF SYMBOLS

A_e	Duct Exit Area, ft.^{2}
A_i	Duct Inlet Area, ft.^{2}
b	Blade Chord, ft.
C_P	Power Coefficient = $\frac{P}{\rho A_e (\Omega R)^3}$.
C_T	Thrust Coefficient = $\frac{T}{\rho A_e (\Omega R)^2}$.
D	Propeller Blade Diameter, ft.
D_e	X-22 Propeller Duct Diameter at Exit, ft.
$D.L.$	Disc Loading = $\frac{T}{A_e} \rho s f$
d	Propeller Duct Diameter at Propeller Centerline, ft.
$^\circ F$	Temperature, Degrees Fahrenheit.
f_a	Aliasing Frequency, cps.
f_s	Sampling Frequency, cps.
g	Acceleration Due to Gravity, ft/sec.^{2}
h	Height of Duct Exit Above Ground, ft.
h_p	Propeller blade Thickness, in.
K	Parameter Relating Disc Loading to Upflc r Air Velocity.
N_2	Propeller Speed, Percent.
n	Propeller Speed, rps.
P	VTOL Gross Weight, lb.
R	Propeller Blade Tip Radius, ft.
r	Propeller Blade Element Radius, ft.
r_p	Propeller Blade Element Radius, in.
T	Propeller Duct Thrust, lb.

LIST OF SYMBOLS (Cont'd.)

T_v	Propeller Duct Thrust Variation, Percent.
V_i	Air Inlet Velocity, ft/sec.
V_u	Air Upflow Velocity Near Inlets, ft/sec.
$\bar{V}_e$	Air Velocity, nondimensional = $\dfrac{V_e}{\sqrt{\dfrac{T}{\rho A_e}}}$
W_a	Airflow Per Simulated Engine Inlet, lb/sec.
W_o	Engine Airflow For Each Engine of Simulated Aircraft, lb/sec.
y	Longitudinal Distance Between Tandem Propeller Ducts, ft.
α	Propeller Blade Element Angle of Attack, Radians.
β	Propeller Blade Angle at 7/8 of the Tip Radius, Degrees.
θ	Propeller Blade Angle at Blade Station, Degrees.
ρ	Air Density, Slugs/ft.^{3}
Ω	Propeller Speed Radians/sec.
$\approx$	Means Approximately.

I INTRODUCTION

A. Kellett Experimental Downwash Programs Conducted for the Bureau of Naval Weapons

Kellett Aircraft Corporation in the past five years, under three Bureau of Naval Weapons contracts, NOw 60-0450-f, NOw 61-0926-c, and NOw 64-0439-f (the present program), has conducted experimental tests to provide systematic full-scale information on problems associated with recirculation of terrain materials due to high velocity downwash during simulated VTOL take-off and landing maneuvers. The scope of the first two programs is described in (1) and (2) below, and the present program under B below.

(1) Initially, a single Pratt and Whitney R-4360 engine-15 foot propeller combination was mounted on the boom of a mobile crane. Tests were conducted over sand, gravel, clay, water and snow. Results are reported in reference 1. Results indicated that recirculation of materials over loose terrain can be a serious problem, with damage resulting from erosion, engine ingestion and flying debris.

(2) Because of the limited applicability of the isolated propeller/engine tests, the program was extended to include tests of a representative full-scale VTOL aircraft configuration, namely,

the tandem tilting duct arrangement. Take-off-and-landing operations of a semi-span tandem duct aircraft were simulated utilizing two YT-53 engines mounted in the ducts, with each engine providing power for an eight-foot diameter propeller. A semi-span wing was attached to the aft duct, and a fuselage, tail, dummy engine nacelles, and a landing gear represented the complete half-model configuration. Results are reported in reference 2. Tests were conducted at heights of less than two duct diameters above sand and water terrain at propeller disc loadings up to 60 pounds per square foot. An engine power loss due to ingestion occurred when operating at low altitudes over water. Severe damage to unprotected engines, propellers, ducts and airframe resulted from downwash recirculation and particle ingestion when operating over sand. Ground coupled interference effects caused by aerodynamic interaction between the ducted propellers indicated high vibratory stress levels. An upflow area occurred between the forward and aft ducts near the sides of the fuselage which acted to increase damage caused to the engine, ducts and airframe during tests conducted over sand terrain.

FIGURE 1: TANDEM DUCTED VTOL AIRCRAFT TEST RIG.

B. Present Program

The present program was oriented to obtain experimental data which would be directly applicable to the Bell tandem ducted X-22A aircraft. Figure 1 indicates the test arrangement employed, which is the reflection plane half-model arrangement previously utilized under A (2) above. To simulate the X-22A engine airflow arrangement, airflow was provided through the dummy engine-nacelle inlets by use of a J-69 engine. Tests were conducted over sand and stone, and a study was made of the sizes and amounts of terrain particles ingested through the inlets. Various inlet protection devices were tested with the aim of minimizing inlet ingestion, and screens were installed on the ducts to protect the propellers from gravel and stone. The tent-like duct protective screens were fastened to each duct with a four-inch cylindrical sheet metal collar. This collar caused duct lip separation, which reduced the thrust of the duct unit significantly during testing. The use of the duct screens was therefore discontinued. The effectiveness of the inlet protective devices in minimizing inlet ingestion was determined and the results are discussed later in the report.

The second major effort covered during the present testing was to conduct tests over sterile terrain, that is, with terrain recirculation minimized. For these tests, the propeller blades and ducts were instrumented in order to assess the severity of blade stress levels caused by aerodynamic interaction between the ducted propellers. The airframe geometry was also varied

by moving the ducts longitudinally and laterally from the standard X-22A duct positions to determine the differences caused in the blade stress levels as a result of the shifting of the duct positions. Isolated propeller duct testing was also accomplished to form a basis for the evaluation of the effect of airframe configuration on the duct to duct blade stress levels. Instrumented propeller stress data was obtained by Hamilton Standard under sub-contract to Kellett Aircraft. Results are reported herein under Appendix A.

The weather was a test restriction due to the possible effects it could have on the data and test comparisons. Past experience at Kellett led the test personnel to realize that the wind velocity should be less than 10 knots during testing, the terrain moisture content should not exceed 12 percent and the temperature should be above freezing.

II TEST APPARATUS

A. Basic Dual Tandem Test Rig

The test apparatus was a modification of the full scale reflection plane model of the dual tandem ducted propeller VTOL aircraft which had been developed during the prior BuWeps-Kellett downwash programs. As illustrated in the Figure 2, three-view scale drawing, this test rig consisted of two ducted propeller units and a half-airframe mounted on an aerodynamic reflection plane. The two ducted propeller units each consisted of a Hamilton-Standard 8 foot diameter propeller powered by a Lycoming T-53 turboprop engine rated at 960 horsepower. Thrust measuring load cells were inserted in the duct support structure to monitor the thrust which was produced.

B. Engine Ingestion Test Rig

The major addition to the test apparatus was the airflow package which simulated realistic airflows in the engine nacelles. This unit consisted of two simulated engine inlets connected through ducting and a particle separator to the intake of a Continental J-69-T-9 turbojet engine capable of producing an airflow of 18 pounds per second. The engine inlets and simulated nacelles were fabricated following Bell Aerosystems Company drawings for the X-22 aircraft in the space provided between the aft propeller duct and the fuselage similar to the X-22 design. The engine inlets are shown in the Figure 3 photograph. The design of these inlets and the inlet airflow instrumentation is illustrated in Figure 4. An overall view of the airflow equip-

A

TEST RIG FOR [illegible] TANDEM [illegible] PROPELLER VTOL AIRCRAFT

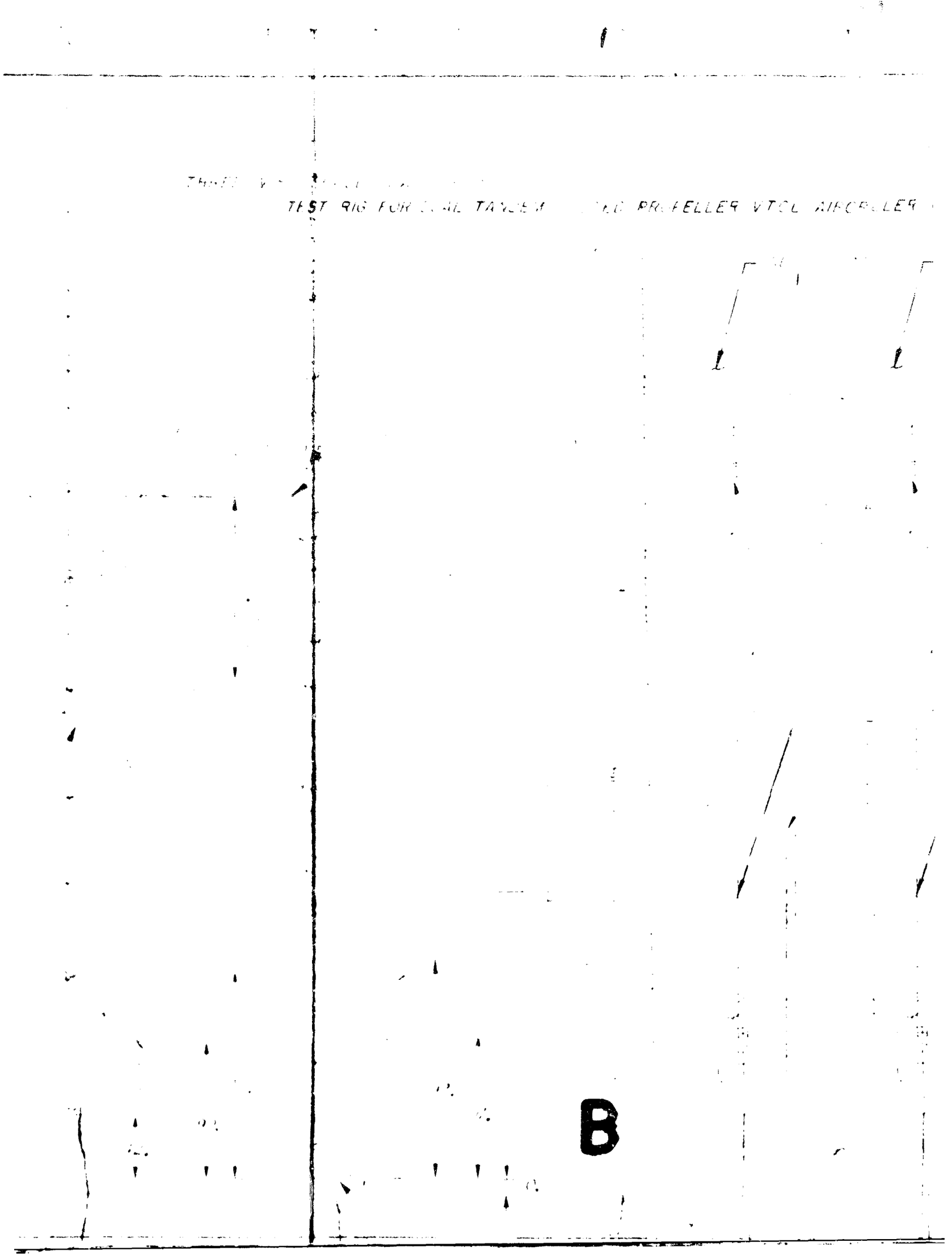

B

7

FIGURE 2

R VTOL AIRCRAFT

C

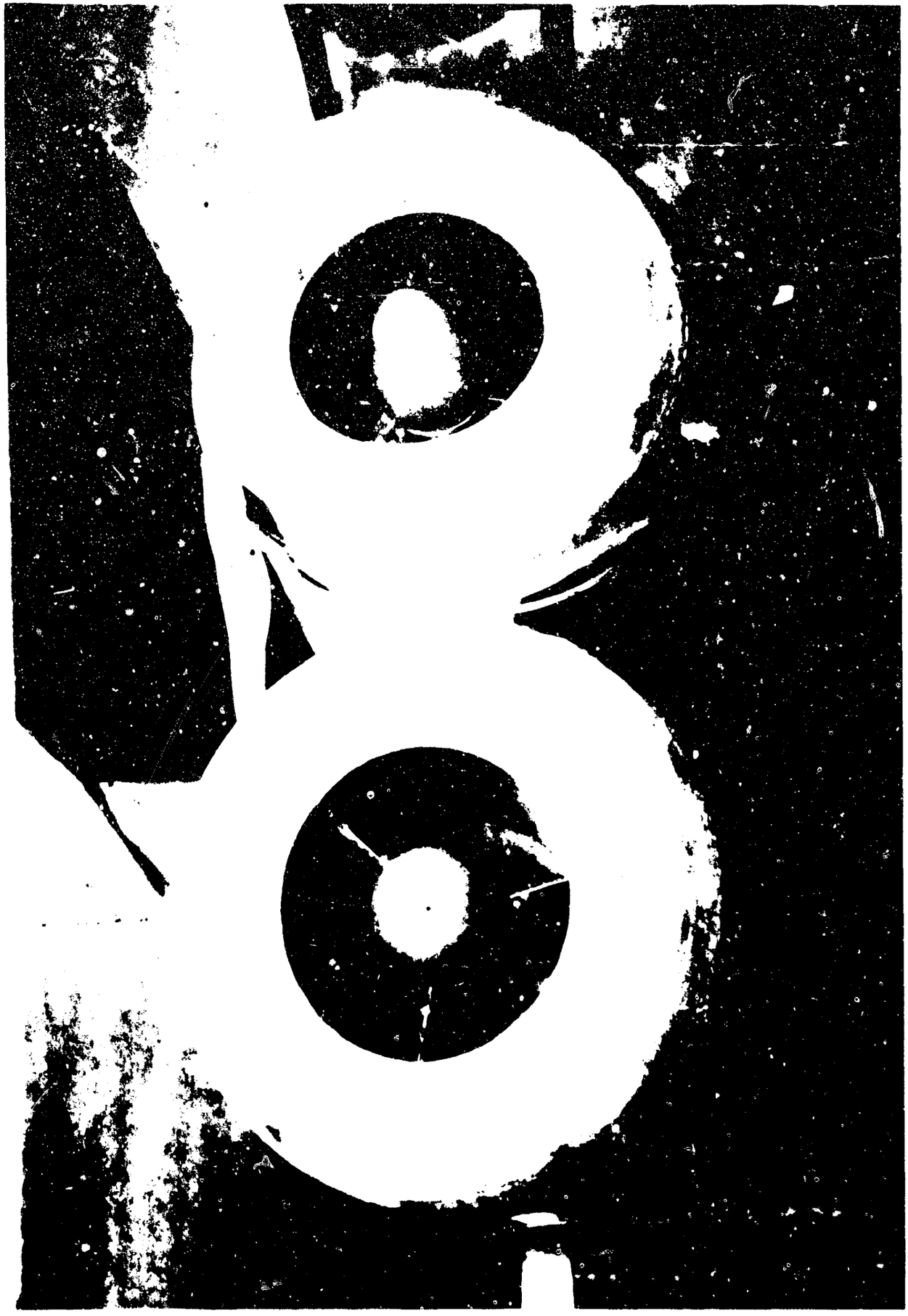

FIGURE 3: SIMULATED ENGINE INSTALLATION

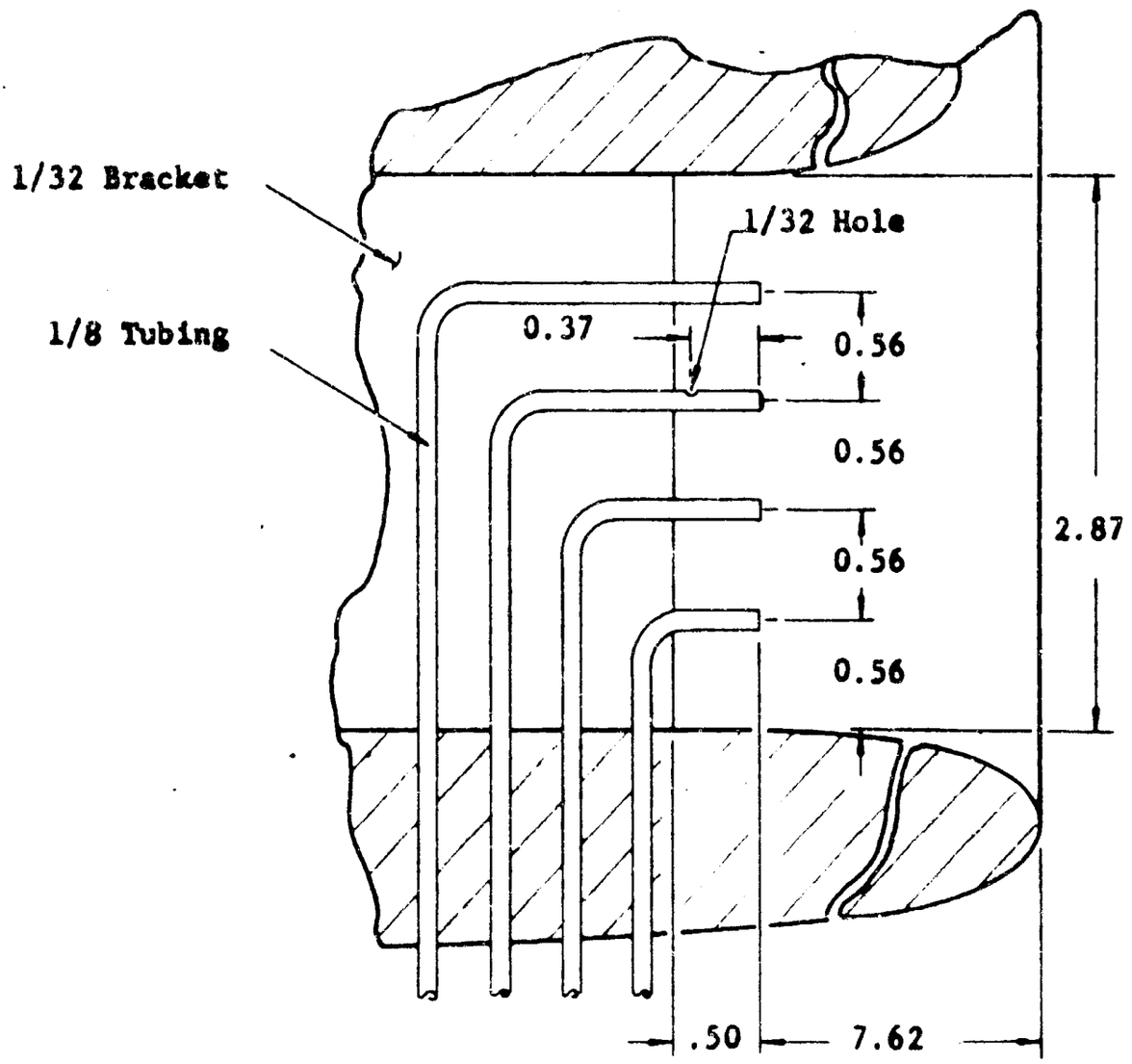

FIGURE 4: AIRFLOW MEASURING PRESSURE PROBES IN SIMULATED ENGINE INLETS

ment located behind the reflection plane is shown in Figure 5.

The particle separator consisted of a plenum chamber and a screen to trap the ingested particles of terrain. The plenum chamber was partitioned with one simulated engine inlet connecting to each half of the chamber so that particles ingested in each inlet were collected separately. The screen was of fine mesh with 200 micron openings and was installed in each chamber in front of the engine intake. The space between the engine intake and the screen acted as an additional settling chamber and collected the particles less than 200 microns in diameter that passed through the screen.

The fundamental parameter of downwash testing which determines the intensity of the downwash is the disc loading. To determine this parameter the combined propeller thrust, duct thrust, and residual engine jet thrust was measured. Two load cells attached to each propeller duct at diametrically opposite positions registered the thrust reaction loads on the supporting structure. The output of the load cells was recorded on a high speed Consolidated oscillograph (Type 5-114) in the ingestion tests and a digital system in the aerodynamic studies. The load cells were calibrated so that the total thrust could be determined from the recorded output. The disc loading was obtained by dividing the total measured thrust by the duct exit area which was 49.0 square feet.

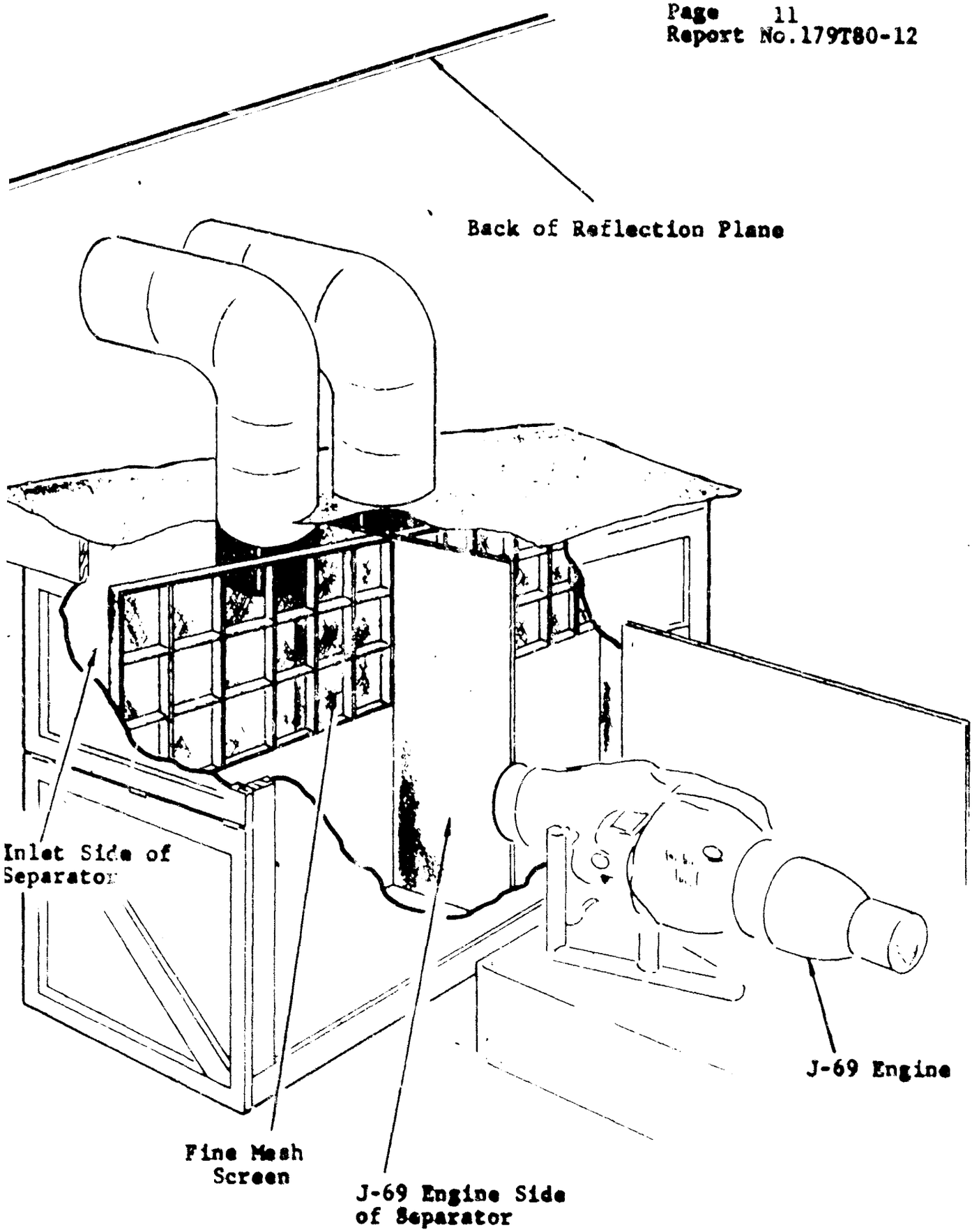

FIGURE 5: SIMULATED ENGINE INLET PARTICLE SEPARATOR AND AIRFLOW EQUIPMENT.

In addition, propeller rpm converted to an appropriate signal throu a suitable transducer was recorded simultaneously to check and support the manually recorded data.

The simulated engine inlets each contained a flow measuring rake consisting of three static pressure tubes and nine total pressure probes. These probes have the appearance of a Y, each leg consisting of three total tubes and one static tube. The configuration at each azimuth is illustrated in Figure 4. The probes were connected with flexible plastic tubing to a multiple tube manometer board. In addition, thermocouples were used to measure the temperature at each inlet. From the above data, the total mass flow into each inlet as well as azimutal variation in the flow was determined.

The particles which were ingested in the simulated engine inlets and trapped by the particle separator were collected and analyzed to determine the weight of terrain ingested and the size distribution of the particles. In addition, samples of terrain circulating through the propeller ducts were collected in especially designed traps shown in Figure 6. Sensitive weighing balances and graduated sieves were used to process the sand and gravel collected. Motion picture coverage using smoke flares to visualize the flow was used to provide corroborating qualitative ingestion data and has served as a permanent visual record of all tests.

FIGURE 6: PROPELLER DUCT PARTICLE TRAP

C. Inlet Protection Devices

Four inlet protection devices were selected for test. Two of these were solid barrier types positioned under the nacelles. The third was a cylindrical wire screen fitting over the nacelles. The fourth was an adaptation of the full screen and consisted of the lower half of the full screen with the cylindrical surface blocked. The details of these devices are described in the following paragraphs.

The long chord deflector had a rectangular planform area of approximately 33 square feet (96 by 50 inches). The thickness was 5.5 inches tapering to 3 inches at the leading and trailing edges. Figure 7 illustrates this device and shows the position of the device relative to the inlet. The deflector was attached to the fuselage side in a horizontal plane approximately 22 inches below the inlet centerline. The long side extended approximately 74 inches forward of the duct inlets.

The short chord deflector had a planform area approximately 10.5 square feet (28 by 54 inches) and a maximum thickness of 5 3/4 inches at the leading edge radius. The thickness tapered to 4 inches at the trailing edge. The detail of the installation of this deflector is illustrated in Figure 8. An overall top view of the deflector is shown in the photograph in Figure 9. The deflector was positioned below the nacelles with the chordline at an angle of 5 degrees to the horizontal and approximately

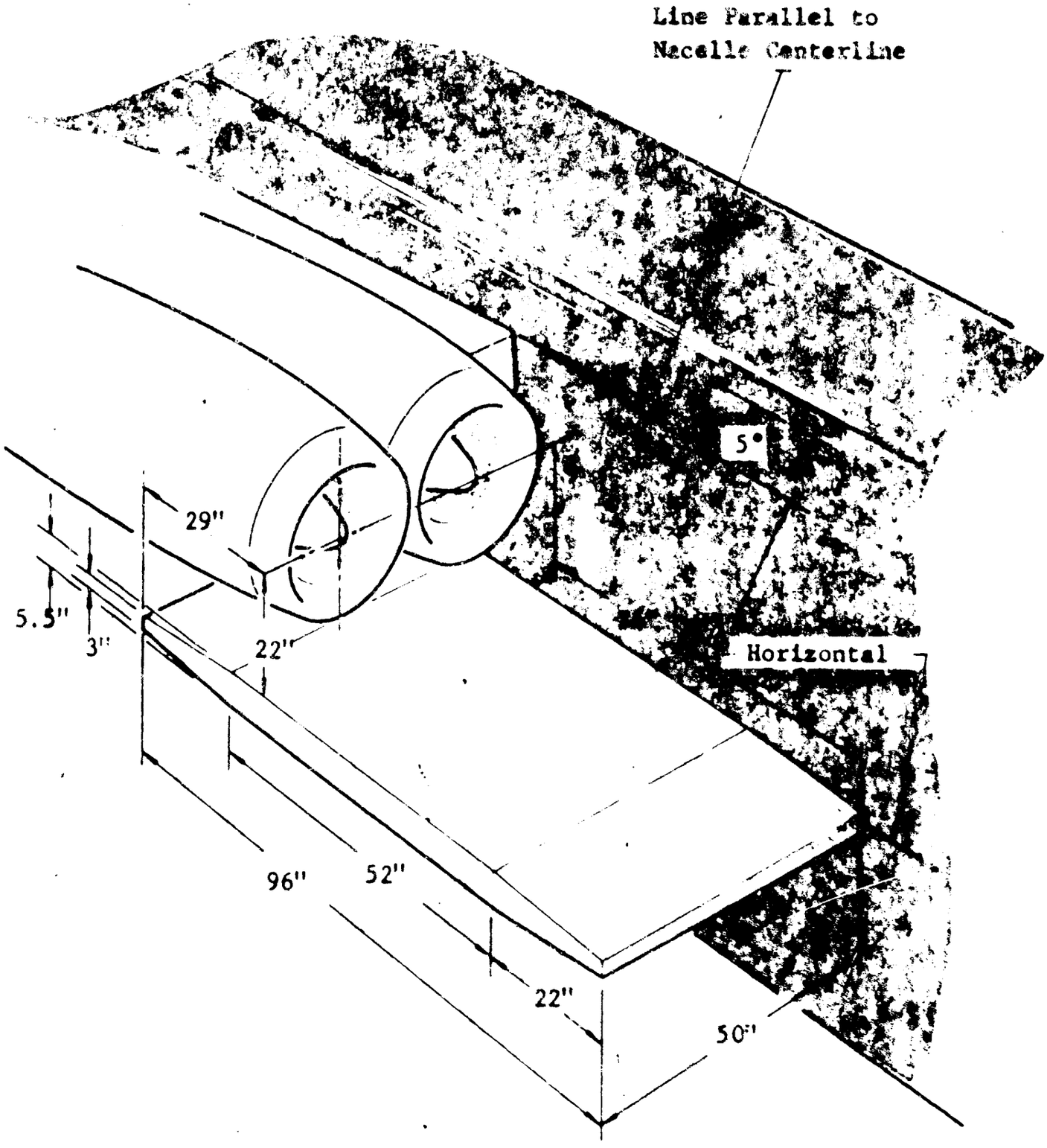

FIGURE 7: SKETCH OF LONG CHORD DEFLECTOR

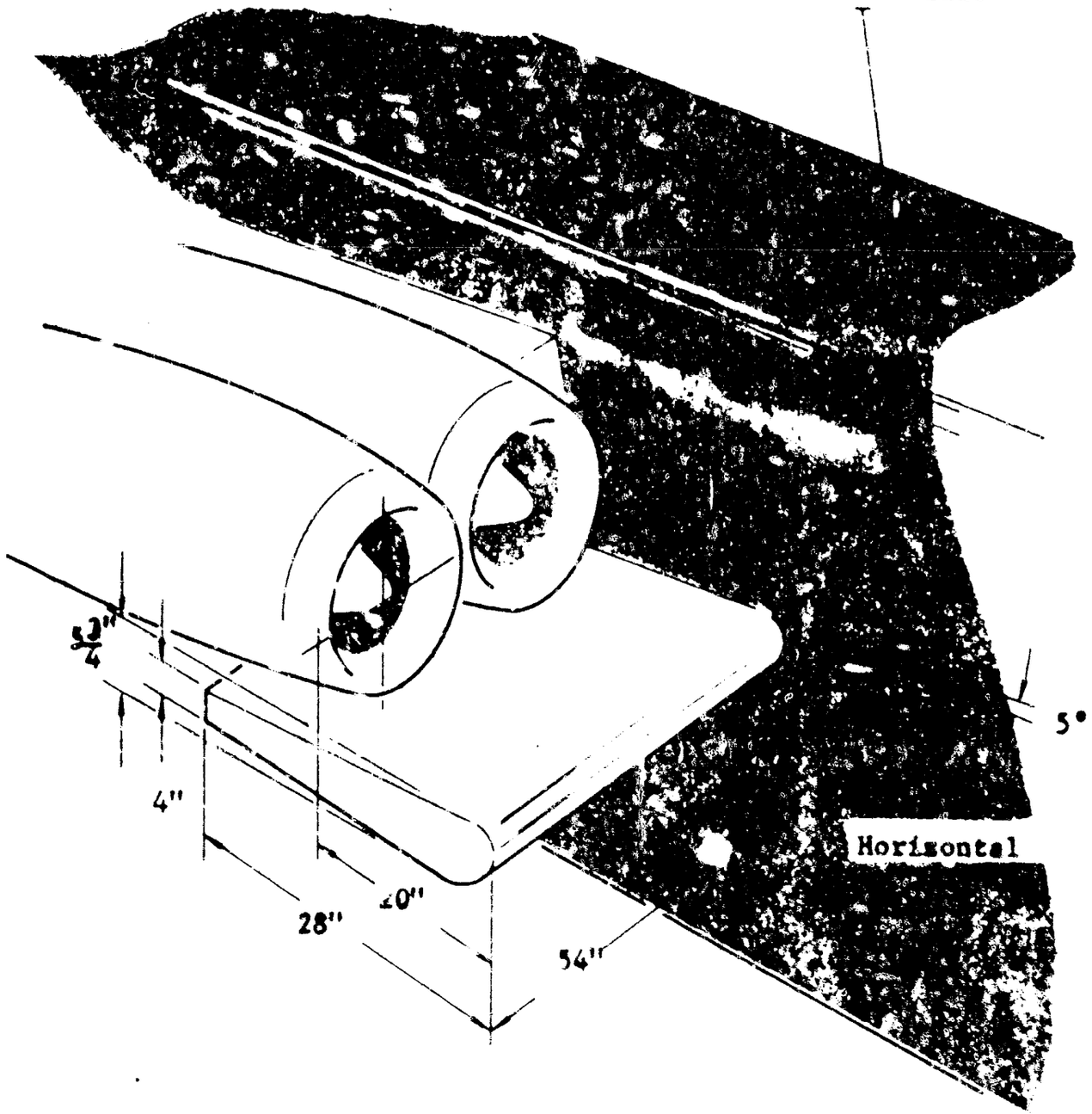

FIGURE 8: SKETCH OF SHORT CHORD DEFLECTOR

FIGURE 9: PHOTOGRAPH OF SHORT CHORD DEFLECTOR

parallel with the inlet centerline. The distance from the leading edge to the inlet is approximately 20 inches.

The third protective device consisted of two cylindrical shapes made of wire screens which fitted over the nacelles and extended 15 inches forward from the inlets. This inlet protection device was made of number 12 mesh screen (0.018 inch diameter wire) layed over a coarse support of number 1 mesh screen (0.080 inch diameter wire). The cylindrical shape covered both the extended circumference and the frontal area of each inlet. The arrangement is shown in Figures 10 and 11. Because of the limited space between the nacelles the parting surface of the top and bottom half of each screen is at an angle with the horizontal.

The fourth device is illustrated in Figure 12. It consists of the two bottom portions of the full screen. The cylindrical surfaces were covered with tar paper and the end surfaces were left open. The orientation was the same as that of the full screen with the parting surface inclined 30 degrees with the horizontal plane.

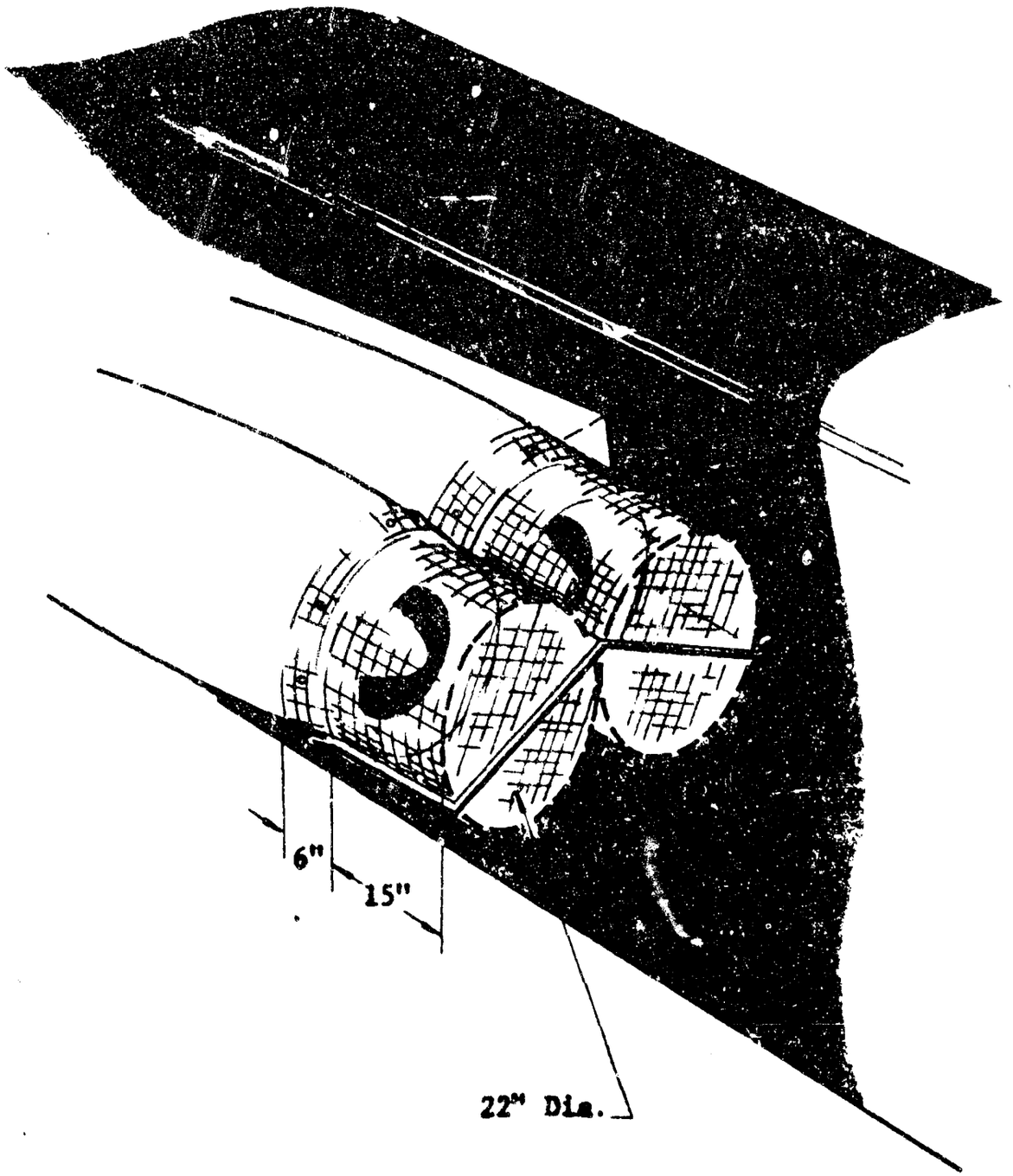

FIGURE 10: SKETCH OF FULL SCREEN INLET PROTECTION

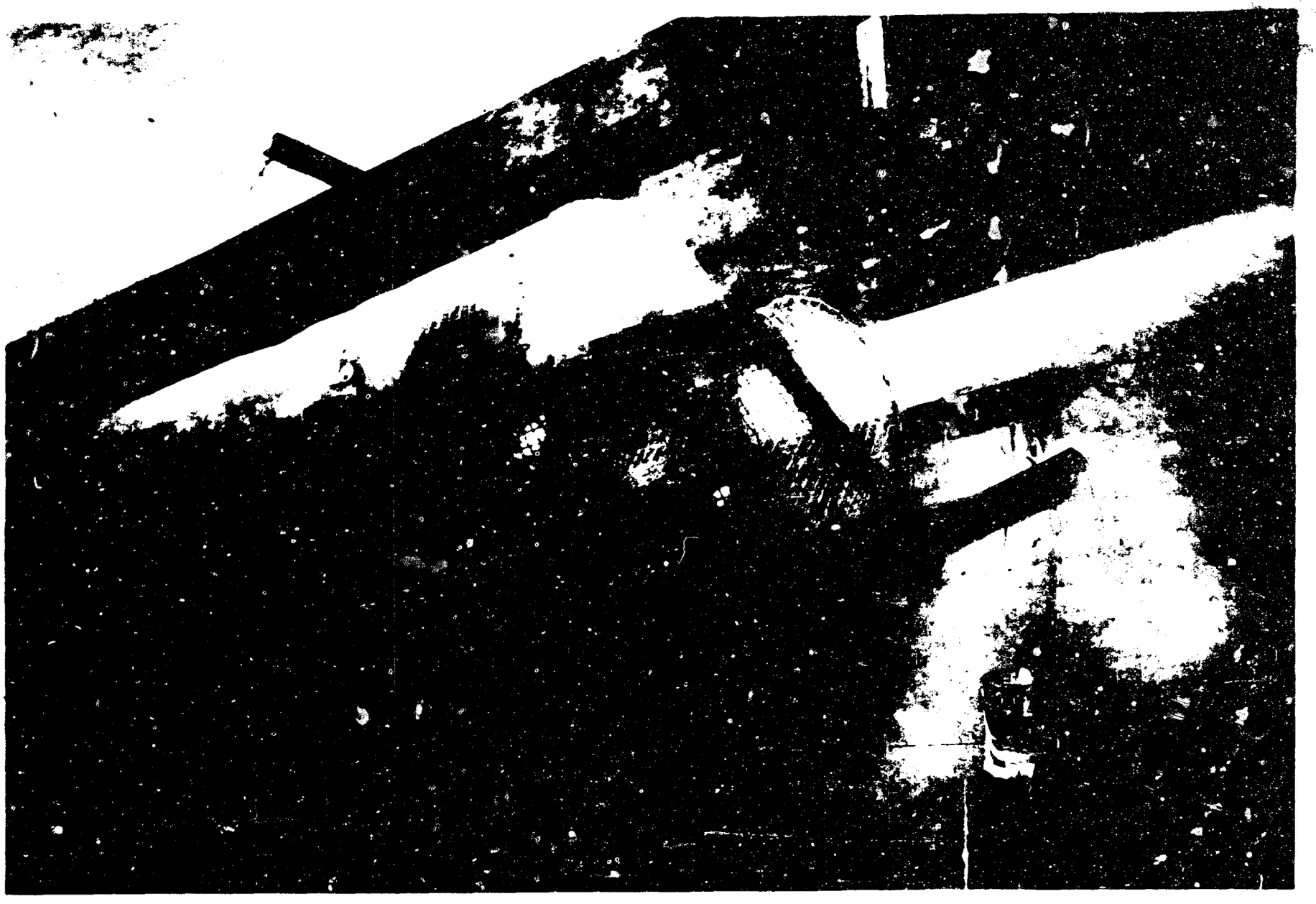

FIGURE 11: PHOTOGRAPH OF FULL SCREEN INLET PROTECTION

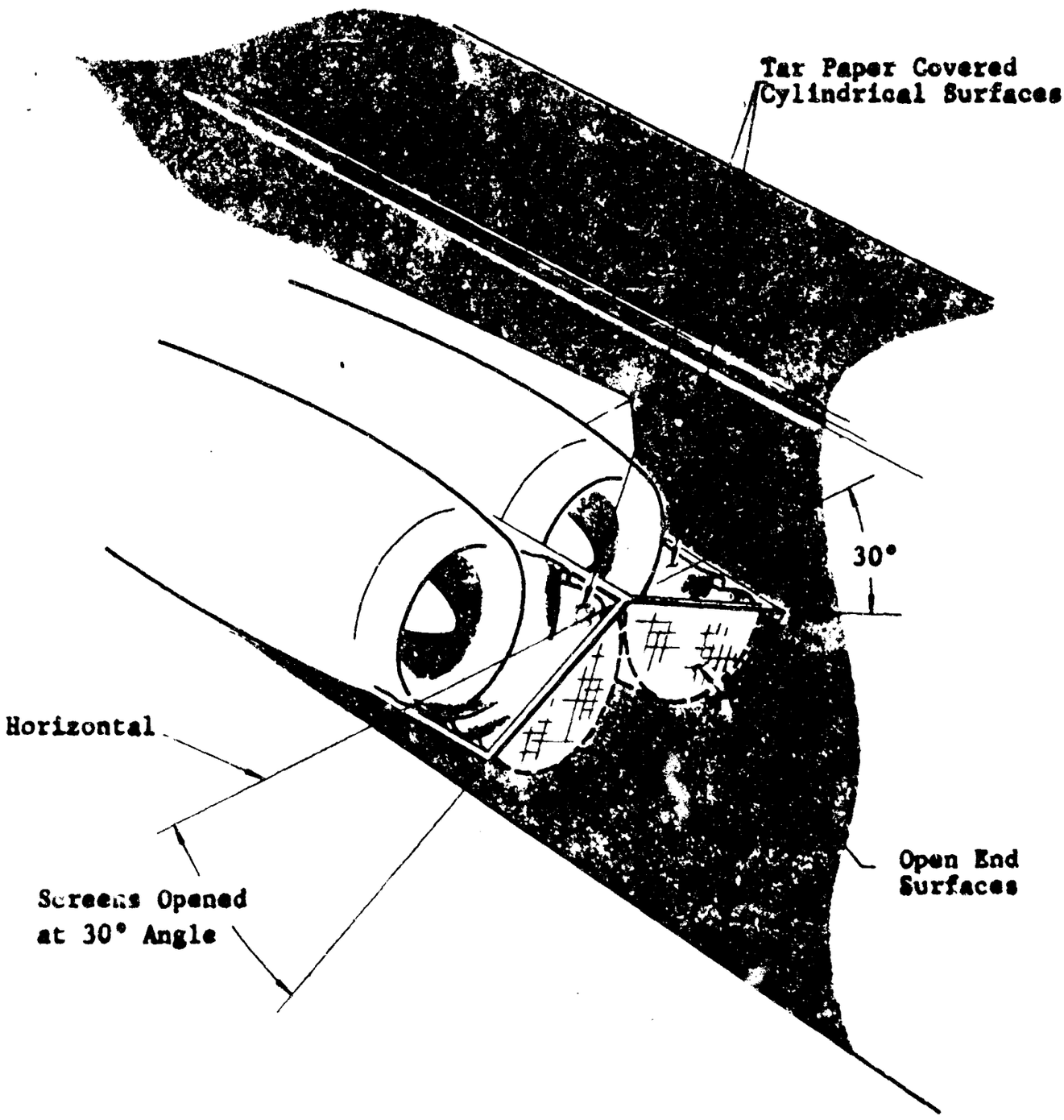

FIGURE 12: SKETCH OF BLOCKED HALF-SCREEN INLET PROTECTION

III TEST PROGRAM

A. Engine Ingestion Tests

Tests were conducted as described in Table 1 to determine the significance of the ingestion problem over sand and stone covered terrain and to evaluate inlet protection devices over sand and stone. The sand which was utilized was coarse building sand which was 50 percent finer than 700 microns. The stone used was crushed granite of 3/8 inch and 1/2 inch size grades. These stone gradings were too coarse for standard sieve analysis and so were graded as shown in the Figure 13. The 1/2 inch stone was graded in a manner similar to that used for the 3/8 inch grade.

The motion picture cameras utilized to document this testing were positioned to obtain the overall view shown in Figure 1 and also some views of the simulated engine inlets. The cameras were used in conjunction with smoke flares positioned at various locations in the upflow region under the inlets for flow visualization studies. Similar flow visualization studies were used to guide the design of the inlet protection devices described previously.

This test program was significantly influenced by the test conditions, test duration and the correlation of the ingestion engine to the thrust engines. These parameters are discussed in the following paragraphs.

Note: Symbols denote test conditions as shown in Table 9.

	TEST NO.	DATE	TERRAIN	PROTECTIVE DEVICES	REMARKS
	155	4/16	Sand	None	Duct Protection Installed
●	156	4/16	Sand	None	
	157	4/17	Sand	None	
	158	4/17	Sand	None	
■	159	4/27	Sand	Full Screen	
▲	160	4/27	Sand	Half Screen	
	161	Test to Measure Duct Inlet Pressures Only			
△	162	5/21	Sand	Half Screen	No Duct Protection
□	163	5/22	Sand	Full Screen	
△	164	5/22	Sand	Half Screen	
	165	5/22	Sand	None	
○	166	5/25	Sand	None	
	167	5/25	Sand	None	
▷	168	5/28	Sand	Short Deflector	
◁	169	5/29	Sand	Long Deflector	
	170	6/3	3/8 Stone	None	
⬡	171	6/4	3/8 Stone	None	
	172	6/9	3/8 Stone	None	
	173	6/9	1/2 Stone	None	

TABLE 1. DESCRIPTION OF TEST CONDITIONS

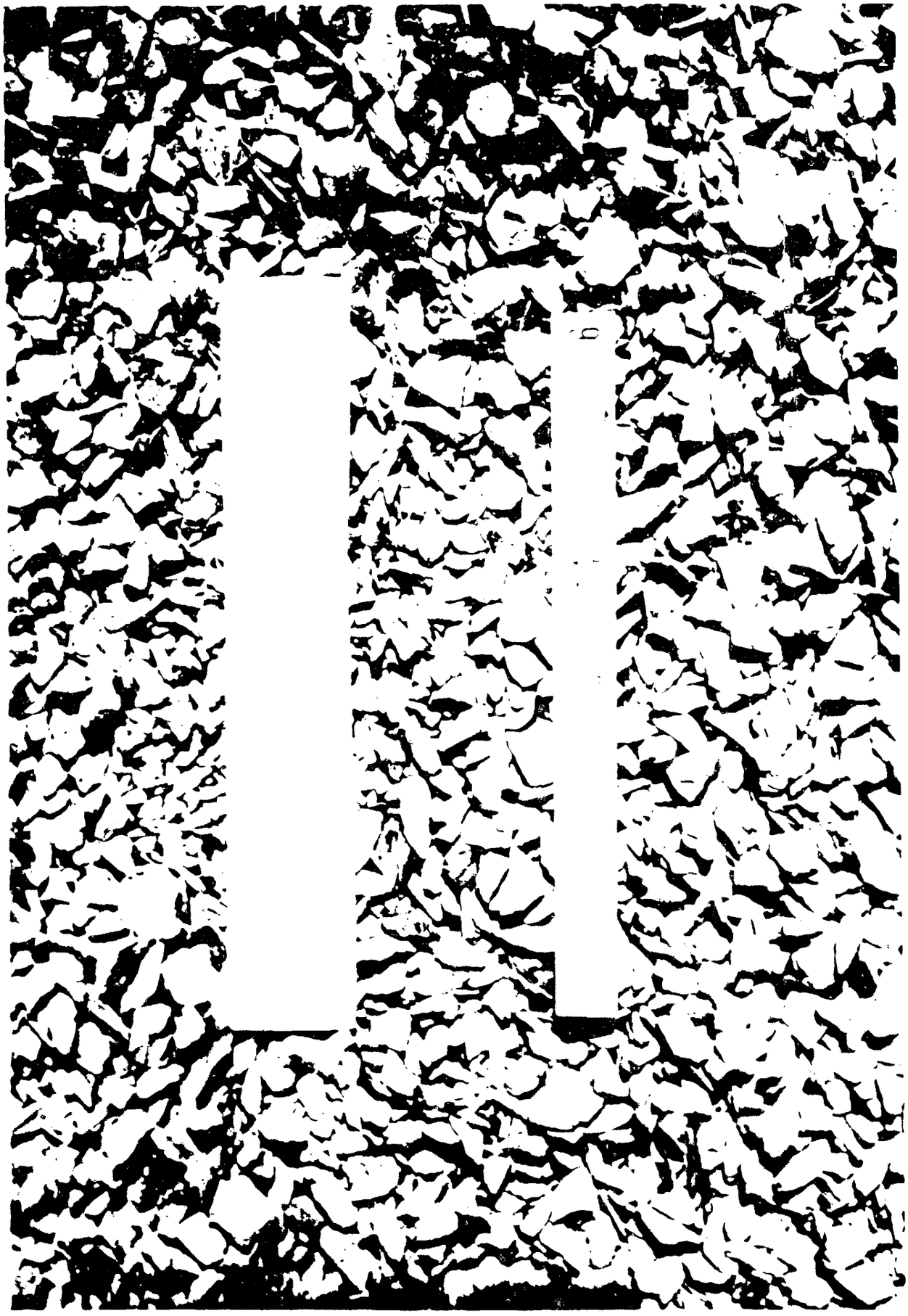

FIGURE 13: PHOTOGRAPH OF 3/8 INCH STONE COVERED TERRAIN

1. Conditions Tested

This test program consisted of tests conducted at an average duct exit height of 0.90 of the duct exit diameter. The aft duct is slightly higher than the forward duct. As shown in Table I, the first tests were conducted over sand terrain with the propeller duct protection devices, referred to as teepees, installed (see Figure 14.). Test 161 was run to determine by pressure studies the effects of the propeller duct protection devices. Results of Test 161 showed that the engine efficiency was reduced to the extent that the thrust capability was compromised, thus significantly reducing the engine performance. Therefore the propeller duct protection screens were removed, (see Introduction, page 4). Tests 162 to 173 (listed in Table I) were conducted without the propeller duct protection.

The ambient conditions experienced during testing are summarized in Table 2. In particular, it should be noted in this table that the terrain moisture was considerably less than that experienced in the tests of Reference 2. The terrain in Reference 2 had a moisture content of about 12 percent. Moisture of 12 percent provided the sand with some cohesion and thus was called wet sand. As shown in Table 2, sand moisture as low as 1.4 percent and up to 6.6 percent was encountered. This range of moisture resulted in sand textures from dry to damp with very little cohesion in this range.

2. Determination of Test Duration

Due to the statistical nature of this testing the determination of the desired length of each test is

FIGURE 14: PHOTOGRAPH OF TEEPEES INSTALLED ON PROPELLER DUCTS

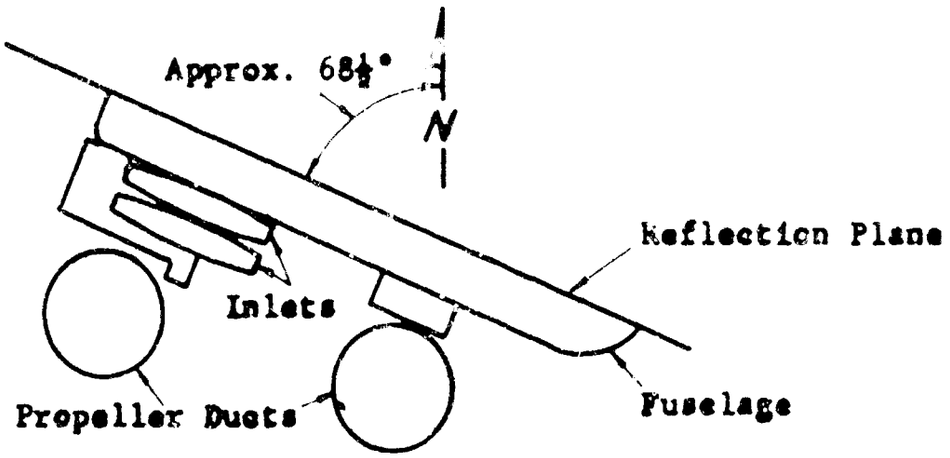

X-22 Test Rig

Test No.	Terrain Moisture, percent	Wind Velocity, knots	Wind Direction	Temperature °F.
155	3.1	10	NW	55
156	3.1	10	NW	55
157	3.1	4	SSW	57
158	3.1	3	WSW	71
159	3.2	7	SSW	51
160	3.2	4	S	62
161		8	ESE	56
162	2.2	6	SW	57
163	6.6	4 to 6	SW	54
164	6.6	8	SW	72
165	6.6	8	SW	72
166	3.4	8 to 10 Gusts to 20	WNW	72
167	3.4	8 to 10 Gusts to 20	WNW	72
168	1.4	5 to 8	NW	57
169	1.4	4	NW	65
170	Stone	10-Gusts to 15	SSW	67
171	Terrain	7	W	62
172		2	NE	68
173		Calm	--	79

Note: The moisture in the sand terrain is calculated from a four pound sample taken on the day of the test. The percentage given is based on weight.

TABLE 2. AMBIENT CONDITIONS OF TERRAIN MOISTURE, WIND AND TEMPERATURE EXPERIENCED DURING TESTING

important. The terrain samples vary widely in particle size and therefore the tests must be of sufficient duration that a representative sample is collected. In reducing the test data, the test duration was obtained from the oscillograph records. Test duration was defined as the time equivalent of the oscillogram length between the intersection of a line parallel to the average thrust reading and a line darined by the average slope of the starting and stopping transients. This relation is shown in Figure 15

The resulting data obtained on test duration is shown in Table 3. It may be noted that the average test duration was about 45 seconds, but tests were as short as 23 seconds and as long as 64 seconds. The wide dispersion in test times indicates that the resulting data should be nondimensionalized by test time.

3. Engine Airflow to Disc Loading Correlation

A fixed relation between the power settings of the thrust engines and the ingestion engine was established as the test criteria. This relation was established to most nearly simulate the X-22 aircraft.

It is realized from previous tests, Reference 2, that the inlet velocity (V_i) is proportional to the upflow velocity (V_u) in the area of the inlet. Since the test rig closely approximates the X-22 configuration we can write the relationship.

$$\left(\frac{V_i}{V_u}\right)_{Test} = \left(\frac{V_i}{V_u}\right)_{X-22}$$

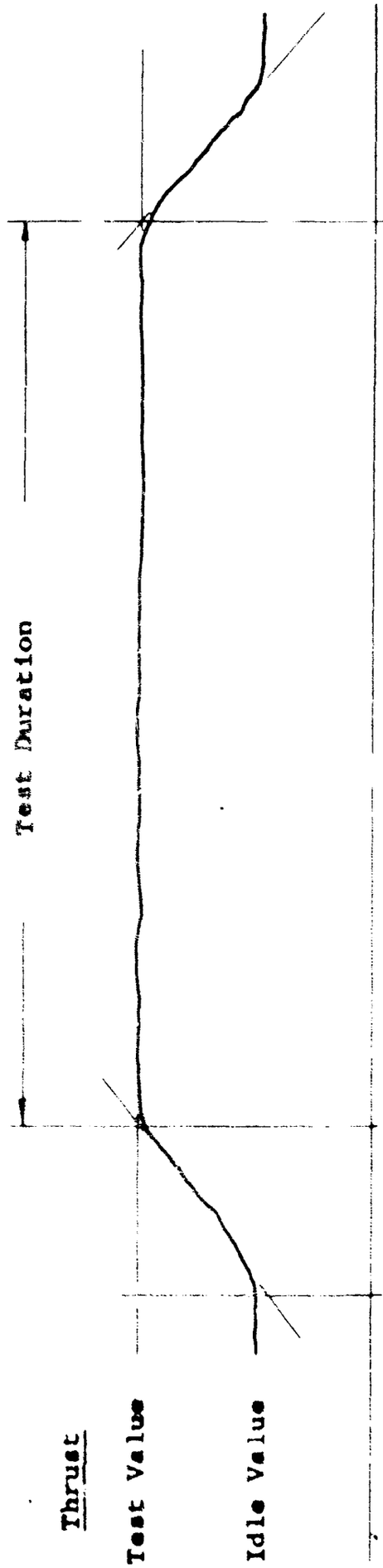

FIGURE 15: TEST DURATION

Test No.	Test Duration, Sec,	Propellor Drive (T-53) Engine Setting		Ingestion (J-69)
		FWD. N_2 (RPM)%	AFT N_2 (RPM)%	Engine RPM %
155	24	84	84	84
156	23	93	93	93
157	33	96	98	98
158	31	93	93	93
159	44	96	98	98
160	46	96	98	98
161	44	96	98	98
162	32	97	98	98
163	45	96	98	98
164	44	97	98	98
165	42	96	98	98
166	41	84	84	84
167	43	93	93	93
168	41	96	98	98
169	41	96	98	98
170	64	86	84	84
171	42	93	93	93
172	31	96	98	98
173	33	96	98	98

TABLE 3: DURATION OF TESTS AND ENGINE POWER SETTINGS

since

$$V_i = \frac{W_2}{\rho_s A_i} = \frac{W_o}{\rho_s A_i}$$

and

$$V_u = K\sqrt{\frac{T}{A_e}}$$

substituting in the above velocity relationship

$$\left(\frac{\frac{W_2}{\rho_s A_i}}{K\sqrt{\frac{T}{A_e}}} \right)_{TEST} = \left(\frac{\frac{W_o}{\rho_s A_i}}{K\sqrt{\frac{T}{A_e}}} \right)_{X-22}$$

simplifying we get

$$\left(\frac{W_2}{\sqrt{\frac{T}{A_e}}} \right)_{TEST} = \left(\frac{W_o}{\sqrt{\frac{T}{A_e}}} \right)_{X-22}$$

realizing

$$\frac{T}{A_e} = D.L.$$

we may write

$$\left(\frac{W_2}{\sqrt{D.L.}} \right)_{TEST} = \left(\frac{W_o}{\sqrt{D.L.}} \right)_{X-22}$$

Futhermore, the X-22 aircraft as given in Reference 3 will have a normal VTOL gross weight of 15,000 pounds. The diameter of the duct exits of this aircraft is approximately 7.9 feet, resulting in a normal VTOL disc loading (D.L.) determined as follows:

$$D.L. = \frac{P}{A_e \times 4 \text{ ENGINES}}$$

where $P = 15{,}000$ Pound

$$A_e = \pi \frac{D_e^2}{4} = 3.1416 \frac{(7.9)^2}{4} = 49.0$$

Therefore

$$D.L. = \frac{15{,}000}{49.0 \times 4 \text{ ENGINES}}$$

resulting in

$$D.L. = 76.5 \text{ PSF}$$

Continuing, the X-22 engine airflow (ω_o) can be obtained from Reference 4 as about 11.5 pounds per second.

Therefore

$$\left(\frac{\omega_o}{\sqrt{D.L.}}\right)_{X-22} = \frac{11.5}{\sqrt{76.5}} = 1.32 \frac{\text{LB/SEC.}}{\sqrt{\text{LB/FT}^2}}$$

Since

$$\left(\frac{\omega_a}{\sqrt{D.L.}}\right)_{TEST} = \left(\frac{\omega_o}{\sqrt{D.L.}}\right)_{X-22}$$

$$\frac{\omega_a}{\sqrt{D.L.}} = 1.32 \left|\text{LB.}\right|^{\frac{1}{2}} / \text{FT. SEC.}$$

This relation was used to reduce the test data to the coordinates airflow (ω_a) and the square root of the disc loading $(D.L.)^{\frac{1}{2}}$ shown in Figure 31.

B. Inlet Protection Device Tests

The program for the Inlet Protection Device Tests was basically the same as for the Engine Ingestion Tests.

C. Aerodynamic Interference Tests

The following parameters were varied during this testing.

1. Duct height from ground.
2. Propeller blade pitch.
3. Propeller RPM.

The time variation of duct static pressure distribution, duct flow velocity, total thrust, propeller torque and propeller blade stresses were determined.

The objective of this phase of the research was to determine the nature of the aerodynamic interference between two ducted propellers operating in close proximity, located near the ground adjacent to a reflection plane, to simulate a four duct VTOL aircraft shown in Figure 16. Note the protective ground cover. The thrust axes of the ducts were oriented in a vertical direction representing a VTOL aircraft hovering near the ground. Earlier tests discussed in Reference 2 indicated low frequency variations in thrust of 9 percent of the average thrust.

Particular emphasis in the present series of tests was placed on measuring the time history of the thrust of the ducts while operating at various blade angles and propeller rotational speeds in various geometric locations with respect to one another. Isolated duct measurements were conducted to serve as a reference for the tandem experiments.

FIGURE 16: PHOTOGRAPH OF AERODYNAMIC INTERFERENCE TEST RIG SHOWING THE GROUND COVER.

The phenomenon of interest is the nature of the recirculation caused by the presence of two ducts near one another. Recirculation refers to the fact that the wake produced by a ducted propeller or other thrusting device flows back through the duct. If this occurs, then it would be expected that the variation with time of the aerodynamic forces acting on the device would be increased since the wake as seen from a stationary reference system is unsteady due to the finite number of blades. A significant fluctuation of the flow at a frequency of the number of blades times the RPM as well as other frequencies would be expected due to the random nature of the flow and the various aerodynamic nonlinearities present.

Physically, recirculation develops as a result of the following influences. If we first consider an isolated duct operating with its thrust axis vertical over a perfectly flat surface with zero wind velocity, no recirculation would be expected and the wake would spread out over the ground as shown in Figure 17. If we move the duct down close to the ground, as shown in Figure 18, then some recirculation may occur. Appreciable recirculation in this perfectly symmetrical situation probably does not occur until the duct is less than one diameter from the ground. If the duct is operating over a surface that is eroded or distorted by the wake (water) then the resulting change in shape of the surface will probably cause recirculation to occur as shown in Figure 19. The

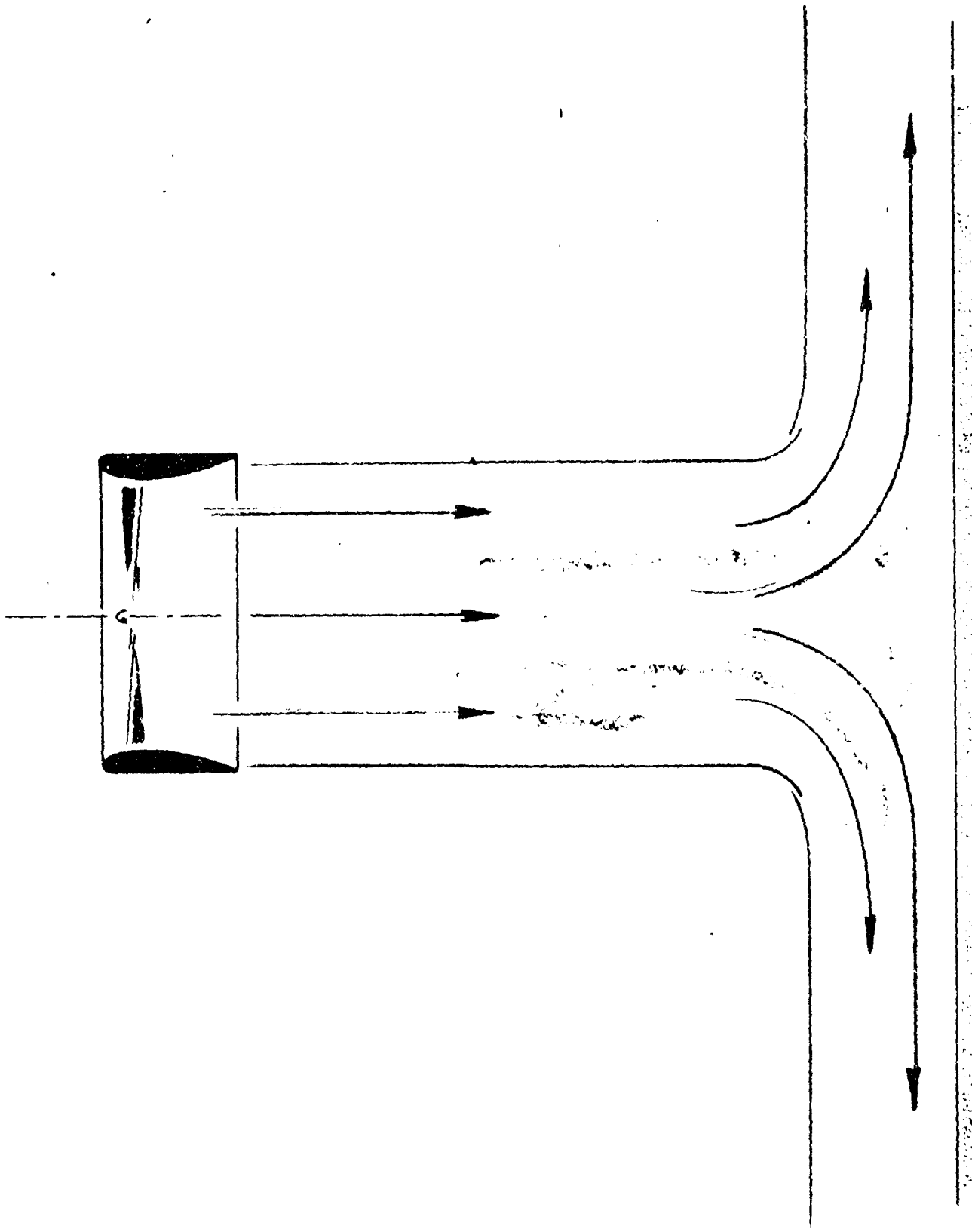

FIGURE 17: ISOLATED DUCT AIRFLOW

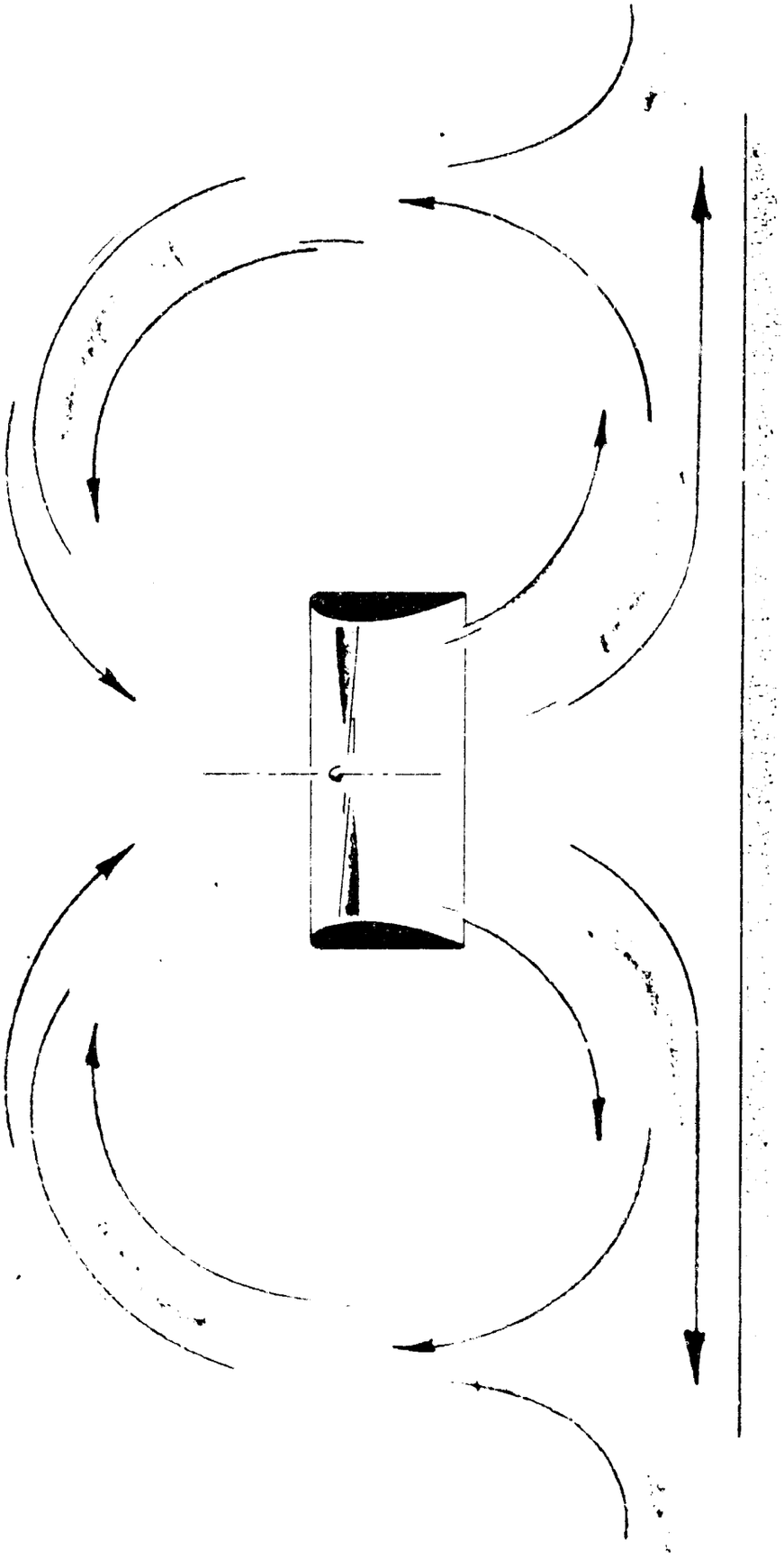

FIGURE 18: ISOLATED DUCT AIRFLOW CLOSE TO GROUND

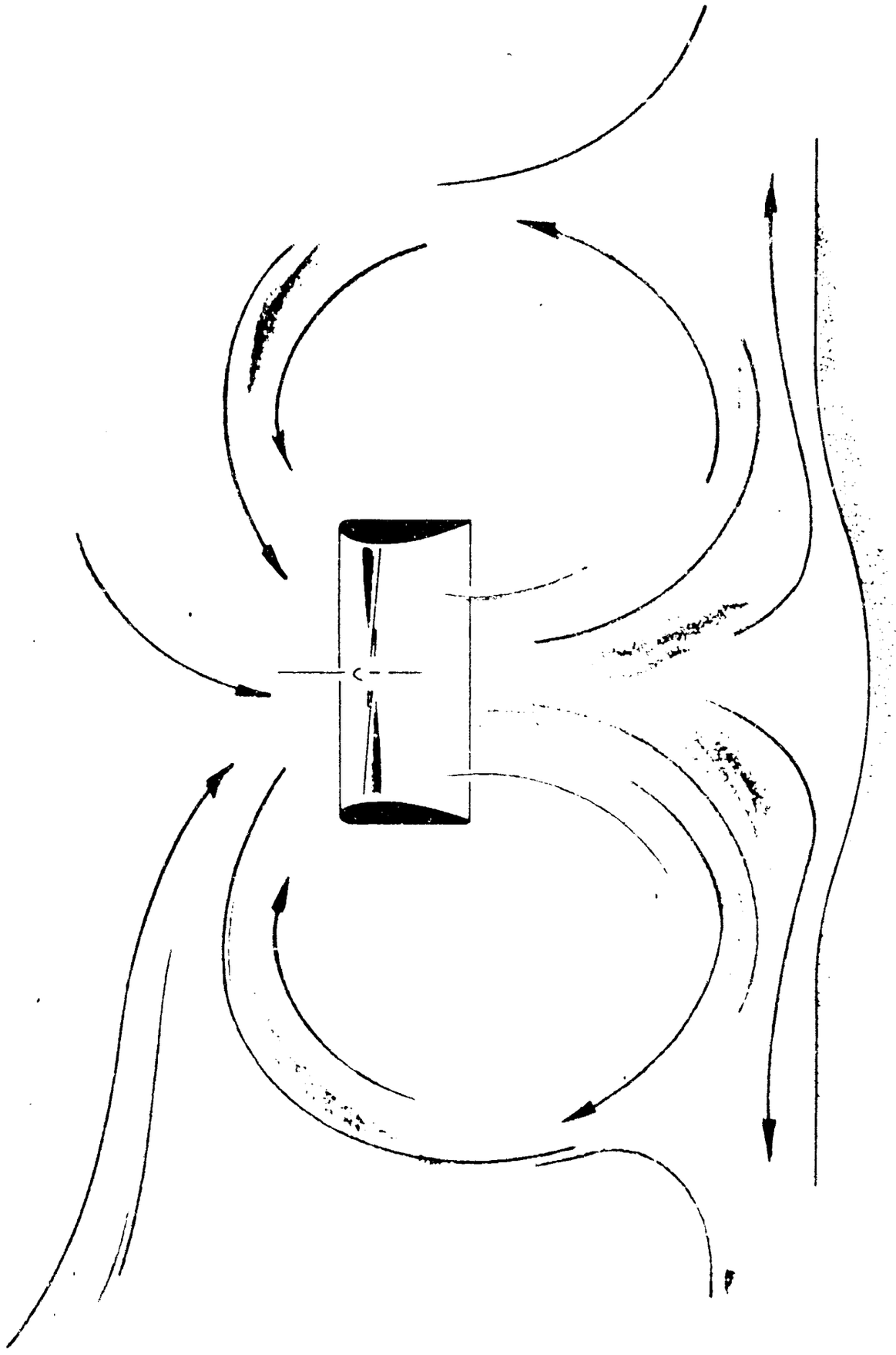

FIGURE 19: ISOLATED DUCT AIRFLOW WITH SURFACE EROSION

presence of a wind will also cause a recirculation as it will stop the flow along the ground. The resulting upward flow would be more likely to be sucked into the incoming flow as shown in Figure 20. Recirculation would also occur when the ducted fan is operated in a closed building or wind tunnel at zero forward speed.

Basically, the propeller or ducted fan is using a large volume of air per unit time and any external influence that deflects the spreading wake upward would be expected to result in some recirculation of the wake as the upward flow would be induced into the inlet.

Now if we place two ducted fans close to one another near the ground as shown in Figure 21, a plane of symmetry will be present with a strong upward flow near this plane of symmetry. Again this upward flow will be sucked into the inlet as shown in the sketch with the resulting recirculation pattern. The presence and magnitude of this up-flow is discussed in Reference 2. The movies that accompany Reference 2 show this phenomenon as well as presence of recirculation.

Now we turn to the question of the aerodynamic effects of a recirculating flow. First, it would be expected that the average thrust of the device at a given blade angle and RPM would be reduced. The presence of an average inflow velocity would act to reduce the average blade element angle of attack with a resulting loss in thrust. In addition, the presence of the

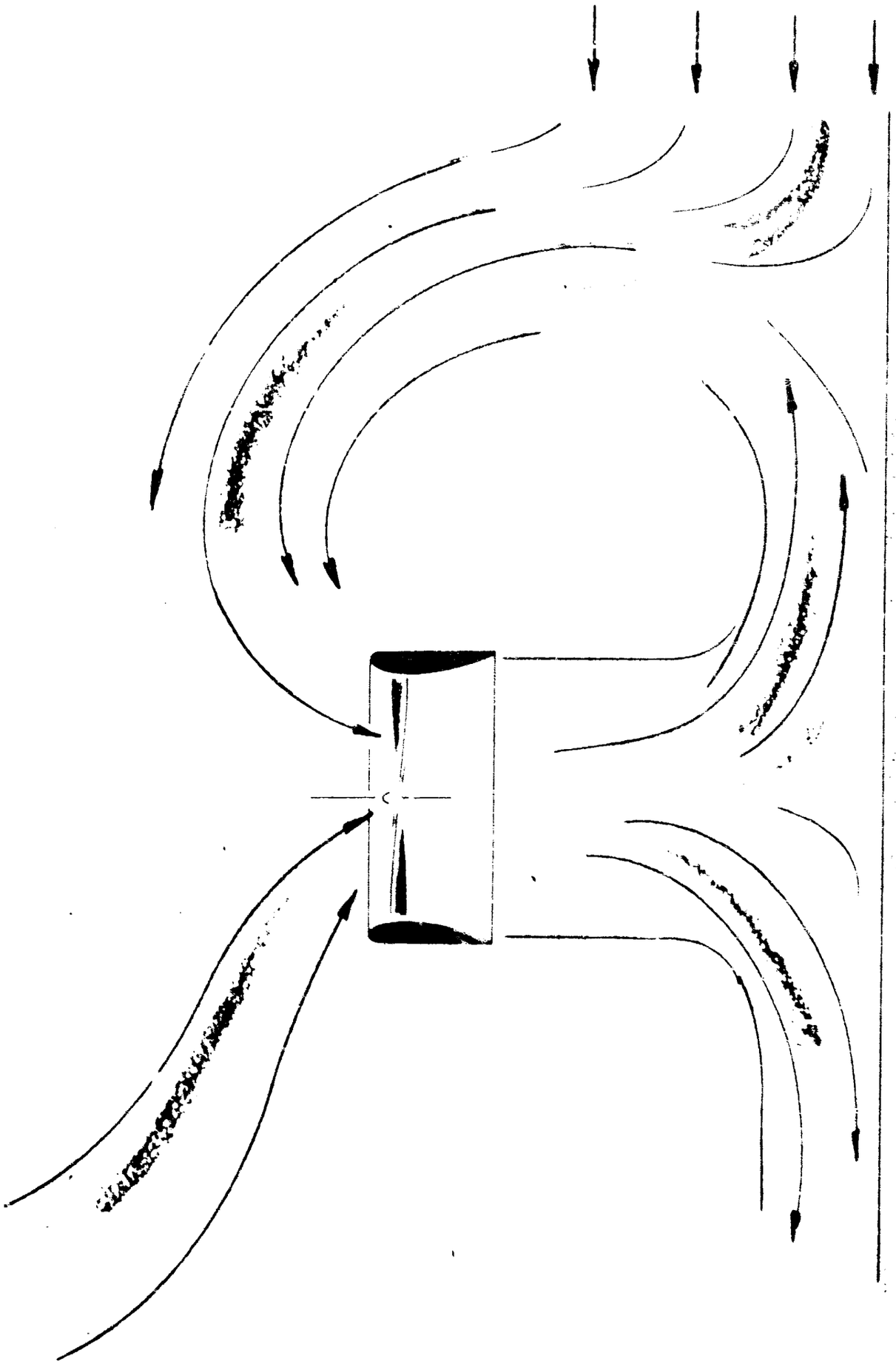

FIGURE 20: ISOLATED DUCT AIRFLOW IN PRESENCE OF WIND

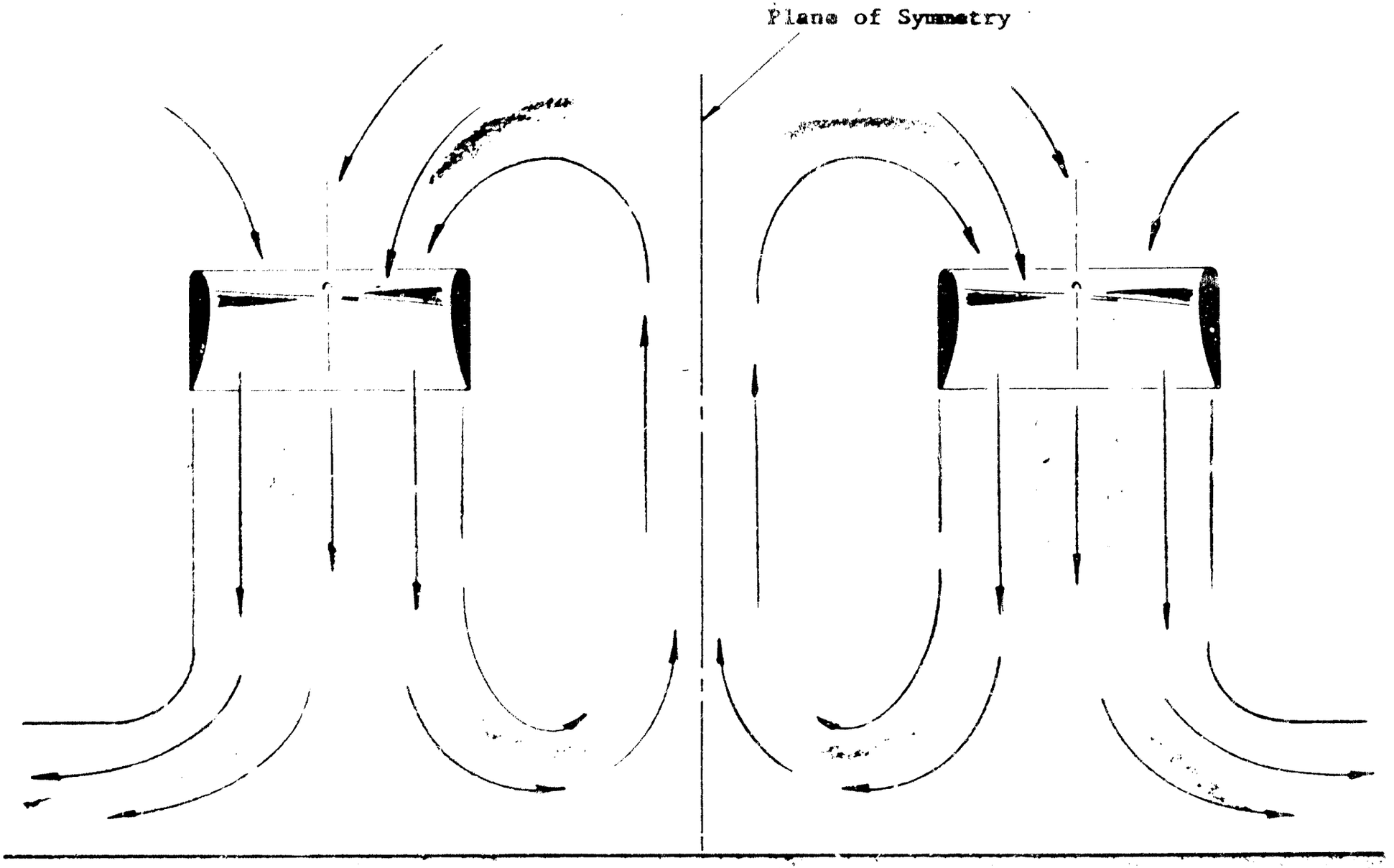

FIGURE 21: TANDEM DUCTS AIRFLOW

Recirculation would be expected to cause roughness perhaps similar in nature to that experienced by a helicopter in a vortex ring state of operation, Reference 5. Any disturbances in the wake would tend to be magnified as a result of recirculation. The importance of the roughness or thrust variation on the operation of an aircraft would tend to fall into three categories based on the frequency range of the disturbances. Very low frequency variations in thrust would appear as random disturbances to the pilot in attempting to hover and control the airplane close to the ground. Recirculation is probably one of the sources of erratic behavior of many VTOL aircraft noticed near the ground, Reference 6. In a mid frequency range, disturbances may be significant in causing amplification of various structural frequencies of the aircraft. In addition, it may be expected that the level of the disturbances at the number of blades times the RPM would be increased and this high frequency fluctuation would be of significance in the stress level experienced by the propeller blades.

The program conducted by Kellett Aircraft Corporation described here was aimed at determining the low frequency components of the thrust as caused by the presence of two adjacent ducts in configurations similar to the X-22 aircraft. In addition, tests were conducted simultaneously by Hamilton Standard Division of UAC to measure the higher frequency components of stress in the blades. See Figure 22 for a photograph of the slip ring and strain gage installations. Strain

FIGURE 22: PROPELLER INSTRUMENTATION AND SLIP RING INSTALLATION

gages were installed on one propeller only. The isolated ducted propeller and the aft ducted propeller were the propellers on wnich the strain gages were applied for the stress investigations.

IV INSTRUMENTATION

A. Aerodynamic Instrumentation

The apparatus consisted of transducers to measure the following parameters associated with the duct:

1. Total ducted fan thrust - Baldwin SR4 load cell type U-1, two provided for each duct.
2. Duct exit velocity - Four hot wire velocity probes, Flow Corporation Model 55A1. They were mounted radially in each duct as shown in Figures 23 and 24.
3. Duct static pressure at two lip stations at four radial locations. Statham Model No.PM60TC±1-350. Locations shown in Figure 23 and 24. The corner frequency is 3500 cps.
4. Propeller torque. Oil pressure Giannini 46129J-D-7-50.
5. Propeller RPM. Tachometer generator. Jack and Heintz Inc. MS-25038-4 Indicator G.E. MS-28000-1.

The geometry of the ducted fan is shown in Figures 23 and 24 and the propeller characteristics are given in Figure 25. A photograph of the isolated duct is shown in Figure 26, and of the tandem configuration is shown in Figure 16. The propeller propulsion engine was mounted in the duct as shown in Figure 23. The transducer outputs were recorded through a digital readout system and recorded on a punched tape. (Wang Labs. Inc. 26 Channel System).

Since the results of this program are dynamic in nature, care must be taken to evaluate the dynamic characteristics of all the components involved in the system.

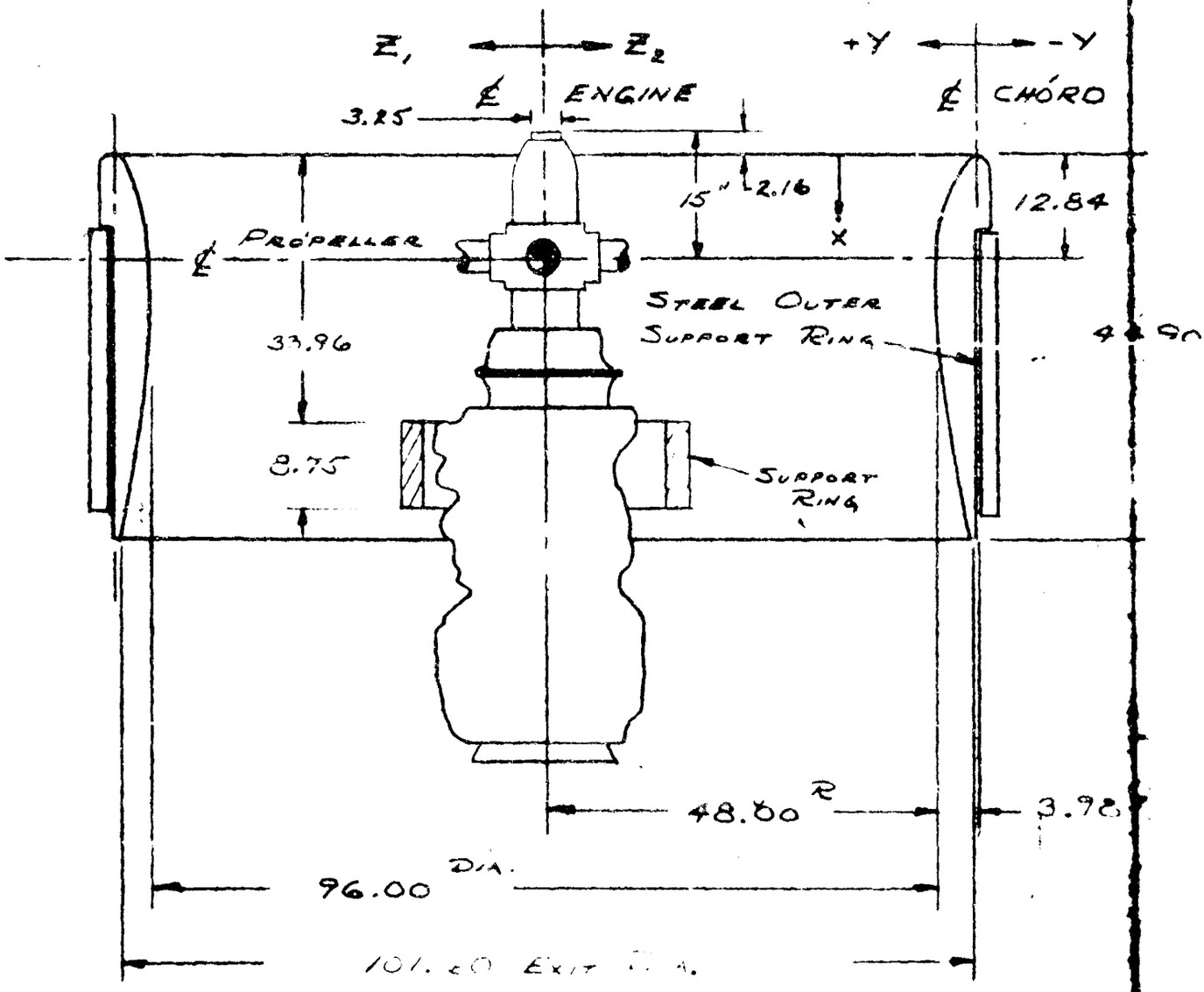

*Velocity Probes Numbered 1, 2, 3, and 4 are on the Forward Duct. The Remainder are on the Aft Duct.

FIGURE 23.

Chord X Inches	Duct		Engine	
	Inner Ord. + Y Inches	Outer Ord. - Y Inches	Ordinate Z_1 Inches	Ordinate Z_2 Inches
0	0	- 0.512	2.30	2.30
0.321	-	- 1.284	-	-
0.385	0.942	-	2.60	2.60
0.642	-	- 1.475	-	-
0.961	1.580	- 1.603	-	-
1.284	-	- 1.643	3.00	3.00
1.796	2.222	-	3.25	3.25
2.245	-	- 1.670	3.25	3.25
2.887	2.869	-	3.25	3.25
4.490	3.570	-	3.25	3.25
6.097	3.830	-	3.25	3.25
9.609	-	- 1.670	3.80	3.80
10.956	3.987	-	3.80	3.80
12.840	3.987	- 1.670	6.30	6.30
16.029	3.969	-	3.80	3.80
18.140	-	- 1.603	3.80	3.80
19.262	3.870	-	3.80	3.80
22.540	3.740	-	3.80	3.80
23.528	-	- 1.367	7.20	7.20
25.683	3.538	-	8.96	8.96
28.870	-	- 0.950	11.40	9.20
28.916	3.282	-	11.60	9.10
32.104	2.977	-	12.60	7.90
34.214	-	- 0.430	13.20	8.40
35.336	2.613	-	12.60	9.00
38.479	2.200	-	11.04	7.50
39.512	-	+ 0.207	10.48	7.50
41.757	1.740	-	9.80	10.00
44.900	1.185	+ 1.123	8.80	8.00
48.400	-	-	10.60	11.60
51.900	-	-	11.40	11.40
53.730	-	-	11.04	11.04
58.100	-	-	11.32	11.32
59.500	-	-	11.10	11.10
63.500	-	-	8.90	8.90
66.200	-	-	7.60	7.60
	Pressure Transducer		Eng. Support Ring	
0.940	0.383	-	-	-
2.800	2.768	-	-	-
34.687	-	-	17.750	17.750
	Velocity Probes			
*No. 1&5	-	-	48.8	-
No. 2&6	-	-	42.6	-
33.840	-	-	35.3	-
No. 3&7	-	-	26.8	-
No. 4&8	-	-		

GEOMETRY OF DUCTS USED IN DOWNWASH TEST RIG.

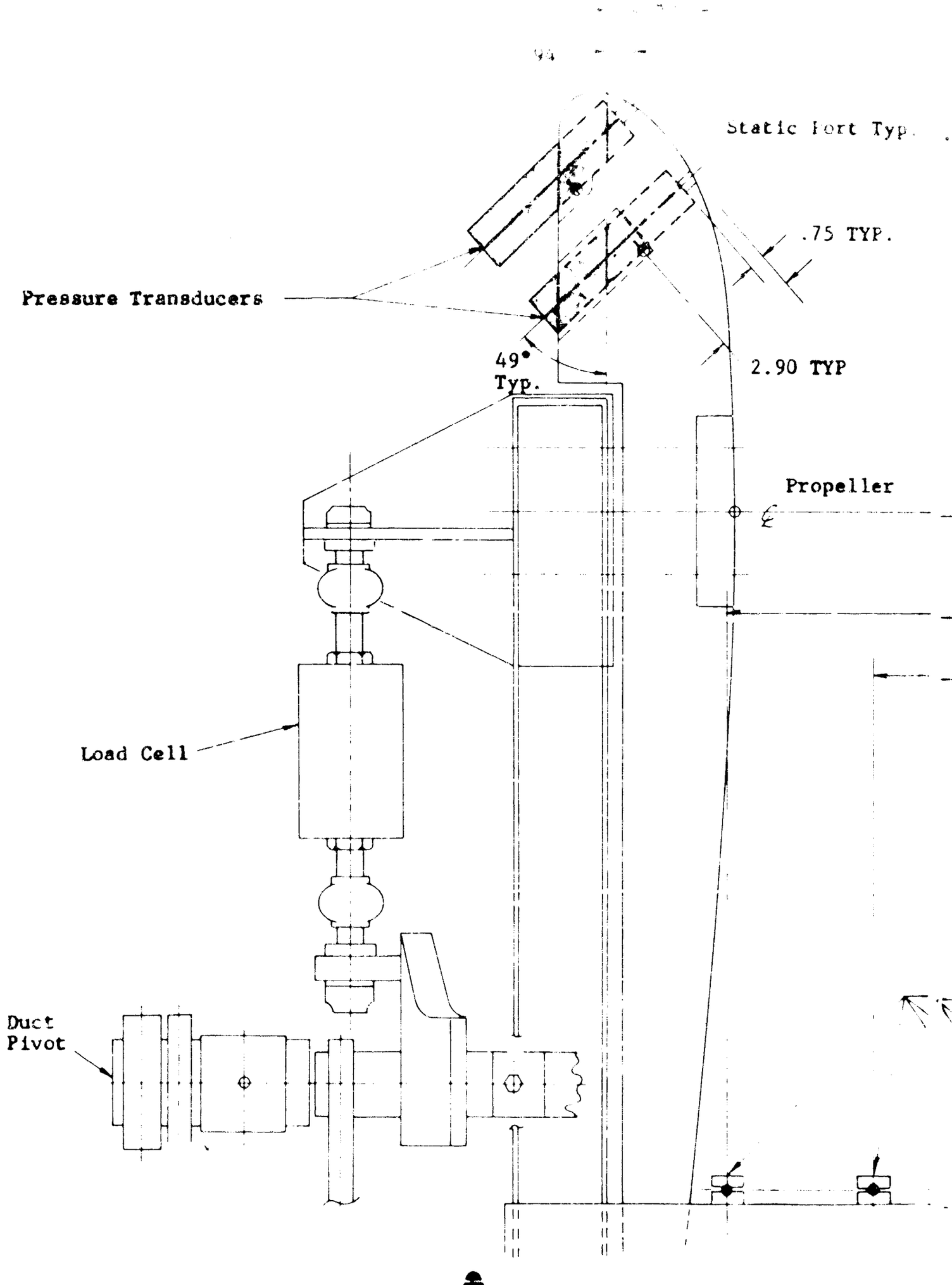
Static Port Typ.
.75 TYP.
Pressure Transducers
49°
Typ.
2.90 TYP
Propeller
Load Cell
Duct
Pivot

FIGURE 24

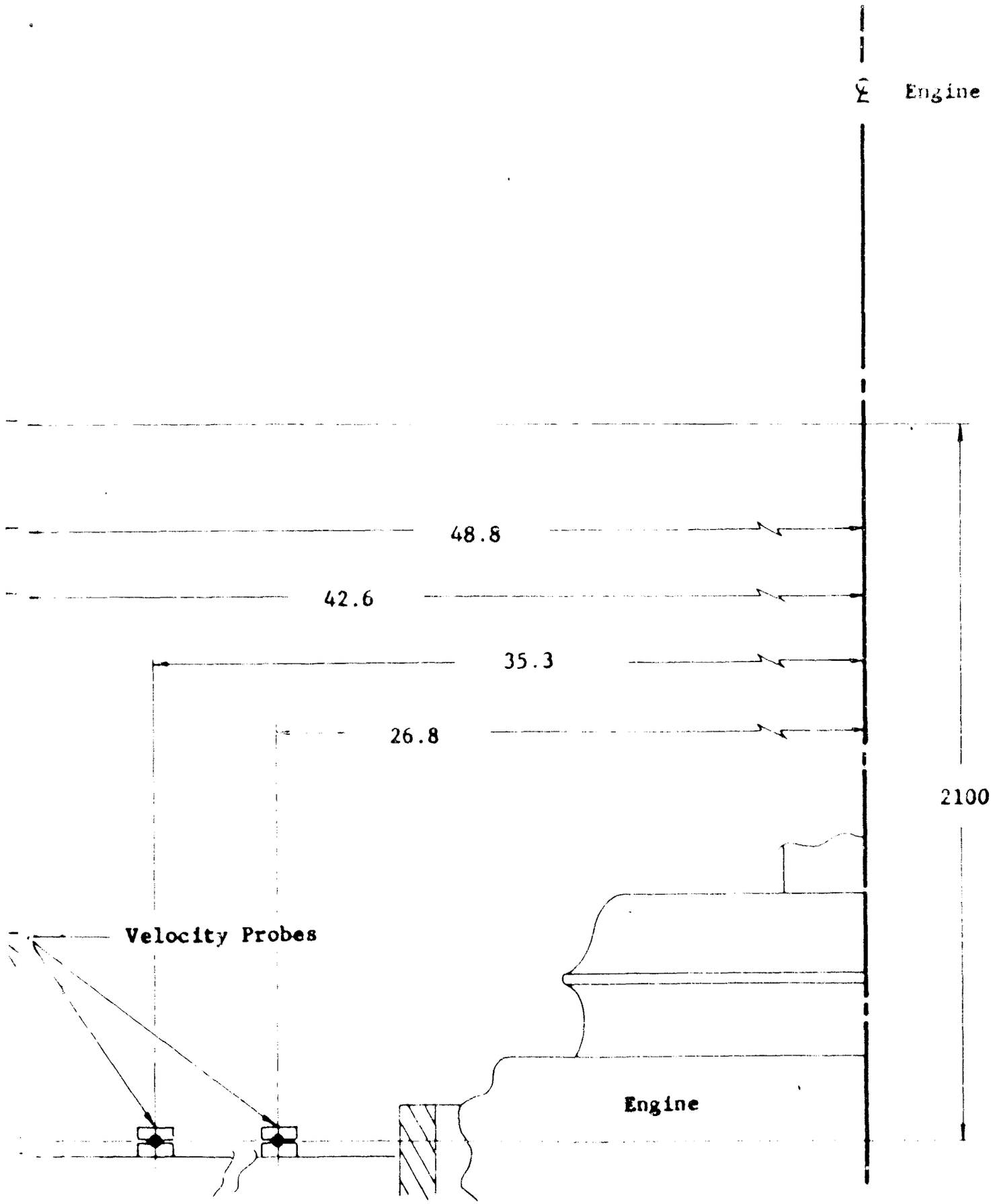

SECTION OF PROPELLER DUCT SHOWING INSTALLATION OF THE PRESSURE TRANSDUCERS AND AIR VELOCITY PROBES.

Hamilton Standard Propeller 7063-6 (Modified)

D Blade Diameter 8 Feet
h Blade Thickness
b Blade Chord
Three Blades

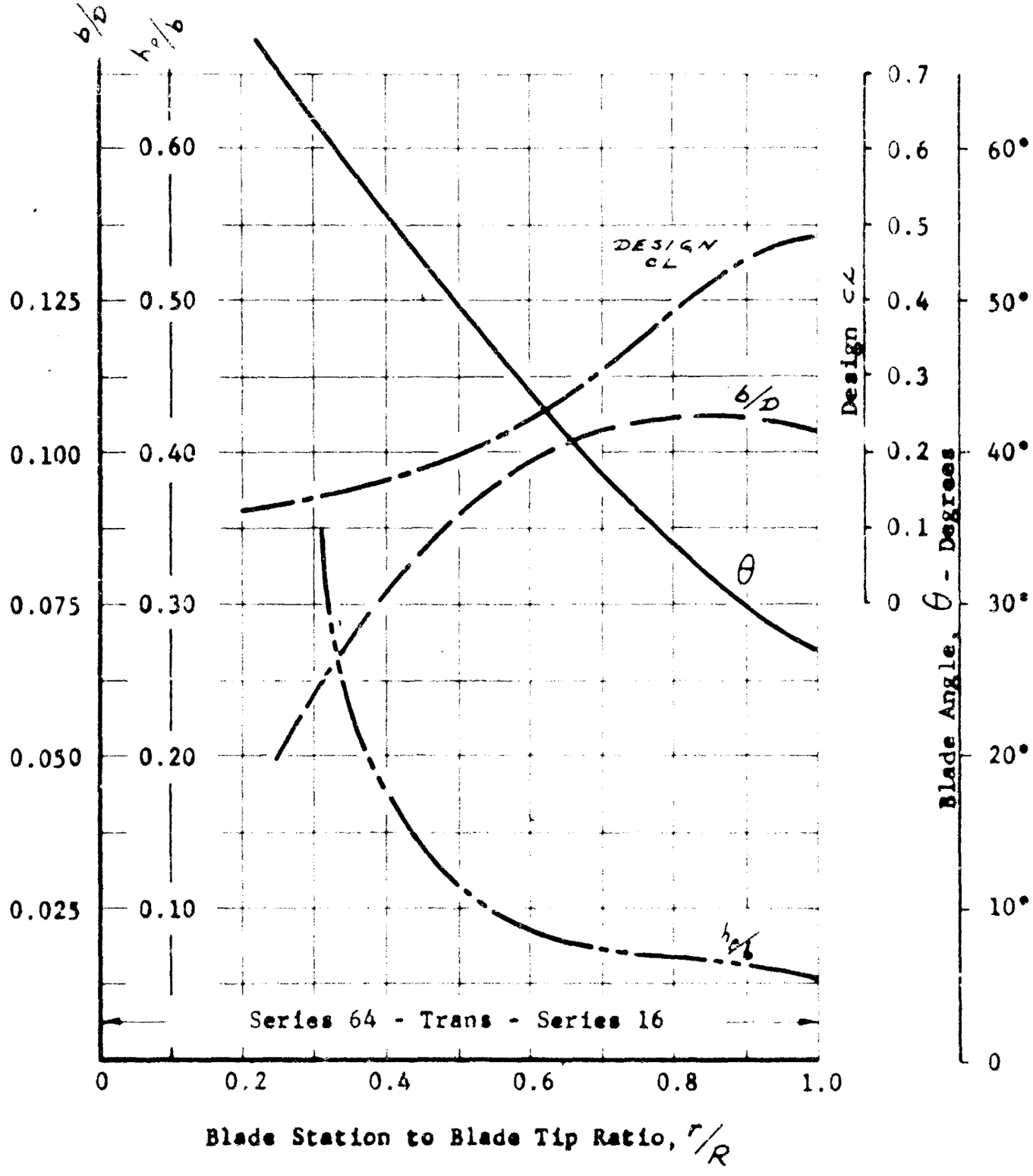

FIGURE 25: CHARACTERISTICS OF PROPELLER BLADES USED IN DOWNWASH TEST RIG.

FIGURE 26: PHOTOGRAPH OF ISOLATED DUCT TEST RIG

The digital readout system had a sampling frequency of 50 samples per second. This places a limitation on the frequencies that may be read in the output theoretically to below 25 cps and practically speaking to below probably 10 or 12 cps, irrespective of the frequency response of the transducers used, Reference 7. In fact, as discussed in Reference 7, whenever a sampling system is used, filtering of the transducer outputs should be such that their response is compatible with the limitations of the sampling system, otherwise a phenomenon known as aliasing will occur. Sufficient filtering was not done in these experiments. Since this limitation is perhaps not generally recognized in using sampling systems it is considered of interest to point out how this fact presents itself in the data. The corner frequency of the pressure transducers is 3500 cps. A significant 3 per revolution component will be present in the duct lip pressure readings due to the passage of the blades by the transducers. This 3 per revolution component beats with the sampling frequency, or some multiple of the sampling frequency, twice in this case, with the resulting spurious frequency components as shown in Figure 27.

The response characteristics of the other transducers used in this experiment were reasonably compatible with this limitation and so are essentially free of aliasing.

To obtain the variation of the duct thrust with time, consideration must be given to the natural frequency

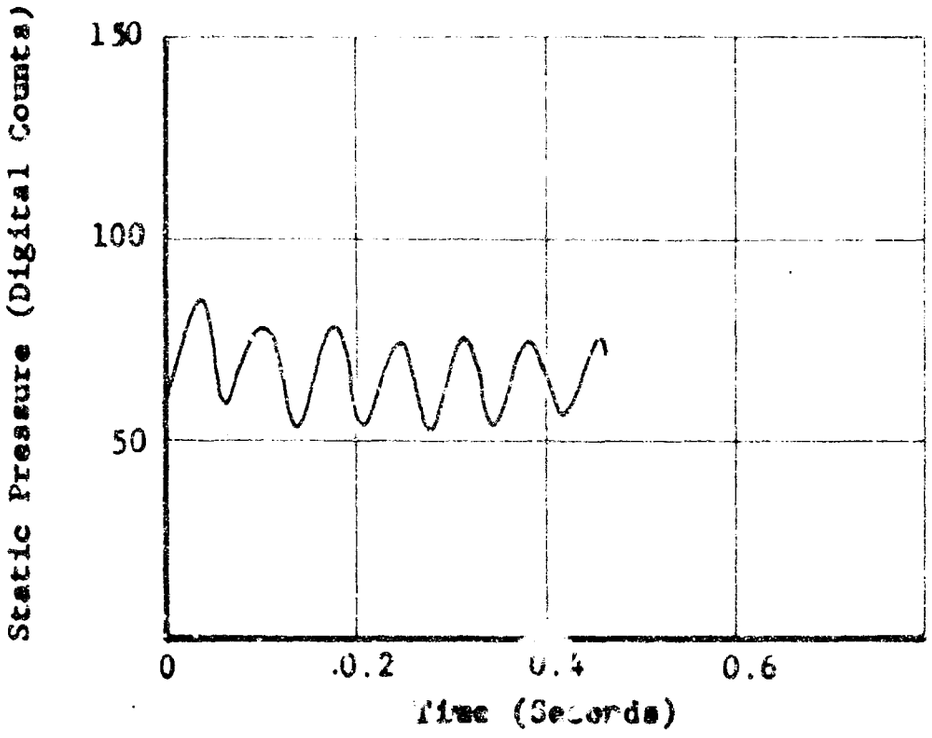

$2f_s - 3n = f_a$
$2(50) - 3(28.3) = 15.1$ rps

a) Propeller Speed 1700 RPM (28.3 cps)

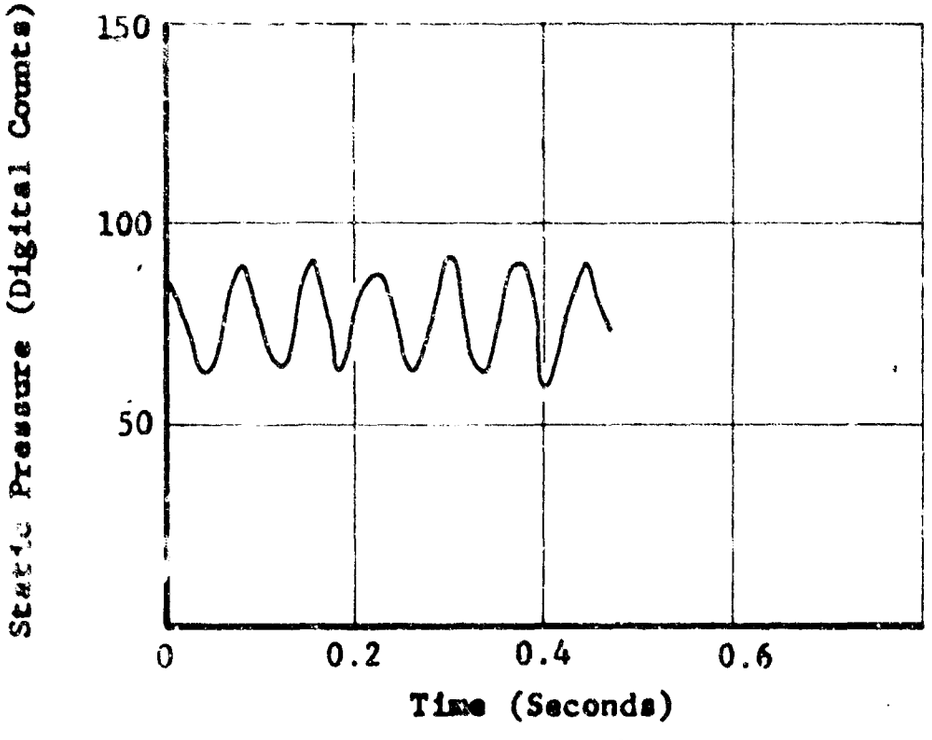

$2f_s - 3n = f_a$
$2(50) - 3(27.8) = 16.6$ rps

b) Propeller Speed 1666 RPM (27.8 cps)

FIGURE 27: PRESSURE MEASUREMENTS.

Aliasing of 3 propeller Blades per Revolution
Pressure Fluctuations With Sampling Frequency.

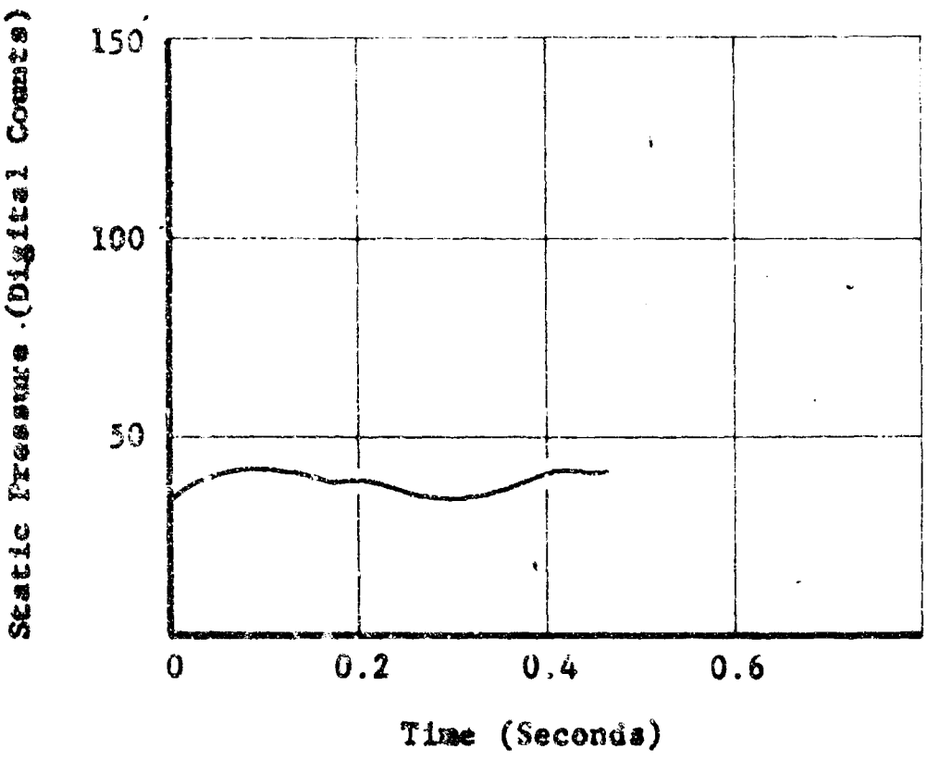

3n - fs =fa
3(17.6) - (50) =2.8 rps

c) Propeller Speed 1054 RPM (17.6 cps)

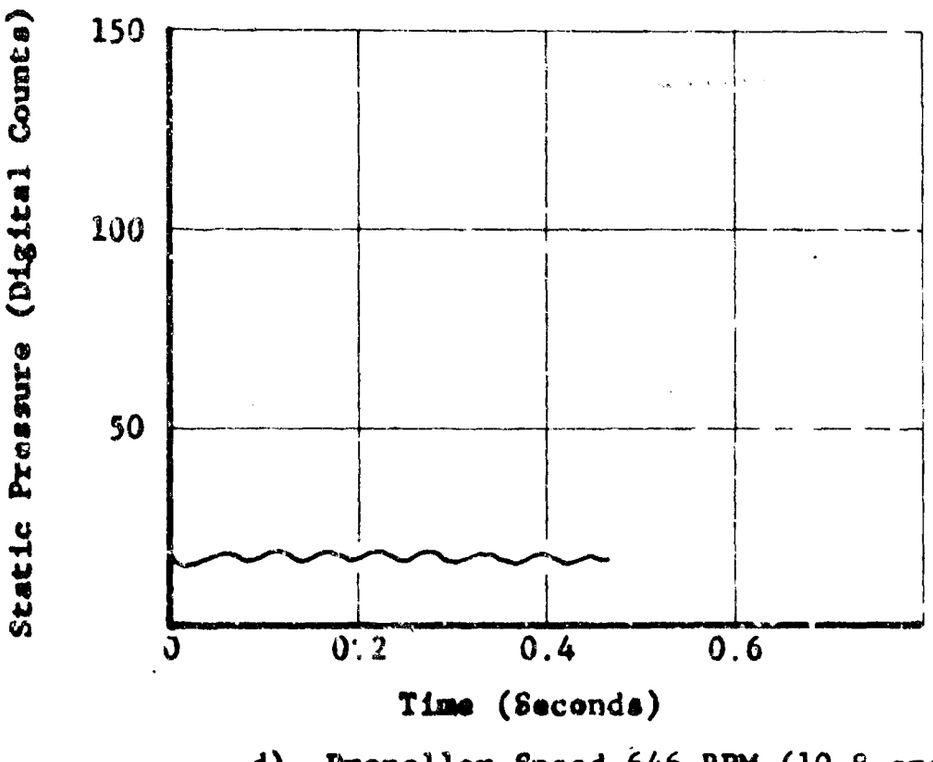

fs - 3n =fa
50 - 3(10.8) =17.6 rps

d) Propeller Speed 646 RPM (10.8 cps)

FIGURE 27: PRESSURE MEASUREMENTS.

Aliasing of 3 Propeller Blades per Revolution
Pressure Fluctuations With Sampling Frequency.

of the duct on the load cells, as well as the possible influence of any structural dynamics associated with the mechanical mounting of the duct that may influence the load cell readings.

The duct load cells have a static deflection of .00042 inches at a load of 5000 pounds. Two load cells are used on each duct, and the mass of the duct is approximately 50 slugs, so the natural frequency of vertical motion of the duct on the load cells is approximately 110 cps.

The duct mounting produces two predominate frequencies, one a torsional oscillation of the duct at about 2 cps due to the flexibility of the duct tilting mechanism which may be observed in the movies accompanying these experiments and a predominate frequency of 7-9 cps (depending upon the duct) which is due to the deflection of the crane as a cantilever, arising from elongation of the cables supporting the boom of the crane. The torsional oscillation did not appear to be present in the load cell readings. The cantilever frequency of the support crane was clearly evident in the previous data on this phenomenon shown in Figure 28 where the period of the vibration is indicated as 0.13 seconds. The frequency was confirmed by striking the duct and determining the resulting load cell output when the propeller was not turning. The amplification of this structural frequency by the recirculating

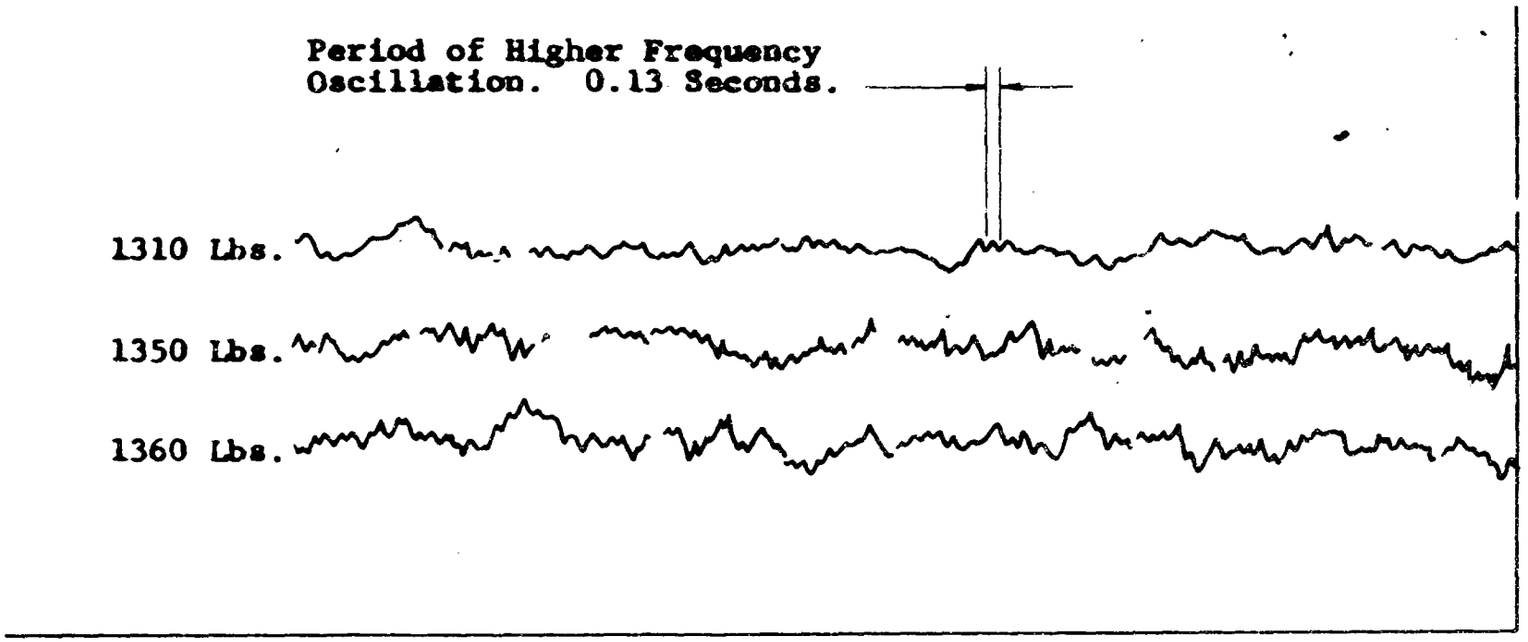

FIGURE 28: TYPICAL GALVONOMETER THRUST TRACE FROM REFERENCE 2.

flow particularly in the tandem configuration is seen in the thrust curves and will be discussed in detail later. The amplitude of this frequency shown in Figure 29 is considerably higher than shown in Figure 28, due to the increased bandwidth of the recording equipment used in this current series of tests. The galvanometers used in the recordings shown in Figure 28 had a time constant of about 0.1 second resulting in a considerable attenuation of this structural frequency of 8 cps.

The significance of the presence of this structural frequency is that the load cell readings will not be indicative of the variations in duct thrust, but instead indicate a displacement amplification due to frequency components in the disturbance forcing the system near resonance. Estimates of the actual motion of the duct when this frequency predominates indicates that these structural motions would have a negligible effect on the duct aerodynamics. That is, consider the simple example of measuring a sinusoidally varying force applied to a mass mounted on a spring by measuring the displacement of the mass. The amplitude of the displacement of the mass will only be proportional to the amplitude of the force when the frequency of the disturbing force is considerably less than the natural frequency of the mass on the spring.

The dynamic system involved in these tests may be visualized in a highly simplified way as a mass (the duct-propeller system) mounted on two springs in series. One spring,

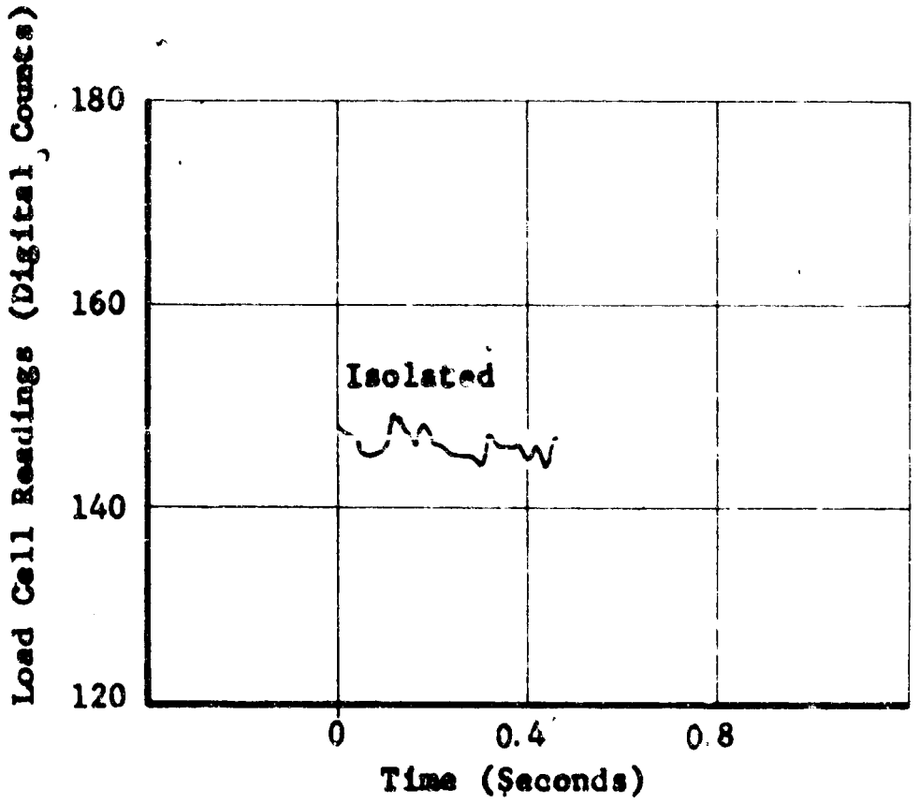

Propeller Speed 90% RPM

a) Test Number 201

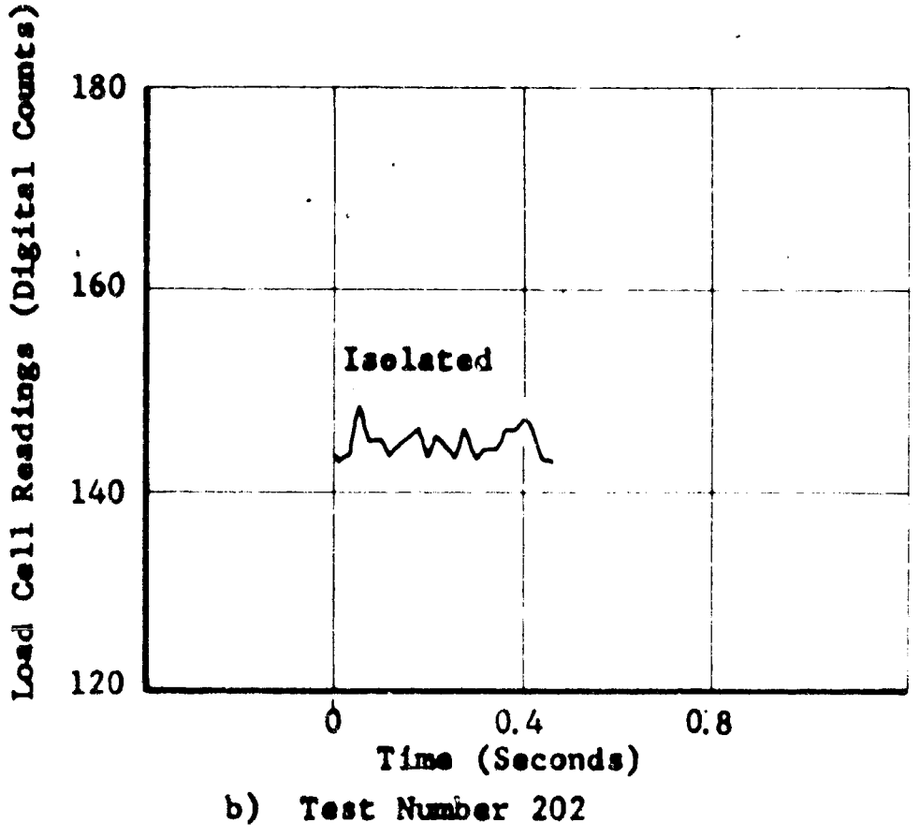

Propeller Speed 95% RPM

b) Test Number 202

FIGURE 29: TYPICAL TIME HISTORY OF LOAD CELL READINGS SHOWING STRUCTURAL EXCITATION.

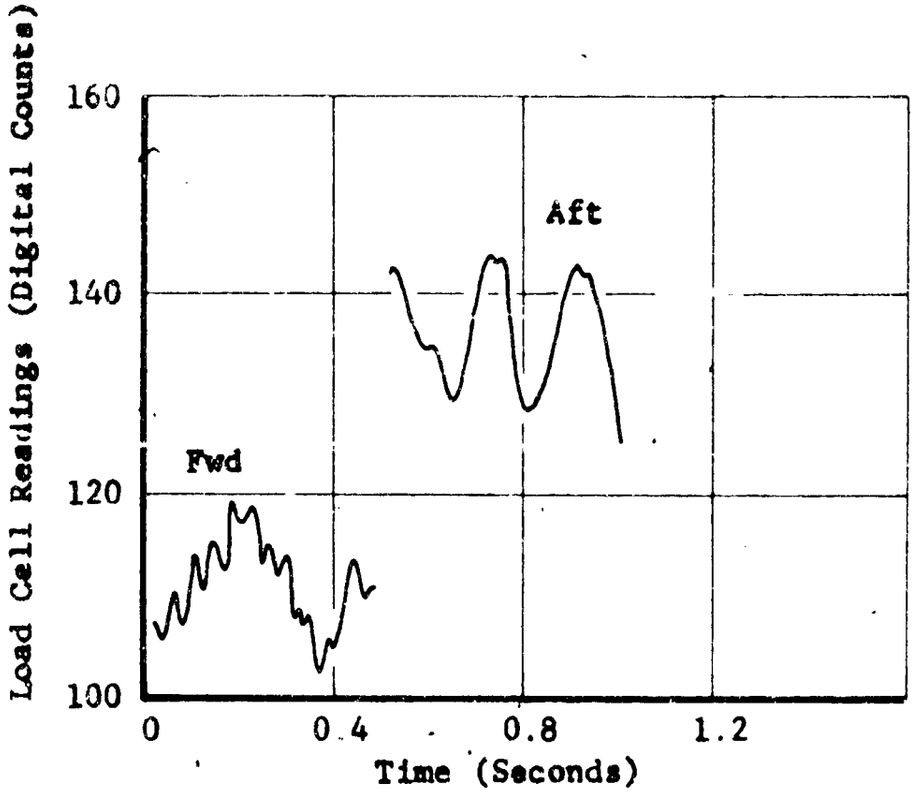

Propeller Speed 90% RPM

c) Test Number 211

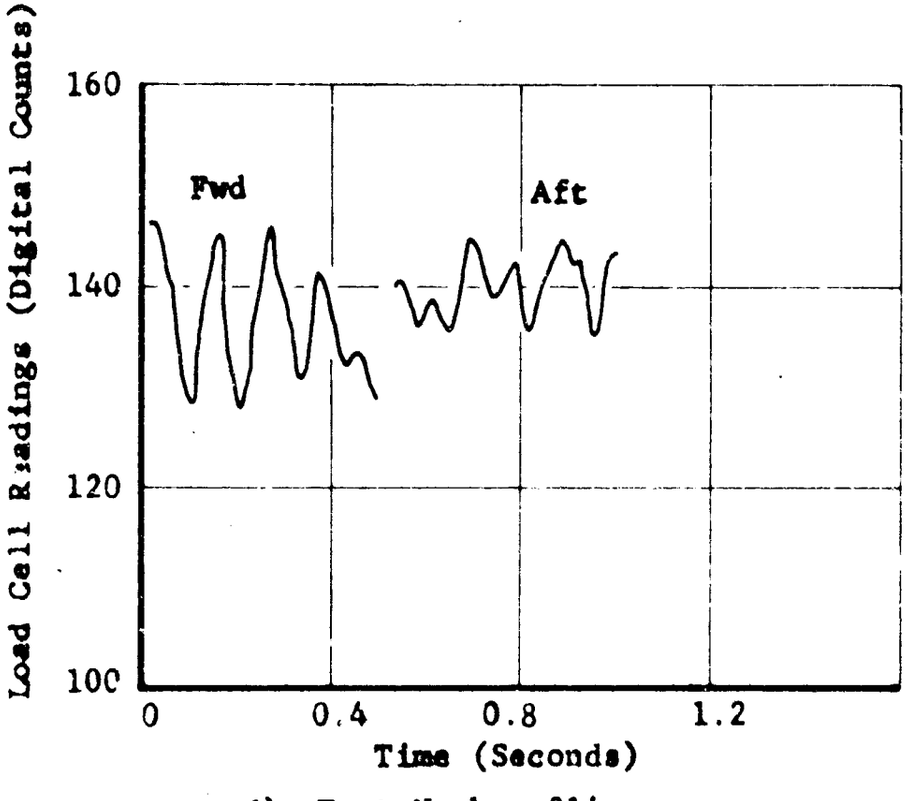

Propeller Speed 100% RPM

d) Test Number 214

FIGURE 29: TYPICAL TIME HISTORY OF LOAD CELL READINGS SHOWING STRUCTURAL EXCITATION.

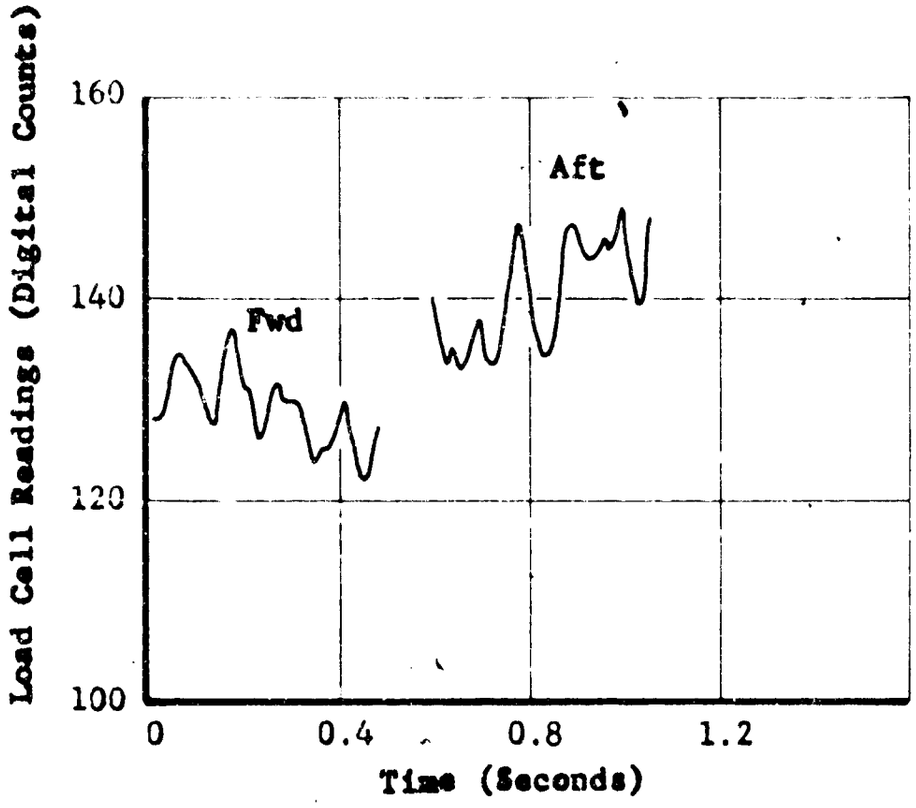

Propeller Speed 100% RPM

e) Test Number 217

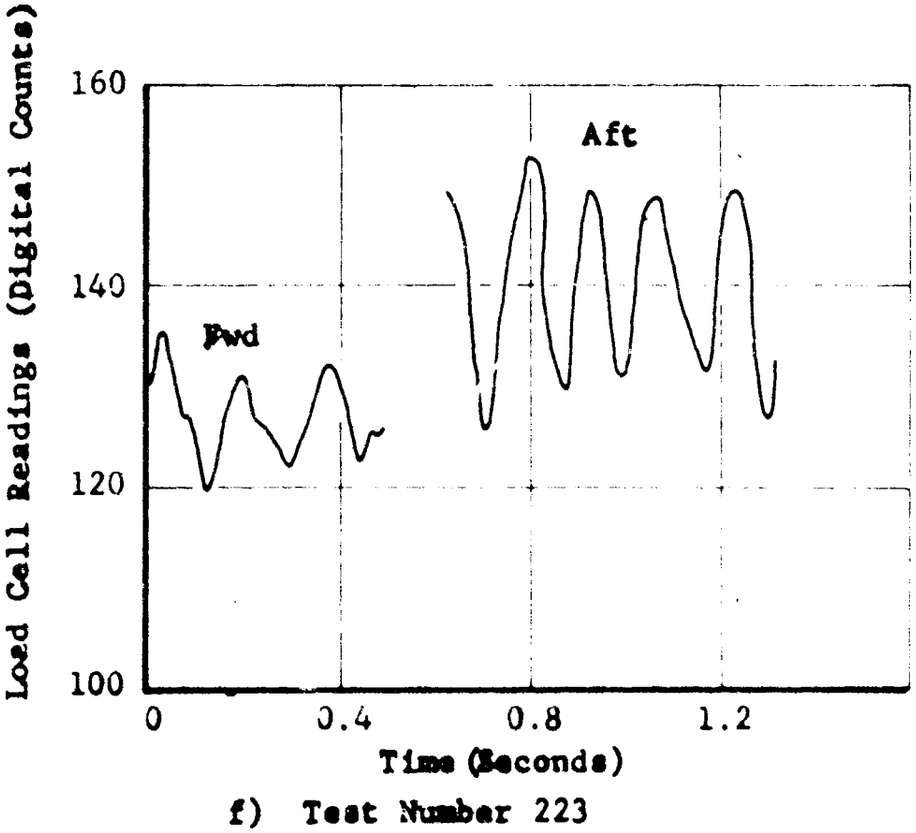

Propeller Speed 100% RPM

f) Test Number 223

FIGURE 29: TYPICAL TIME HISTORY OF LOAD CELL READINGS SHOWING STRUCTURAL EXCITATION.

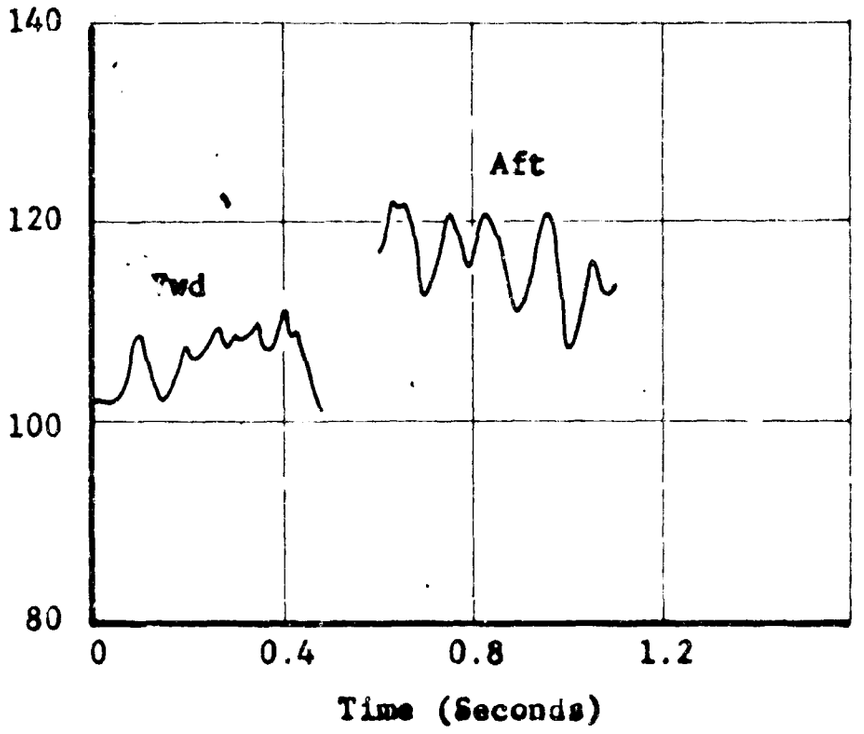

Propeller Speed 100% RPM

g) Test Number 225

FIGURE 29: TYPICAL TIME HISTORY OF LOAD CELL READINGS SHOWING STRUCTURAL EXCITATION.

very stiff, would represent the load cells, and the second spring, more flexible, representing the flexibility of the crane. When there are frequency components in the disturbances near the natural frequency of the system, determined primarily by the crane flexibility, the motion of the duct will be amplified and this will be reflected in an amplification of the load cell readings. Thus it would appear that in the following we can not interpret the high frequency fluctuations as actual fluctuations in the thrust, but rather as an amplification of the structural deflections due to forcing of the system near a structural resonance. This particular aspect of the data will be discussed in more detail later in the results of the aerodynamic tests.

B. Engine Ingestion and Inlet Protection Instrumentation

The same sensors were used in the Engine Ingestion and Inlet Protection studies as in the aerodynamic tests. There were however, static and dynamic pressures taken at the simulated engine inlets with banks of manometers.

The data except for the manometer readings were recorded on oscillographs.

V TEST PROCEDURES

A. Engine Ingestion Test Procedure

The inlet ingestion engine was started. The duct engines were then started in the horizontal position as required by their design. The inlet ingestion engine was brought to the desired airflow conditions. The ducts were rotated to the vertical position, the oscillograph was turned on and the duct engines brought to their required power settings. The test was run for a fraction of a minute and then the duct engines were throttled back, and the ducts rotated back to the horizontal position. The inlet engine was run at full throttle for a short time to blow the terrain particles out of the manifold pipes connecting the inlets with the particle collector. The oscillograph was then shut off followed by engine shut down.

B. Inlet Protection Test Procedure

The inlet protection procedure was essentially the same as during the engine ingestion tests.

C. Aerodynamic Test Procedure

After the turboprop engine was started and turned for the duct axis to become vertical, the turboprop engine speed was brought up to 50% of full speed.

The speed was held constant and the punch was allowed to punch the data for approximately 15 seconds which completed the 50% run.

Similarly, the speed was brought to 60% - 70% - 80% - 90% and 100% of full turboprop engine power. When Hamilton Standard was looking for specific propeller stress patterns, other speeds were run to suit their requirements.

Later tests were run with a procedure of locking the digital recording system on the aft and forward duct thrust channels prior to the above procedure. In this manner, extended thrust readings over several seconds of operation were recorded.

VI TEST RESULTS

A. Engine Ingestion and Inlet Protection Test Results

The results presented in this report are all quantitative. Prior downwash programs, References 1 and 2, have been mostly qualitative judgments of the severity of problems and summaries of experience. However, the problem is now sufficiently defined and adequate test equipment is now available to provide quantitative results. Some minor exceptions to this conclusion have been discussed previously.

1. Comparison with Prior Test Series

The most significant quantitative data available from Reference 2 is the rate of sand transportation to the sensitive areas of the airframe above the fuselage. This rate is a function of the average propeller disc loading. To reduce this rate of sand transportation for the variation in test time, the total amount of sand collected on the top of the half-fuselage was divided by the time of test. This procedure follows Reference 2 and the faired curve through the data obtained in this prior program is shown with the present data in Figure 30. It is apparent that while the data shows considerable scatter, the curve from Reference 2 is fairly representative. If curves are faired through the extremes of the data obtained in runs with no protective devices, sand collection rates of 1 to 4.5 pounds per minute can be expected at a disc loading of 30 psf.

The stone test data of Figure 30 are surprisingly consistent with all four test points in the region of 4 pounds per

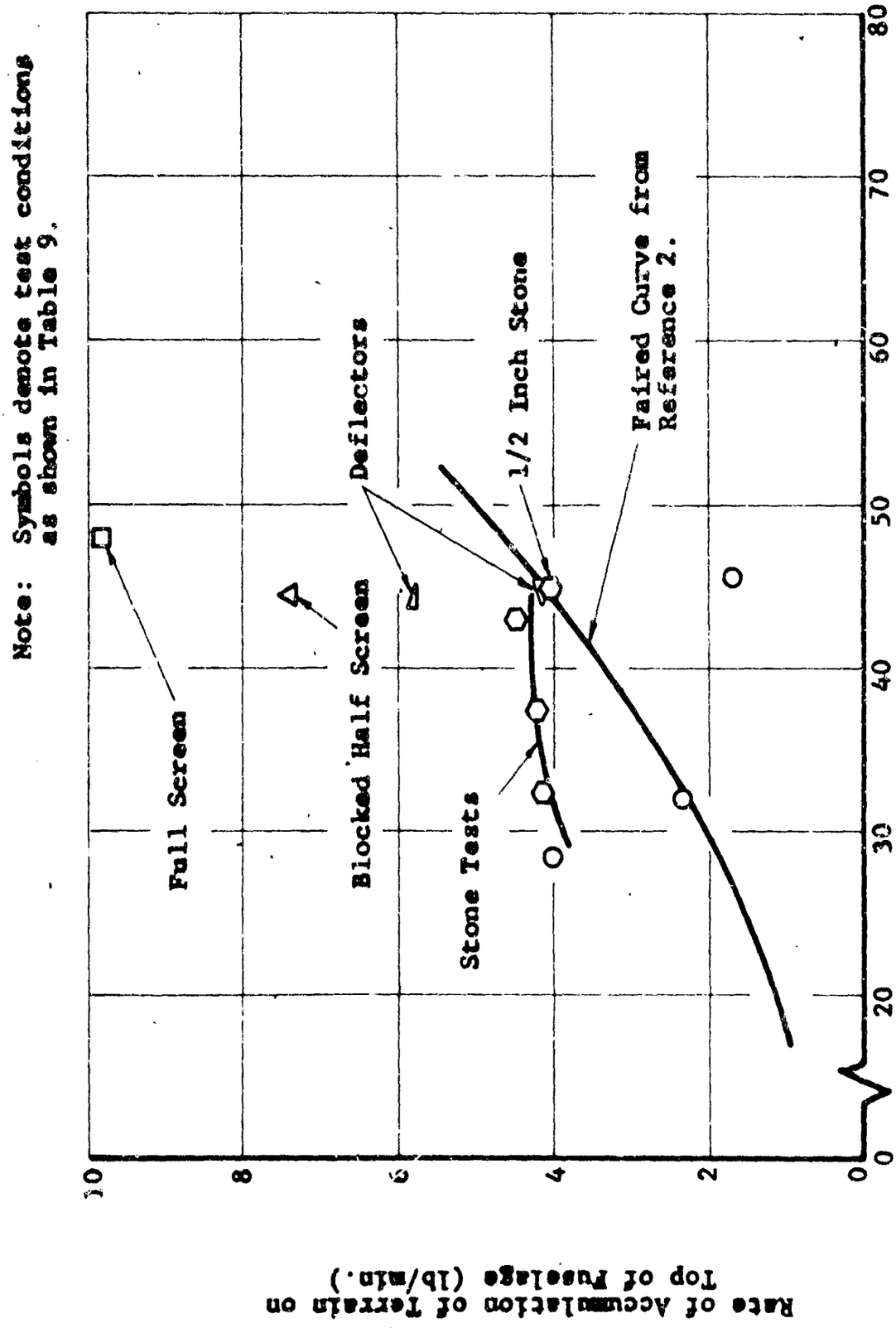

FIGURE 30: COLLECTION OF SAND AND CRUSHED STONE ON TOP SURFACE OF FUSELAGE.

minute. The point which was obtained over 1/2 inch stone is the highest disc loading point. These data show that there is no significant influence of particle size on the amount of terrain which was transported to this sensitive area for either the sand or the two sizes of crushed stone tested.

The influence of the inlet protection devices on the terrain ingested by the engine inlets is shown in Figure 32. These devices cause a significant blockage in the upflow region which apparently causes more particles to be transported to the region above the fuselage. This effect was also reported in Reference 2, where an increase in the flow up around the aft end of the fuselage was noted when the upflow region between the ducts was blocked.

In general, these data are in accord with prior results and indicate the sizeable amount of terrain which can be transported to the top surface of the fuselage and ingested. It can also be concluded from these data that engine or other inlets located in this region should be protected. Also, an increase in the terrain transported to these areas can be expected if the upflow is only partially restricted as with a screen.

2. Engine Inlet Ingestion Over Sand and Stone

The aft and forward propeller duct disc loadings and inlet airflows for each test are given in Table 4. The

Test No.	Disc Loading, psf			Air Mass Flow, lb./sec.		Air Mass Flow Avg. lb/sec.
	FWD	AFT	$\sqrt{D.L.}$ Avg.	Inboard	Outboard	
155	20	20	4.47	6.78	6.82	6.80
156	26	31	5.34	7.64	7.59	7.62
157	30	34	5.66	8.31	8.24	8.28
158	26	28	5.20	7.59	7.70	7.65
159	32	39	5.96	7.70	7.94	7.82
160	32	39	5.95	8.72	8.72	8.72
161	——	30	5.48	——	——	——
162	41	48	6.65	8.88	9.04	8.96
163	43	53	6.93	6.51	6.67	6.59
164	41	48	6.67	8.64	8.02	8.33
165	41	50	6.75	7.59	7.99	7.79
166	27	30	5.34	6.19	6.35	6.27
167	25	39	5.65	7.35	7.35	7.35
168	41	48	6.67	8.26	8.38	8.32
169	42	48	6.70	8.16	7.54	7.85
170	30	35	5.70	6.38	6.83	6.61
171	34	41	6.12	7.22	7.07	7.15
172	40	50	6.74	7.26	7.25	7.26
	39	47	6.56	7.18	7.55	7.36

TABLE 4. DUCTED PROPELLER DISC LOADINGS AND INGESTION AIR MASS FLOW DATA

airflow versus the square root of the disc loading are then shown plotted in Figure 31. Referring to Figure 31, it can be noted in general that there are two types of data. These types are data from tests with duct protection and data from tests without duct protection. As noted on pages 4 and 25, the duct protection devices caused reduced engine performance, and were therefore removed.

3. Engine Inlet Protection Devices Over Sand and Stone.

While the tested environment is probably the most severe which can be expected to be encountered with this type of aircraft, the basic data on ingestion point out the need for inlet protection. These data are listed in Table 5 and are plotted in nondimensional form in Figure 32. The plotted data are presented as the ratio of the weight of ingested sand to the weight of ingested air. To obtain this ratio the total sand ingestion data from Table 5 was averaged between the two inlets and divided by the test duration to obtain the average rate of sand ingestion. The sand to air weight ratio was then obtained by dividing the rate of sand ingestion by the rate of air ingestion obtained from Table 4. The sand ingestion data show a fairly consistent relation with the average propeller disc loading. It is reasonable to assume that ingestion rates larger than the 0.004 pounds of sand per pound of air measured at 45 psf can be expected at higher disc loadings.

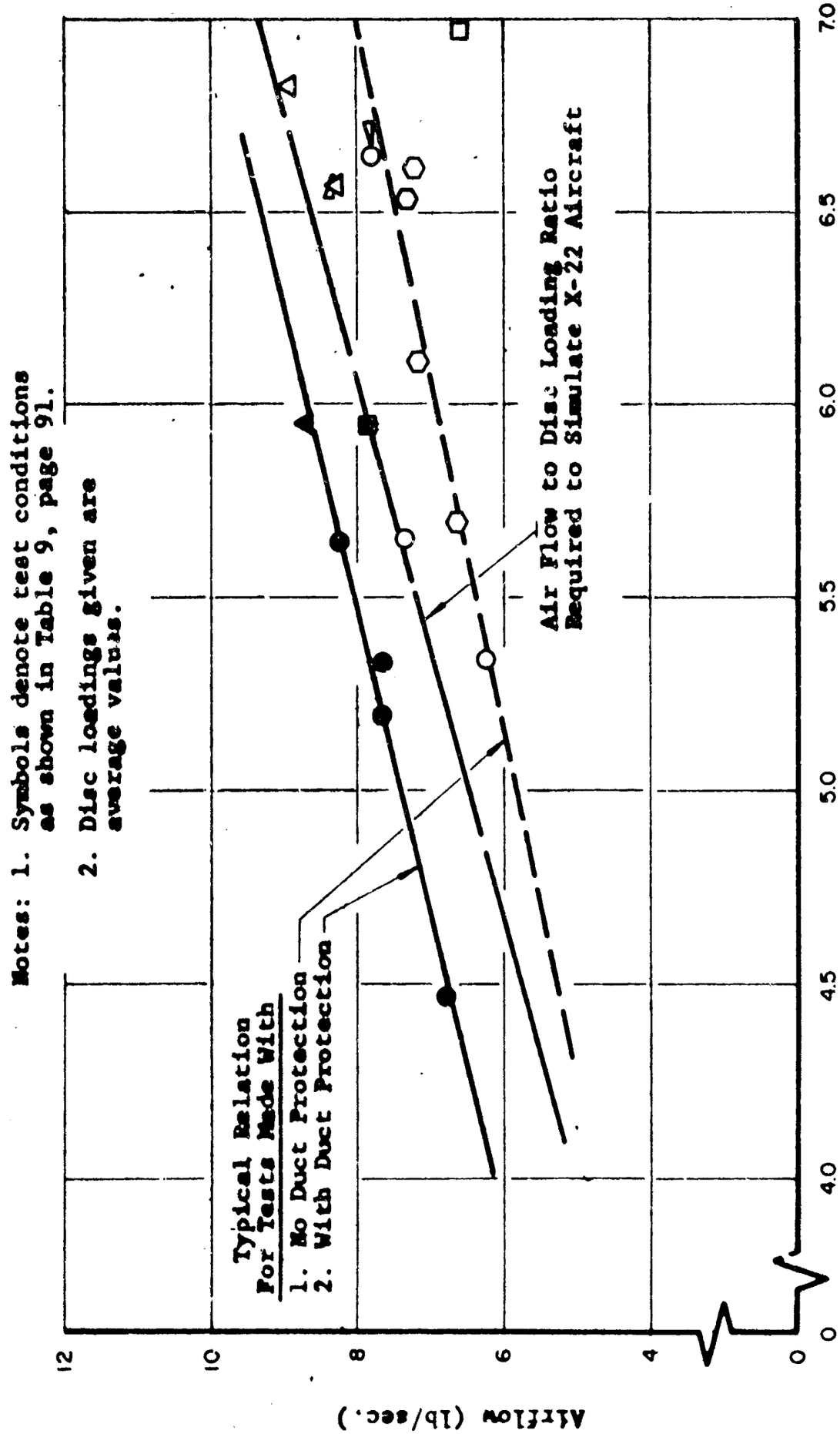

FIGURE 31: TEST SETTINGS OF INGESTION ENGINE AIRFLOW COMPARED WITH DESIRED AIRFLOW TO PROPELLER DISC LOADING RELATION

a). Tests Over Sand Terrain

Test No.	Disc Loading (Average) psf	Sand (Grams) Inboard Nacelle		Outboard Nacelle	
		*J-69 Eng.Side	Inlet Side	*J-69 Eng.Side	Inlet Side
155	20	8.1	138.4	12.1	147.0
156	28.5	9.3	166.3	15.1	178.0
157	32	12.8	196.0	20.3	207.2
158	27	8.0	185.1	29.3	207.0
159	35.5	53.6	1,663.3	78.1	1,321.0
160	35.5	16.4	186.5	30.0	255.0
161	30	———	———	———	———
162	48	25.0	278.0	44.0	350.0
163	48	40.0	1,340.0	55.0	978.0
164	44.5	15.0	265.0	19.0	148.0
165	45.5	26.5	887.0	22.0	288.0
166	28.5	20.0	267.0	17.0	225.0
167	32	24.0	180.0	22.0	235.0
168	44.5	25.0	137.0	40.0	125.0
169	45	21.0	193.0	26.0	161.1

b). Tests Over Sand Mixed With Crushed Stone

Test No.	Disc Loading (Average) psf	Sand and Stone (Grams) Inboard Nacelle		Outboard Nacelle	
		*J-69 Eng.Side	Inlet Side	*J-69 Eng.Side	Inlet Side
170	32.5	11.0	112.4	22.0	60.3
171	37.5	8.3	55.5	5.5	63.4
172	45	3.8	153.8	6.0	120.1
173	43	5.0	137.2	5.0	88.0

*Smaller Size Particles Collect on the J-69 Engine Side of the Particle Separator Screen as Shown in Figure 5.

TABLE 5. WEIGHT OF SAND AND STONE COLLECTED IN SIMULATED ENGINE INLET PARTICLE SEPARATOR.

a). Tests Over Sand Terrain

Test No.	Test Duration Sec.	Terrain Ingested Lb/Sec.	Air Ingested Lb/Sec.	Ingestion Ratio Weight of Terrain Per Weight of Air
155	24	6.37	6.80	.0021
156	23	8.02	7.62	.0023
157	33	6.61	8.28	.0018
158	31	6.93	7.65	.0020
159	44	35.41	7.82	.0097
160	46	5.30	8.72	.0013
161	44	—	—	—
162	32	10.89	8.96	.0027
163	45	26.81	6.59	.0090
164	44	5.08	8.33	.0013
165	42	14.57	7.79	.0041
166	41	6.45	6.27	.0023
167	43	5.36	7.35	.0016
168	41	3.99	8.32	.0011
169	41	4.89	7.85	.0014

b). Tests Over Sand Mixed With Crushed Stone

Test No.	Test Duration Sec.	Terrain Ingested Lb/Sec.	Air Ingested Lb/Sec	Ingestion Ratio Weight of Terrain Per Weight of Air
170	64	1.53	6.61	.0005
171	42	1.58	7.15	.0005
172	31	4.58	7.26	.0014
173	33	3.56	7.37	.0011

TABLE 5. WEIGHT OF SAND AND STONE COLLEDTED IN SIMULATED ENGINE INLET PARTICLE SEPARATOR. (Continued)

Notes: 1. Symbols denote test conditions as shown in Table 9, page 91.
2. Data presented are average for inboard and outboard inlets.

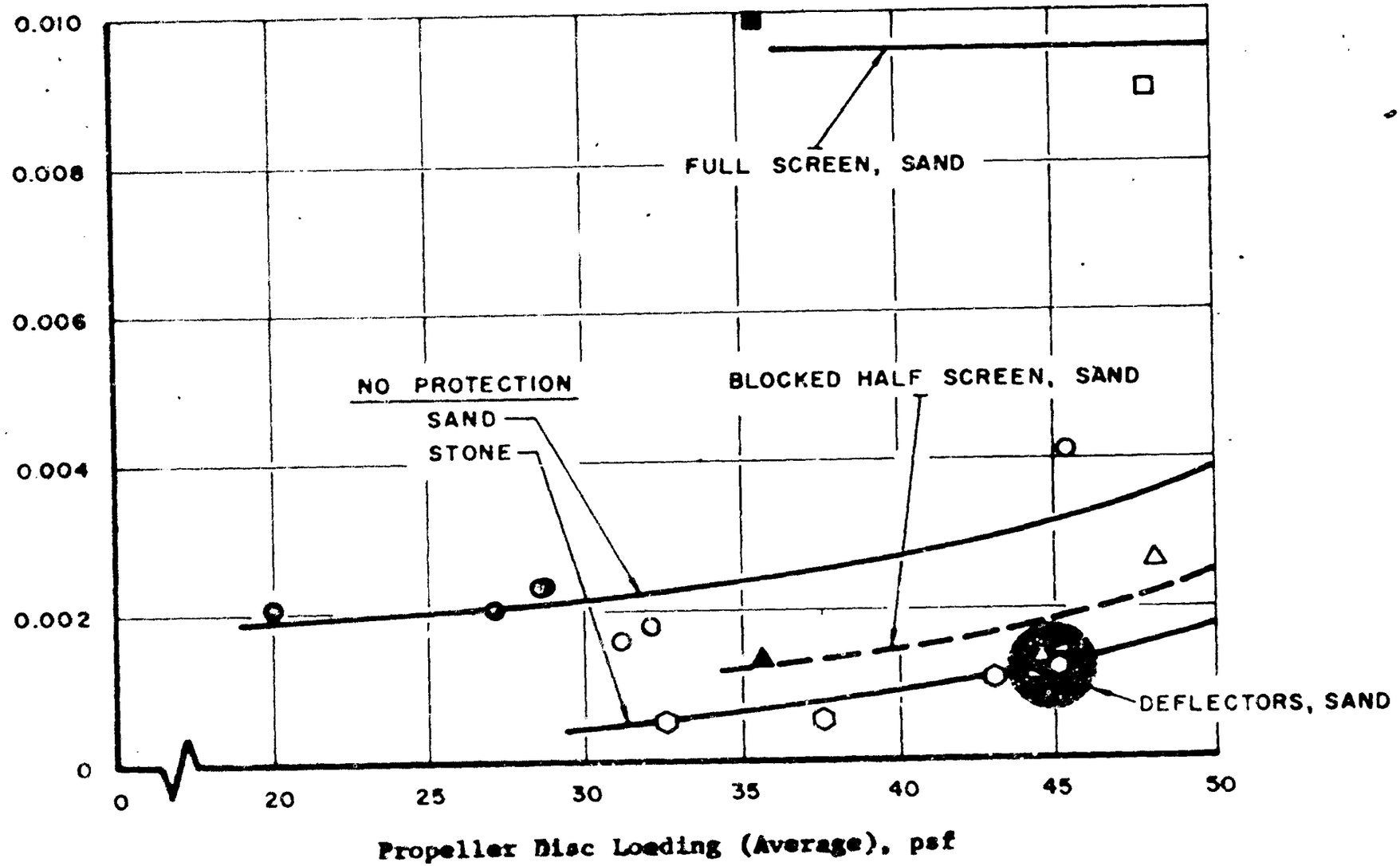

FIGURE 32: EFFECTIVENESS OF INLET PROTECTION DEVICES IN PREVENTING SAND AND STONE INGESTION

Similar stone ingestion data are also shown in Figure 32 and again much less scatter than with sand is shown. The rate of ingestion of stone is less than the sand ingestion rate, and, as will be discussed, the particles ingested are significantly larger when operating over stone covered terrain.

Typical sieve analysis data on the sand ingested by the simulated engine inlets are shown in Figure 33. The data presented are the average between the ingestion of the inboard and outboard i .ets. It should be noted that there is little scatter in these data. A comparison with a random sand sample shows that the ingested sand is significantly finer. However, this is coarse sand as judged by engine ingestion standards with about 95 percent of the particles being larger than 200 microns and about 10 percent being larger than 1000 microns.

It is of particular interest to compare these ingestion rates and particle sizes to an engine test to evaluate ingestion capability. In Reference 8, a T-53 engine was tested and was found to suffer a minimum loss of performance; however, the rate and size of ingestion were both an order of magnitude less than the data obtained in this program. It is doubtful that turbine engines can be developed to tolerate this severe ingestion

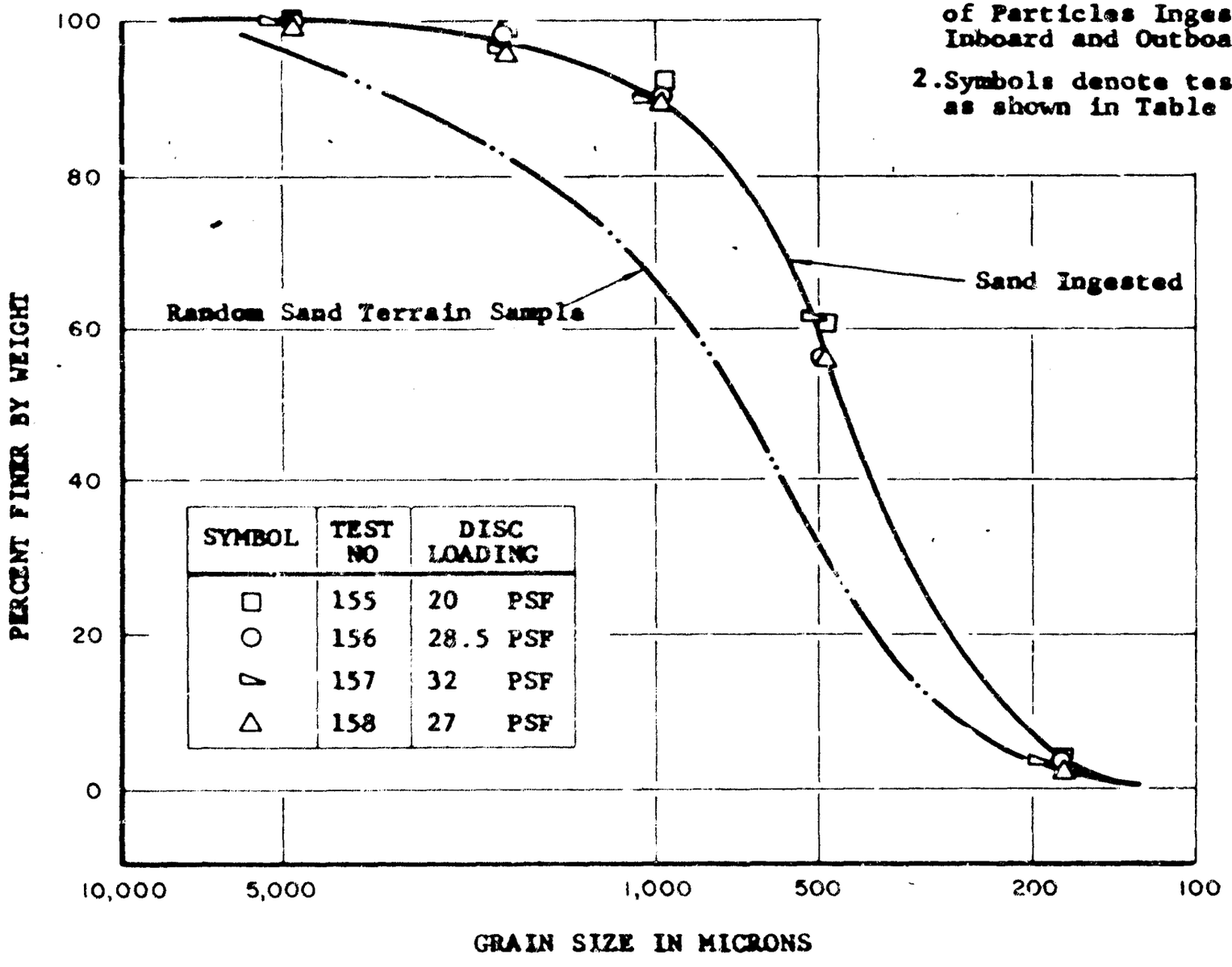

FIGURE 33. SIEVE ANALYSIS OF SAND INGESTED BY SIMULATED ENGINE INLETS WITHOUT INLET PROTECTION

and therefore inlet protection devices are required.

4. Effectiveness of Inlet Protection Devices

The data evaluating the inlet protection devices are shown together with the engine ingestion data without inlet protection in Figure 34. The three deflectors, the blocked half screen and the long and short chord deflectors, each provide about the same level of protection. A reduction of ingestion is shown by the data of Figure 34 for any of these devices at most disc loadings. It should be noted that the ingestion rate was not decreased sufficiently that engine damage would not occur.

The behavior of the full screen is quite different than any of the other devices tested and is shown separately in Figure 34. The amount of sand ingested with the screen is approximately an order of magnitude higher than with any other protection device. At first this paradox seems improbable, the inlets were fully screened but the amount of sand ingested increased. However, two similar independent points were obtained on different test days under somewhat different test conditions lending credulence to these data. Also, it

Note: Symbols denote test conditions as shown in Table 9, page 91.

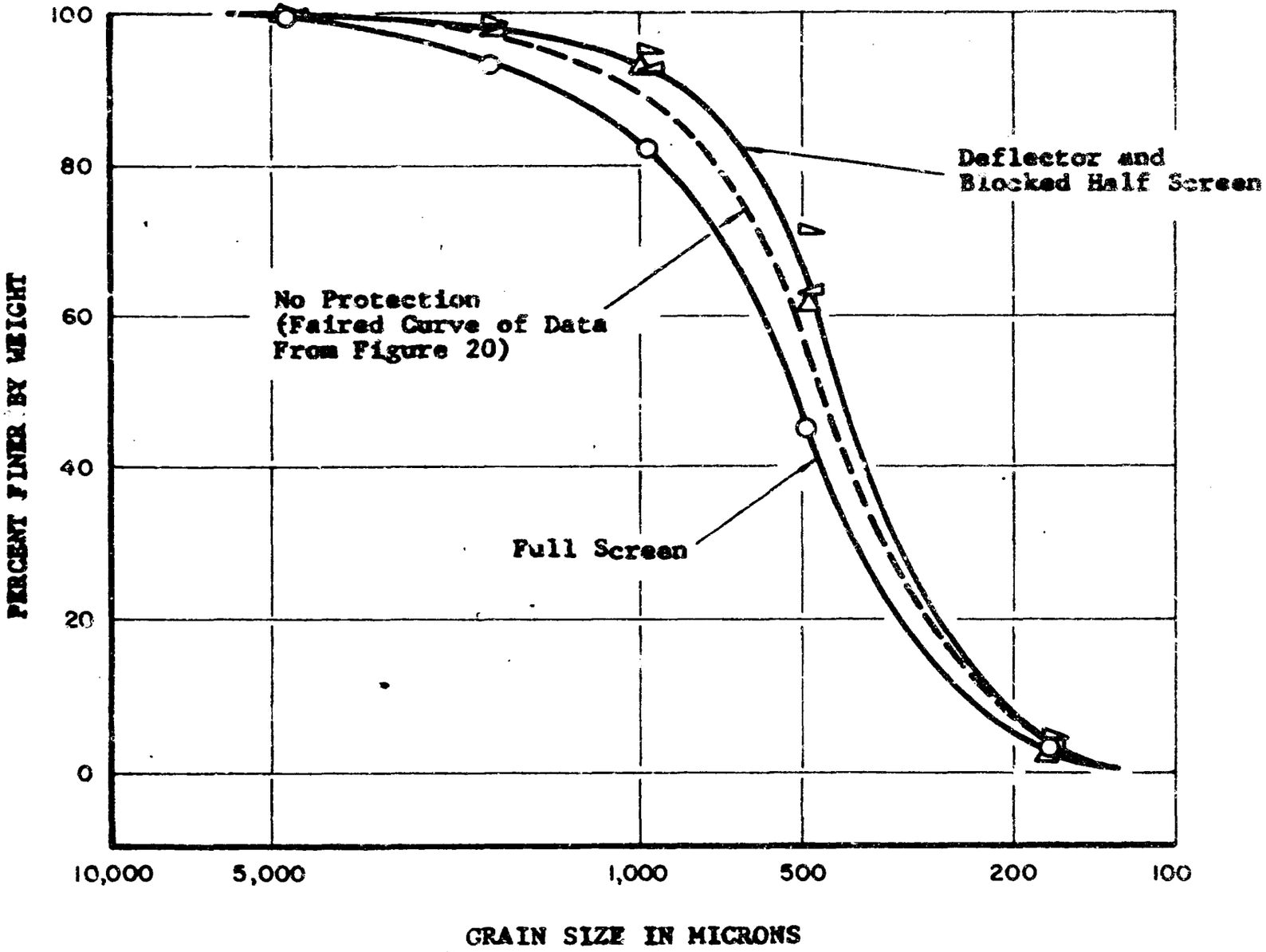

FIGURE 34. EFFECT OF INLET PROTECTION DEVICES ON SIEVE ANALYSIS OF INGESTED SAND

can be noted in the test films that the screens act as a porous blockage to the upflow. In this manner the screens stop the vertical passage of the particles and hold them long enough for the inlet flow to ingest the particles into the inlet. The screens do not deflect the airflow but they do stop and trap the particles. From this it is concluded that screens should not be used where they can block the flow as on the X-22 configuration. In fact, the use of screens in conjunction with a well protected suction device should be considered to stop particles and clear an area.

The influence of the inlet protection devices on the size of particles ingested is shown in Figure 34. It may be noted that the deflectors cause a small but fairly consistent shift toward finer particles. The full screen data show a significant shift toward more coarse particles. In general, it is shown that the effect of these devices on the size of the ingested particles is small.

5. Effect of Terrain Particle Size on Engine Ingestion

The relationship between the accumulation of large particles to total accumulation is of importance in that damage to engines and other high speed rotating components increases

greatly with ingested particle size. Most turbine engines can ingest large quantities of fine particles without suffering undue power loss; however, ingestion of a single stone, bolt, or other similar foreign object can cause catastrophic failure of the engine. For this reason, the data on the larger particles is emphasized.

It is of interest to analyze the present data in an effort to relate this testing to the general problem of ingestion. The sieve analysis data indicates that only a very small amount of the larger particles were ingested; however there was only a small proportion of these particles available. To consider the effect of particle size the largest standard available sieve of 4625 micron (0.185 inch) opening was used as a standard. Particles which would not go through this sieve were defined as large particles. A summary of data on large particle ingestion by the simulated engine inlets is plotted as Figure 35. These data are for the inboard or outboard inlet as noted, not an average as used previously. It is shown in this figure that there is very little large particle ingestion for the tests over sand. In most of the tests over sand there were no large particles collected and these data and the larger sand ingestion rate data are not reflected in Figure 35. It is admittedly realized that the large particle data presented in Figure 35 is based upon very few test points. Subsequent tests, however, of a similar nature have borne out the main aspects of the curves presented in Figure 35. However, even with ingestion rates as great as

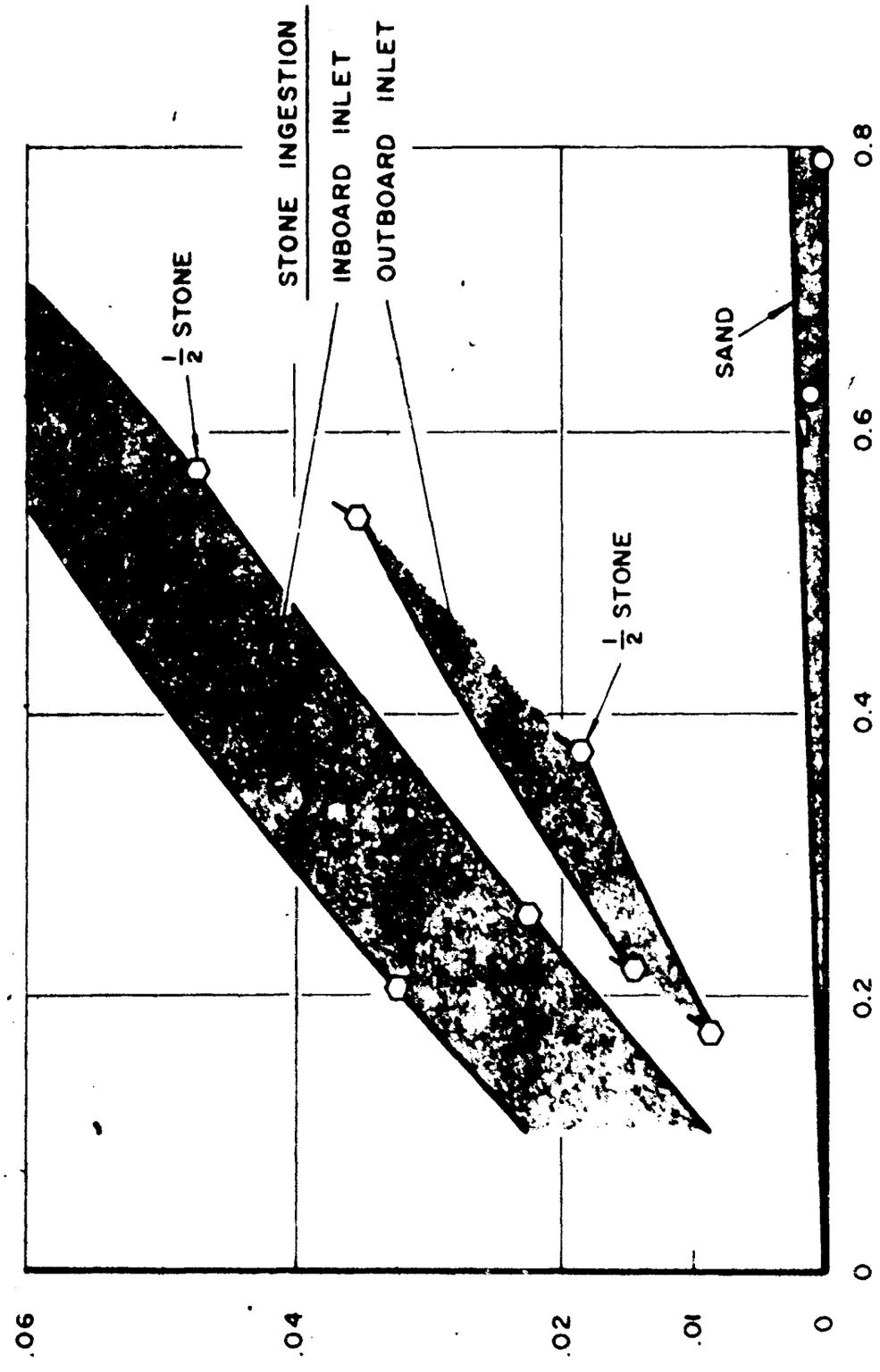

Rate of Ingestion of all Sizes of Terrain, lb/min.

Rate of Ingestion of Terrain Larger Than 4625 Microns, lb/min.

Notes: 1. Symbols for inboard inlet are as shown in Table 9. Same symbols are used for outboard inlet except flag mark is used.

2. Stone size is noted for 1/2 inch stone test. All other points are for 3/8 inch stone.

FIGURE 35: INGESTION OF LARGE SIZE PARTICLES OF SAND AND STONE BY SIMULATED ENGINE INLETS

0.8 pounds per minute, the greatest rate of ingestion of large particles was less than 0.01 pounds per minute with sand terrain.

Referring to Figure 35 it is realized that when operating over crushed stone covered terrain at least 5 percent of the terrain ingested is large particles. The inboard inlet is shown to have ingested more particles than the outboard which is typical and also the inboard inlet ingested significantly larger particles. This effect is probably due to the proximity of the fuselage.

It is significant to note in Figure 35 that there is slightly less ingestion of large particles when the terrain was changed from the 3/8 inch grade stone to the 1/2 inch grade. While it can be argued that this small reduction in ingestion is less than the scatter of the data, this effect is believed to be of sufficient significance to form the following hypothesis. Summarizing, the data for this hypothesis are that there was an order of magnitude change which resulted when the terrain was changed from the 700 microns sand to the 9000 microns (about 3/8 inch) stone but only a small decrease occurred when the terrain was changed to 12,500 micron (about 1/2 inch) particles. It is doubtful that the maximum rate of large particle ingestion occurs between 9,000 and 12,000 microns and also it is unlikely that a sharp peak occurs at particle sizes less than 9000 microns. Thus, it is believed the following sketched relation holds:

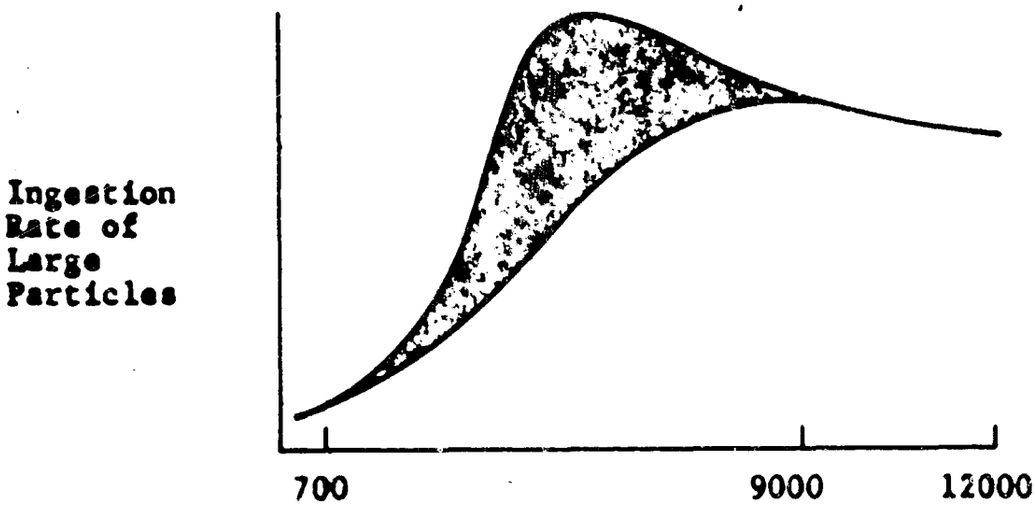

It is thus concluded that there may be a terrain particle size smaller than that tested (3/8 stone) which gives significantly more ingestion of large particles. However, since damage increases with particle size, the damage which was experienced with the crushed stone tested is probably nearly the worst damage which can occur.

6. Large Size Particles Collected on Airframe

A plot of the data on accumulation of large particles of terrain (greater than 4625 microns) on the fuselage is presented in Figure 36. This plot relating large particles to total quantity qualifies the data on total accumulation shown in Figure 30. The accumulation of large particles is of particular interest in the stone runs where they constitute approximately 10 percent by weight in a total accumulation of 3 pounds per minute. For the sand runs of the same total accumulation of 3 pounds per minute the corresponding fraction of large particles is about one-half of one percent. This relation remains approximately linear up to six pounds per minute accumulation with sand.

7. Ducted Propeller Ingestion

The sand and stone ingestion data for the forward and aft propellers are plotted in Figures 37 and 38 respectively. These data were obtained from the terrain collected in the particle traps located inside the propeller ducts, seen in Figure 6. The scale used for convenience in these figures 37 and 38 is pounds per million cubic feet of air. In examining these curves we note the considerable scatter of data which is to be expected when dealing with such complex phenomena as a high velocity flow of air-sand mixture. The scatter of data is appreciably less for the stone ingestion than the sand. The stone particles,

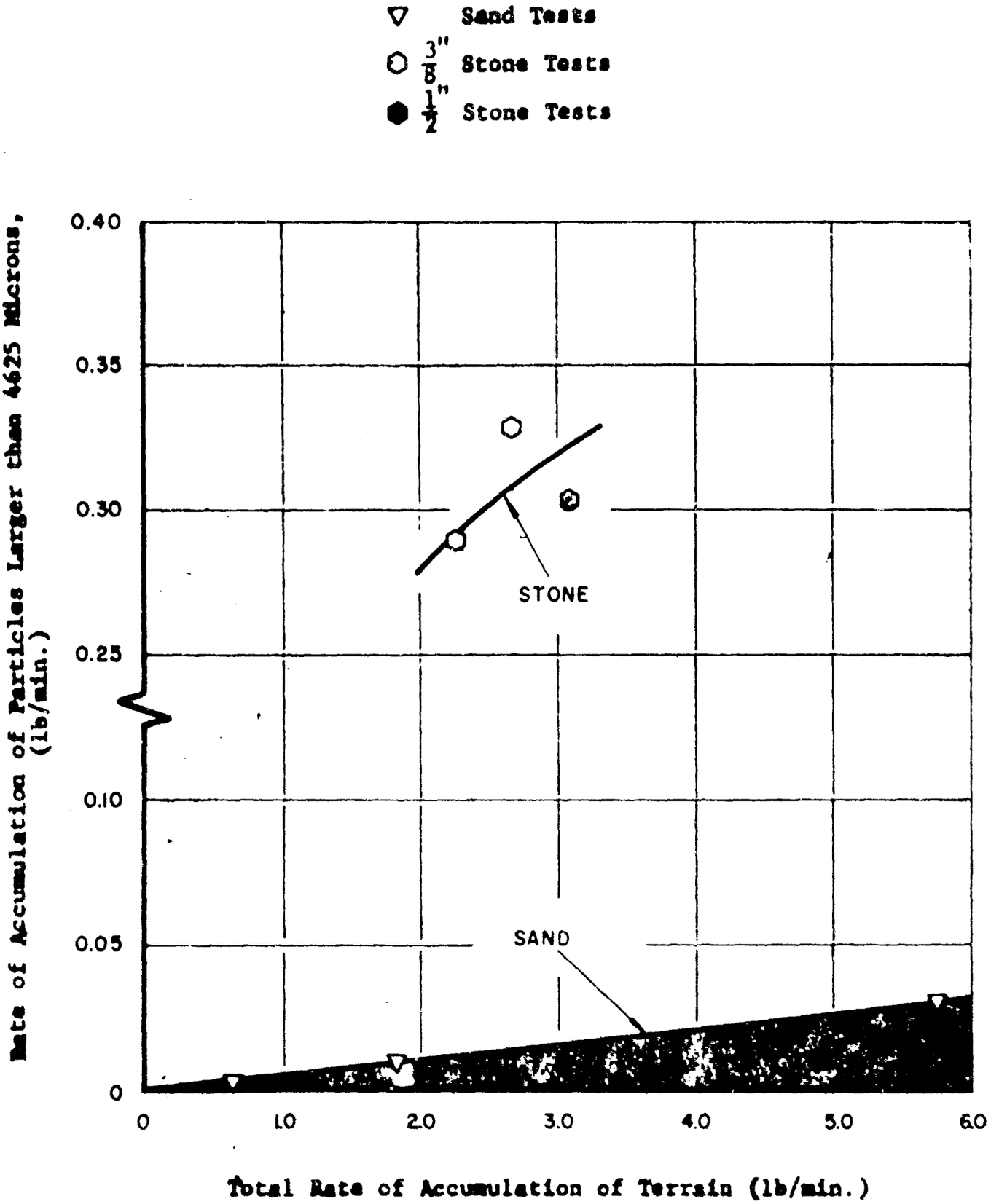

FIGURE 36: COMPARISON OF ACCUMULATION OF LARGE PARTICLES TO TOTAL ACCUMULATION OF SAND AND CRUSHED STONE ON TOP OF FUSELAGE.

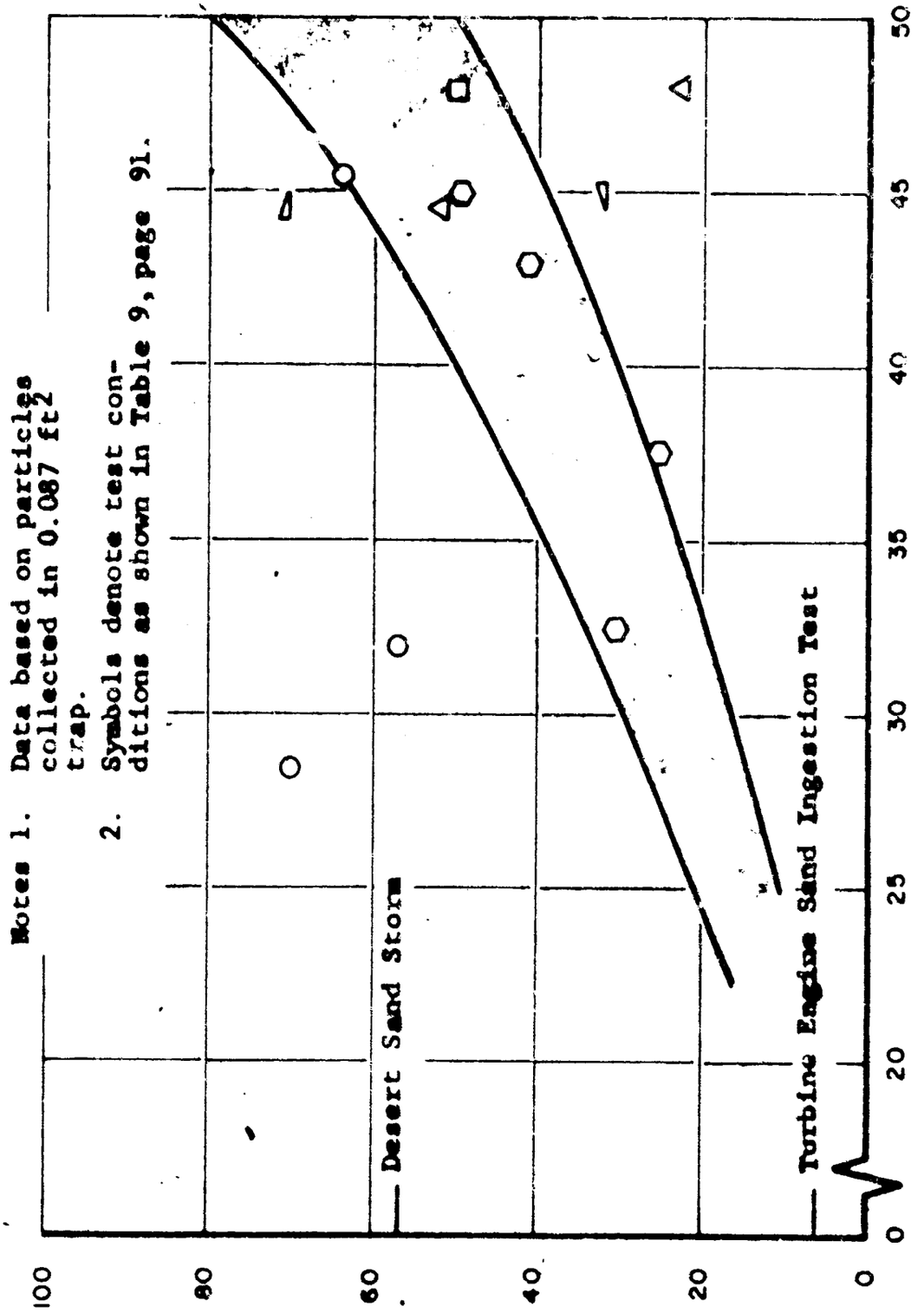

FIGURE 37: SAND AND STONE INGESTION OF FORWARD DUCTED PROPELLER

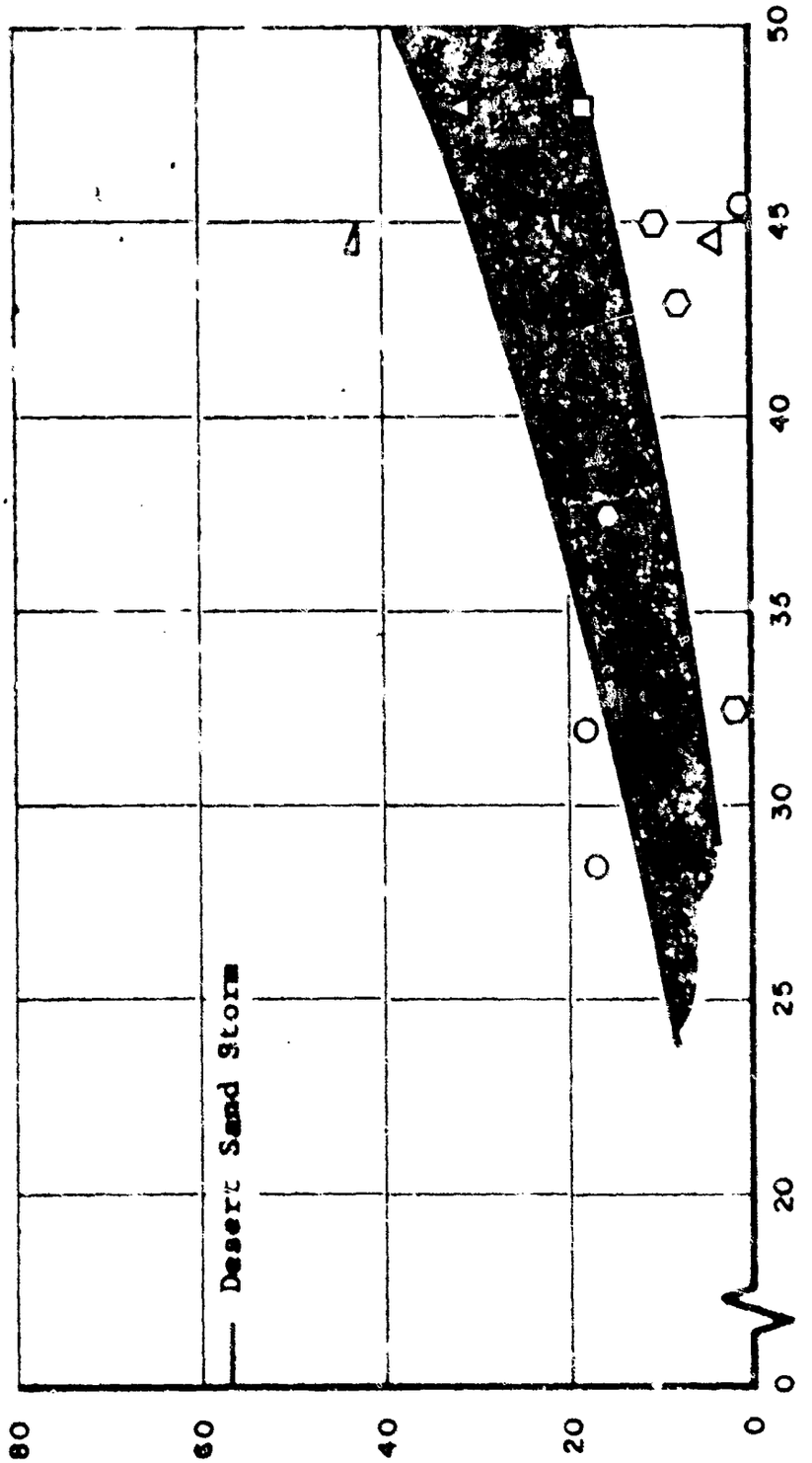

Notes 1. Data based on particles collected in 0.087 ft.^{2} trap
2. Symbols denote test conditions as shown in Table 9, page 91.

FIGURE 38: SAND AND STONE INGESTION OF AFT DUCTED PROPELLER

because of their greater relative inertia do not respond to the aerodynamic forces to the same extent as the sand particles and therefore the concentration of the stone and the scatter of the data is appreciably less than that of the sand.

A comparison of the forward and aft duct ingestion shows that the concentration is considerably higher (approximately two to one) in the forward duct. This apparently results since the flow field was not symmetrical and the lateral streamline illustrated in Figure 39 shows a curvature towards the forward propeller. The sand concentration, taking into account the scatter of data, is of the same order of magnitude as that reported for a desert sand storm in Reference 9. A qualitative and a very striking corroboration of this result was obtained in the motion pictures of this testing.

It is also of interest to realize the extent of the damage to the propeller and duct as shown in Figures 40 and 41 respectively, which were results the same as experienced in previous downwash programs.

8. Other Data

There are three other tables of data which have been used as guides for the analysis performed on data discussed so far. These data are presented in Tables 6, 7, and 8 which include the distribution of ingested airflow, the temperature of the ingested air and the propeller duct static pressures, respectively.

Table 9 gives the symbols used on many data plots as noted on the fields of the graphs.

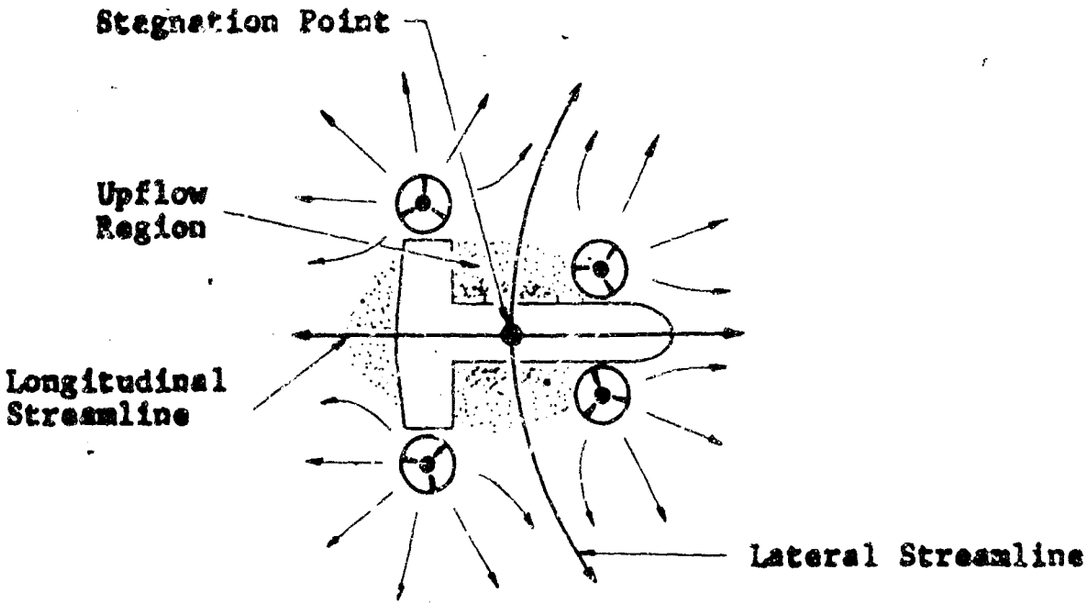

a) Features of Downwash Flow

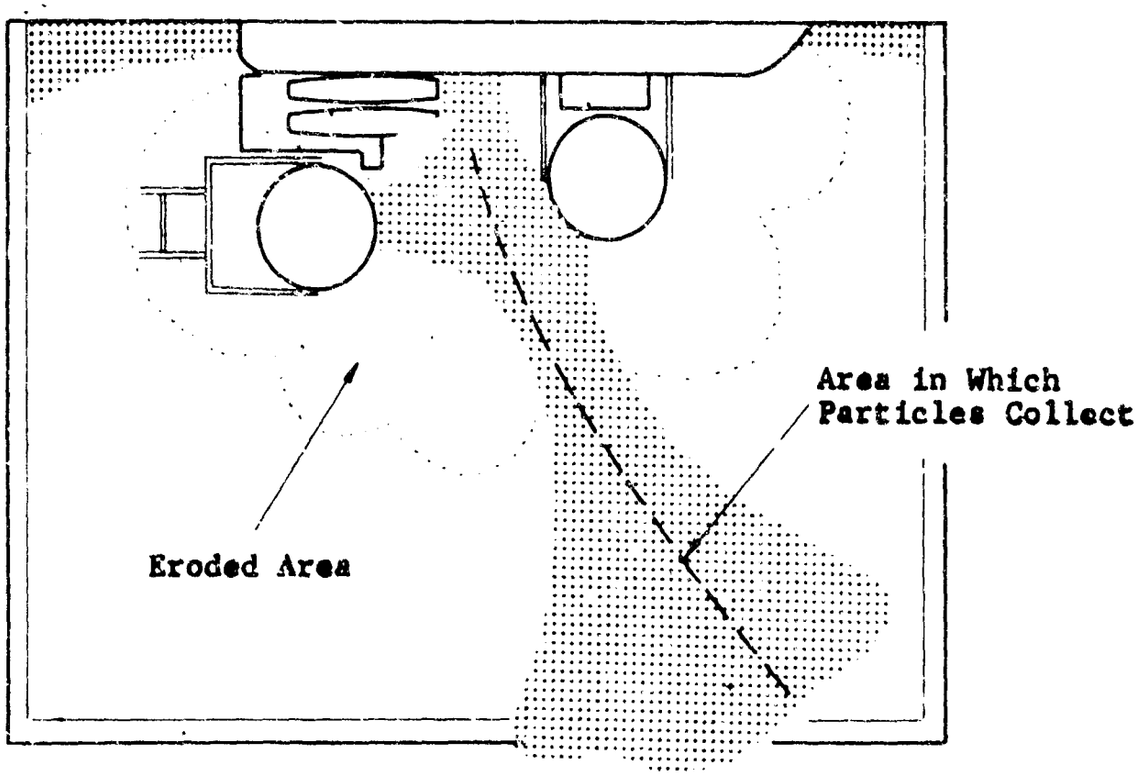

b) Ground Surface Signature

FIGURE 39: AERODYNAMIC DOWNWASH CHARACTERISTICS OF DUAL TANDEM CONFIGURATION.

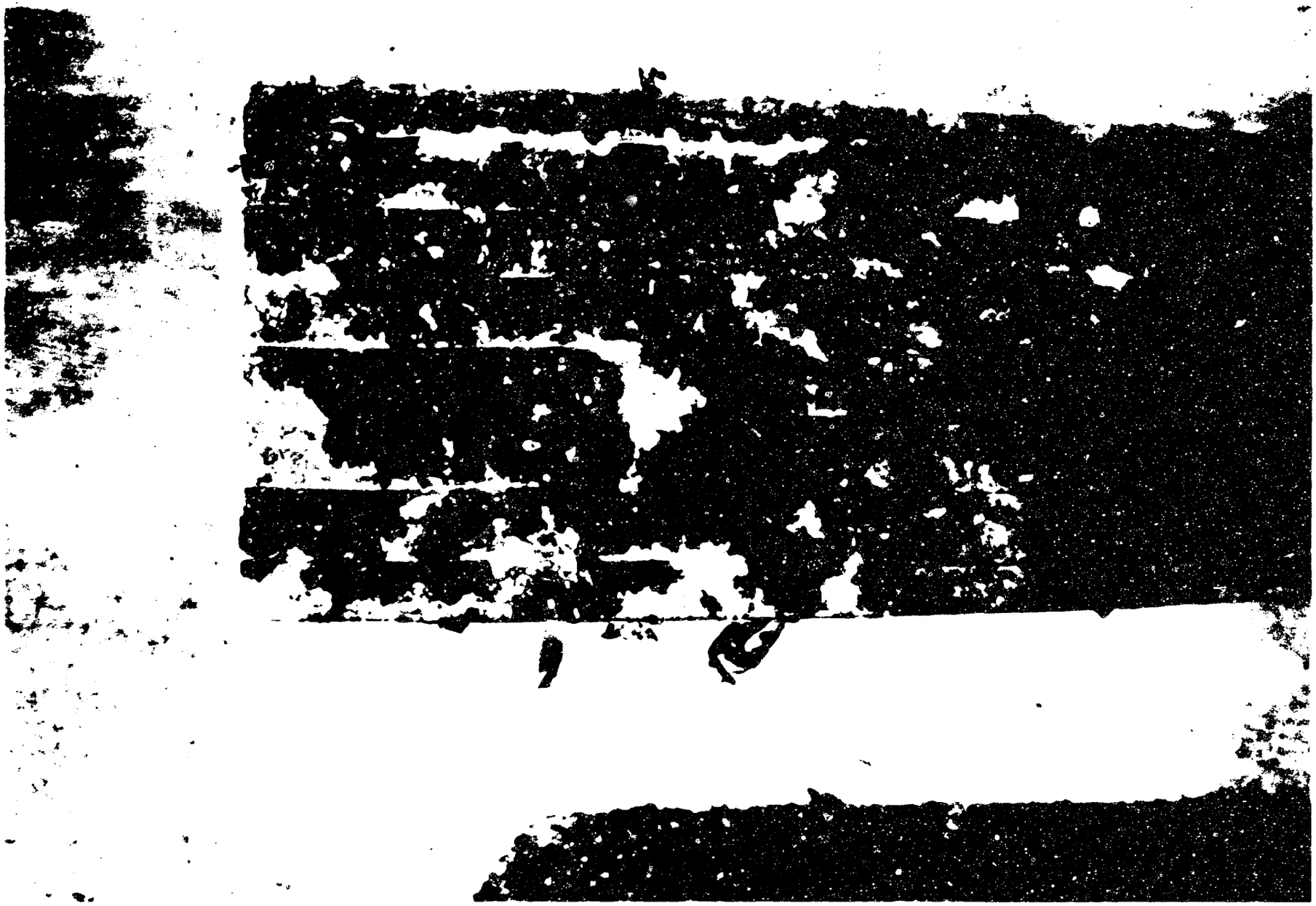

FIGURE 40: DAMAGE TO NEOPRENE SHEET COVERED PROPELLER BLADE AFTER THREE MINUTES OF OPERATION OVER CRUSHED STONE COVERED TERRAIN

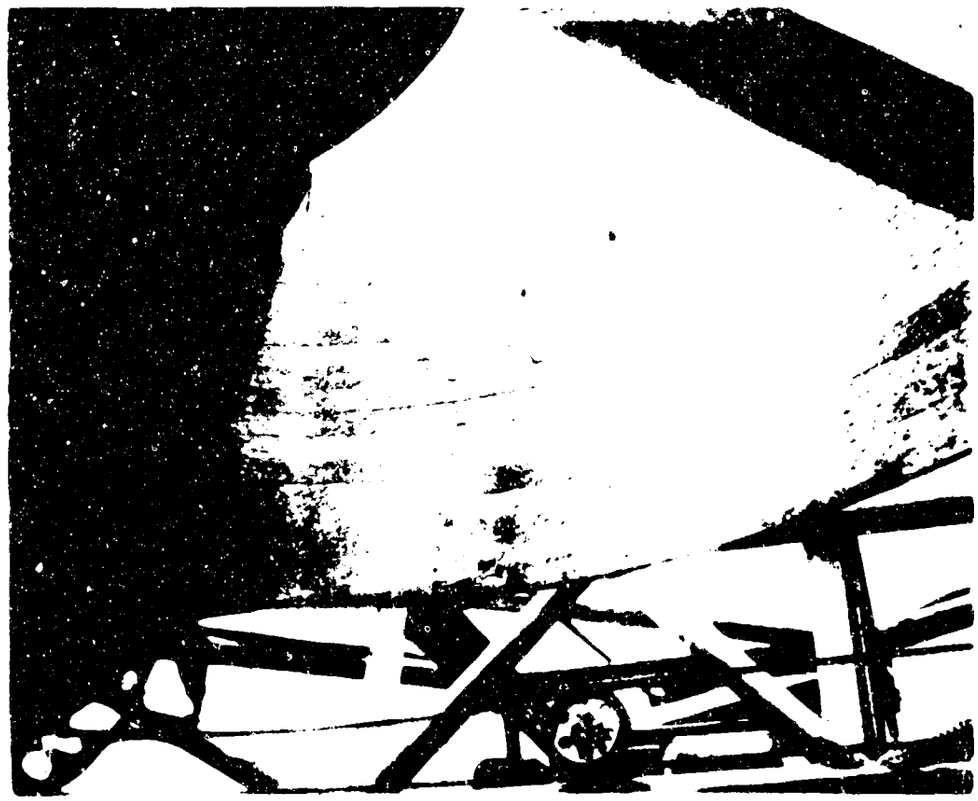

a) View from below shows that most damage occurs near propeller plane

b) Close-up shows erosion of wooden surface

FIGURE 41: CUMULATIVE DAMAGE TO PROPELLER DUCT FROM SAND AND STONE TESTS

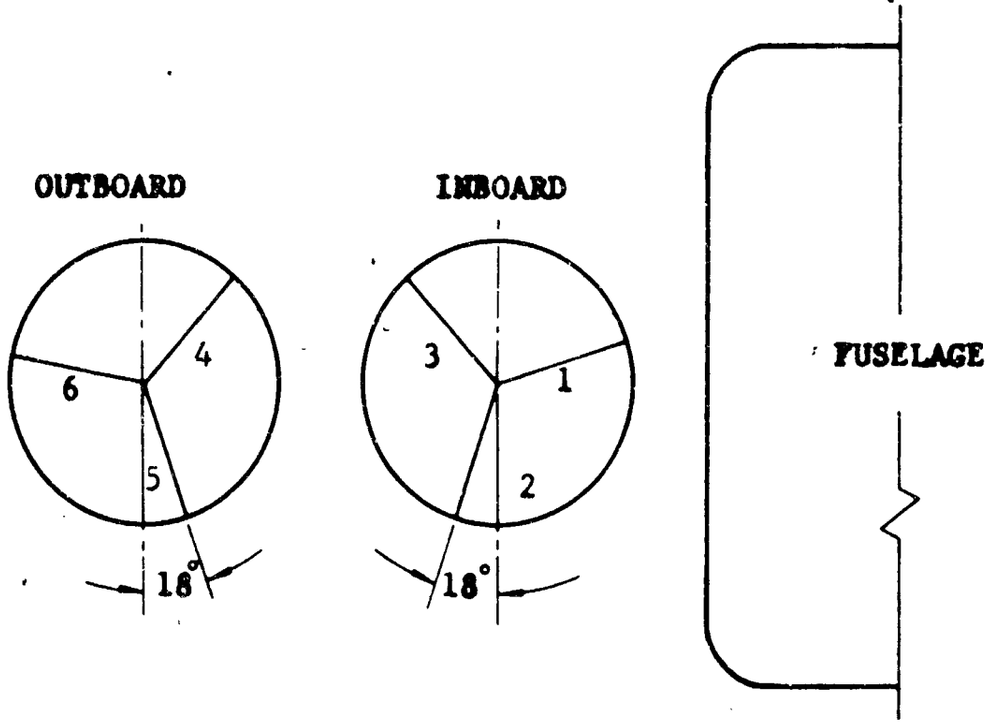

Specific Gravity of Fluid = 0.845

Test No.	INBOARD (Inches)				OUTBOARD (Inches)			
	Average Manometer Height	*Variation			Average Manometer Height	*Variation		
		1	2	3		4	5	6
155	7.89	-1.41	0.89	0.52	8.04	0.22	-0.61	0.41
156	10.04	-1.21	0.92	0.29	10.26	0.23	-0.77	0.54
157	11.97	-2.02	1.14	0.60	11.54	0.16	-0.69	0.48
158	9.98	-1.16	0.92	0.23	10.25	0.25	-0.75	0.50
159	10.27	-2.23	1.77	0.46	11.00	0.50	0.25	-0.75
160	13.17	-2.04	0.95	-0.70	13.13	0.23	-0.99	-1.59
161	13.13	-1.74	1.13	-1.35	13.44	0.79	-1.14	-1.00

*Azimuthal variation of difference between average static pressure and local static pressure for stations shown in above illustration. (Negative sign indicates static (gage) pressure is less than the average).

TABLE 6: STATIC PRESSURE DISTRIBUTION IN SIMULATED ENGINE INLETS

Test No.	INLET DUCT TEMPERATURE (°F.)					
	INBOARD INLET			OUTBOARD INLET		
	Ambient	Gnd. Idle	Power	Ambient	Gnd. Idle	Power
159	62	70	61	62	70	61
160	61	69	75.5	61	61	75.5
161	65	71.5	78.5	65	71.5	77
162	73	74	81	67.5	74	79
163	66	67.5	81	66	67.5	81
164	70	--	74	67.5	--	74
165	66	61	74	66	61	74
172	83	90	101	83	89	101
173	79	79	96	79	79	96

TABLE 7: TEMPERATURE OF SIMULATED ENGINE INLET AIR

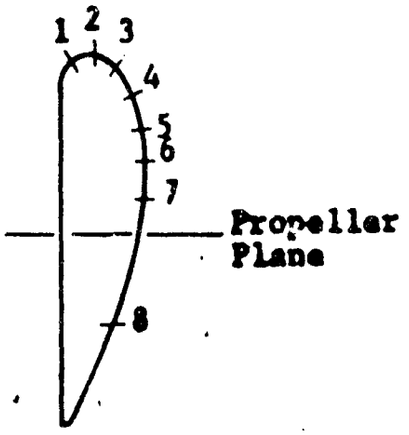

Location of Stations of Pressure Taps at Section A - A

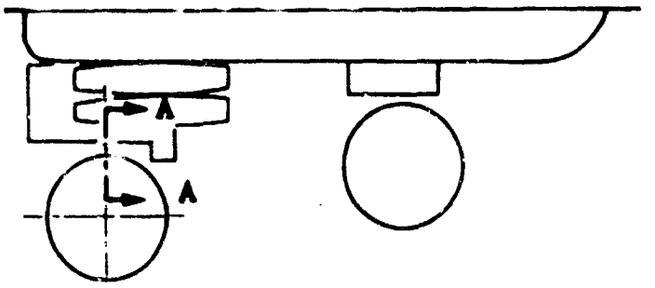

Location of Duct Azimuth of Readings

Station	Static Pressure, psf	
	With Protection (Teepees)	No Protection
	Test No. 161	Test No. 162
1	-48	--
2	-48	-71
3	-48	-61
4	--	-38
5	-46	-37
6	-46	--
7	--	-31
8	--	--
Aft Duct Disc Loading T/Ae, psf	30	54

TABLE 8. PROPELLER DUCT SURFACE STATIC PRESSURES

No Duct Protection	With Duct Protection (Teepees)
○ No Inlet Protection, Sand	● No Inlet Protection, Sand
△ Half Screen, Sand	▲ Half Screen, Sand
□ Full Screen, Sand	■ Full Screen, Sand
◅ Long Chord Deflector, Sand	◅ Long Chord Deflector, Sand
◅ Short Chord Deflector, Sand	◅ Short Chord Deflector, Sand
⬡ No Inlet Protection, Stone	⬢ No Inlet Protection, Stone

TABLE 9. SYMBOLS USED IN DATA PLOTS UNLESS DEFINED ON THE FIELD OF THE GRAPH.

B. Aerodynamic Test Results

1. Thrust and Torque Characteristics

First we consider the average performance characteristics and how they were influenced by the various parameters in the problem. Isolated duct tests were made at three propeller blade pitch angles, 19 degrees, 22.5 degrees and 26 degrees. At 26 degree blade angle, tests were made at one and one-and-a-half duct diameters above ground as indicated in Table 10, at 22.5 degree blade angle at one-and-one-half diameters, and 19 degree at one-and-one-half diameters with the propeller shaft axis horizontal and vertical. The tandem duct tests were conducted at the identical propeller blade pitch angles used for the isolated propeller tests. Tests were conducted in the tandem duct configuration at heights of one-and-one-and-one-half diameters, and three other tandem duct geometric arrangements were investigated at a height of one diameter as indicated in Table 10. The thrust characteristics and the performance of the ducts based on the average values of thrust coefficient and power coefficient are shown in Figures 42 and 43. In Figure 43 thrust coefficient vs. blade angle is shown, and thrust coefficient vs. power coefficient is shown in Figure 42. No noticeable ground effect appears to be present in the 26 degree case or as a result of the difference in orientation of the 19 degree blade angle case. Appreciable effects of the presence of the ground are probably not present until the duct is considerably closer than one diameter. This is also shown to be the case by comparison of the tandem operation in runs 212 and 213 (blade angle 19 degrees, duct exit heights

TEST NO.	*PITCH ANGLE	DUCT ANGLE	h/d	y/d	Remarks
ISOLATED PROPELLER DUCT					
199	19°	Horizontal	1.5		
200	19°	Vertical	1.5		
201	22.5°	Vertical	1.5		
202	26°	Vertical	1.5		
203	26°	Vertical	1.5		
204	26°	Vertical	1.0		
TANDEM PROPELLER DUCTS					
211	26°	Vertical	1.5	2.375	Short thrust run and ducts staggered 46 inches
212	19°	Vertical	1.5	2.375	
213	19°	Vertical	1.0	2.375	
214	22.5°	Vertical	1.0	2.375	
215	26°	Vertical	1.0	2.375	
217	26°	Vertical	1.0	2.0	Long thrust runs and ducts staggered 46 inches
218	22.5°	Vertical	1.0	2.0	
219	19°	Vertical	1.0	2.0	
220	19°	Vertical	1.0	3.0	
221	22.5°	Vertical	1.0	3.0	
222	26°	Vertical	1.0	3.0	
223	26°	Vertical	1.0	3.0	Long thrust runs and ducts inline
224	22.5°	Vertical	1.0	3.0	
225	19°	Vertical	1.0	3.0	

*Note: Pitch angle measured at 7/8 Radius

TABLE 10. AERODYNAMIC INTERFERENCE TESTS

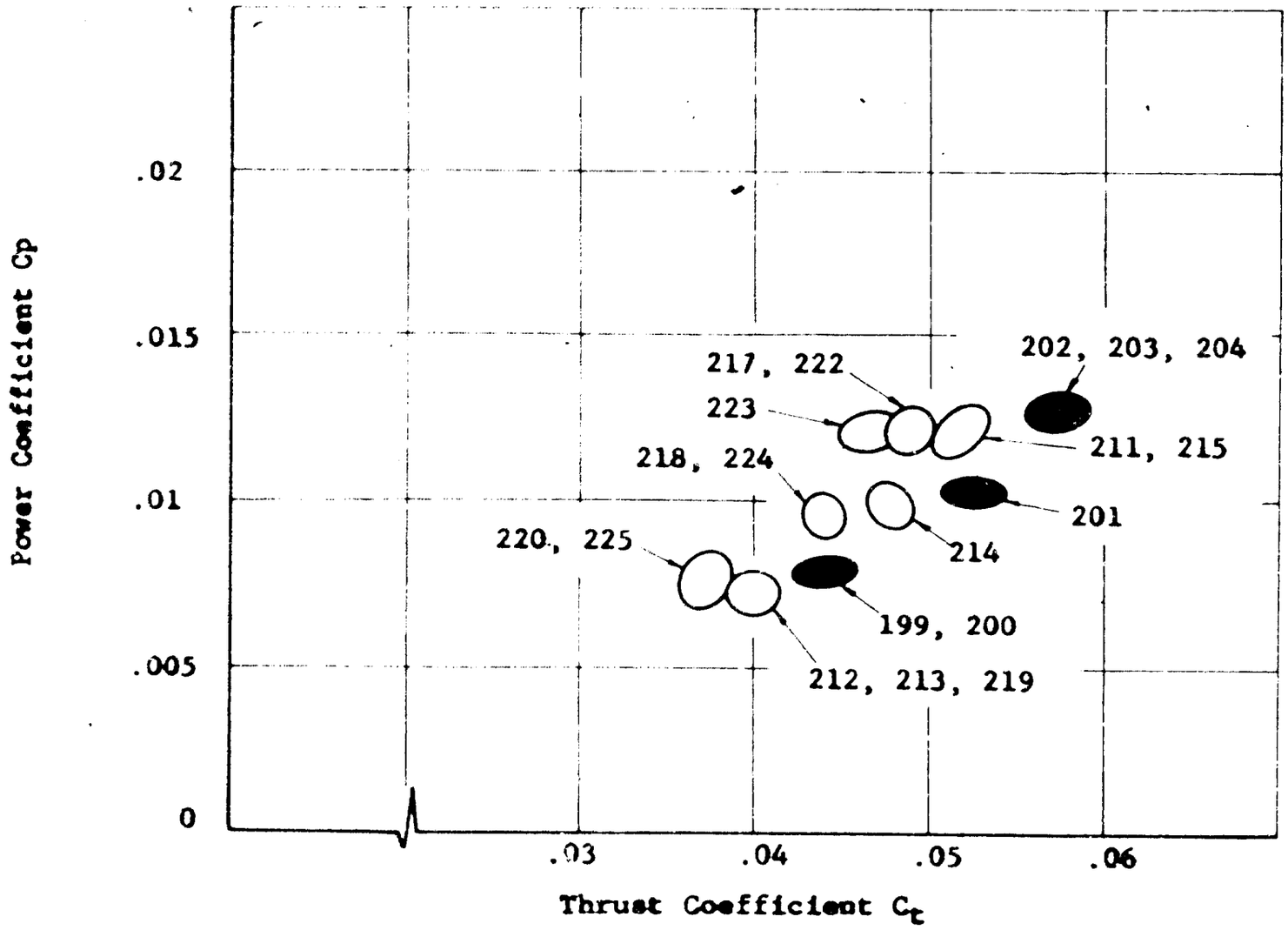

See Table 10, page 93, for test descriptions.

Note: Dark areas are the isolated duct tests.

FIGURE 42: PERFORMANCE CHARACTERISTICS

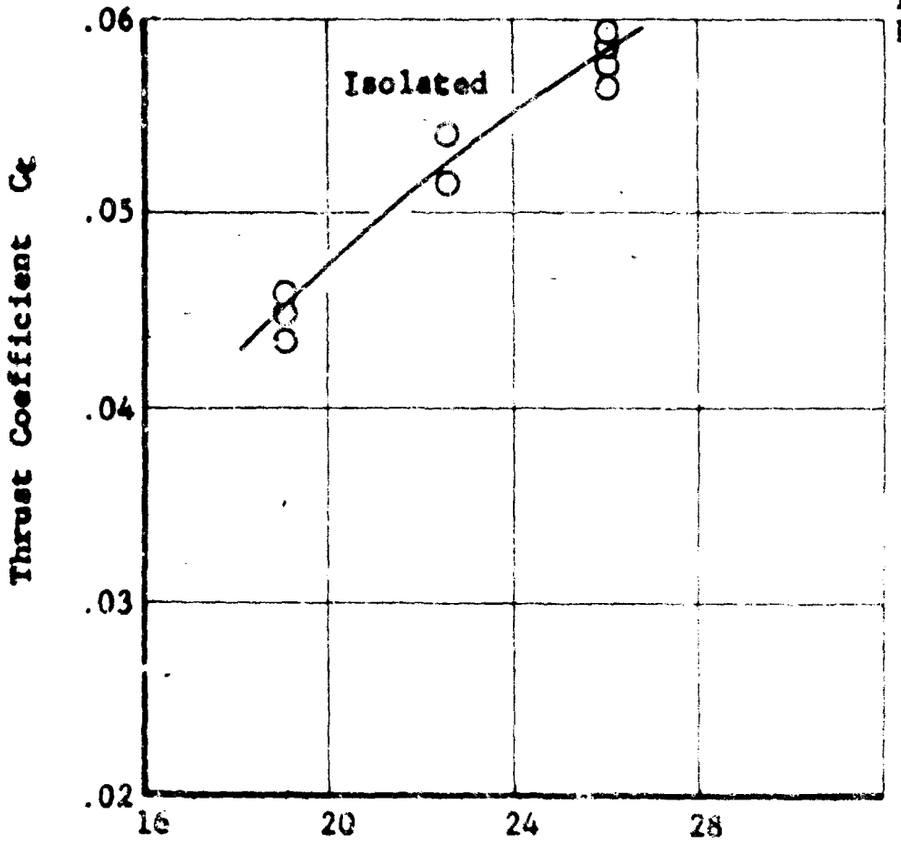

a) Isolated Duct Tests 201, 202, 203 & 204

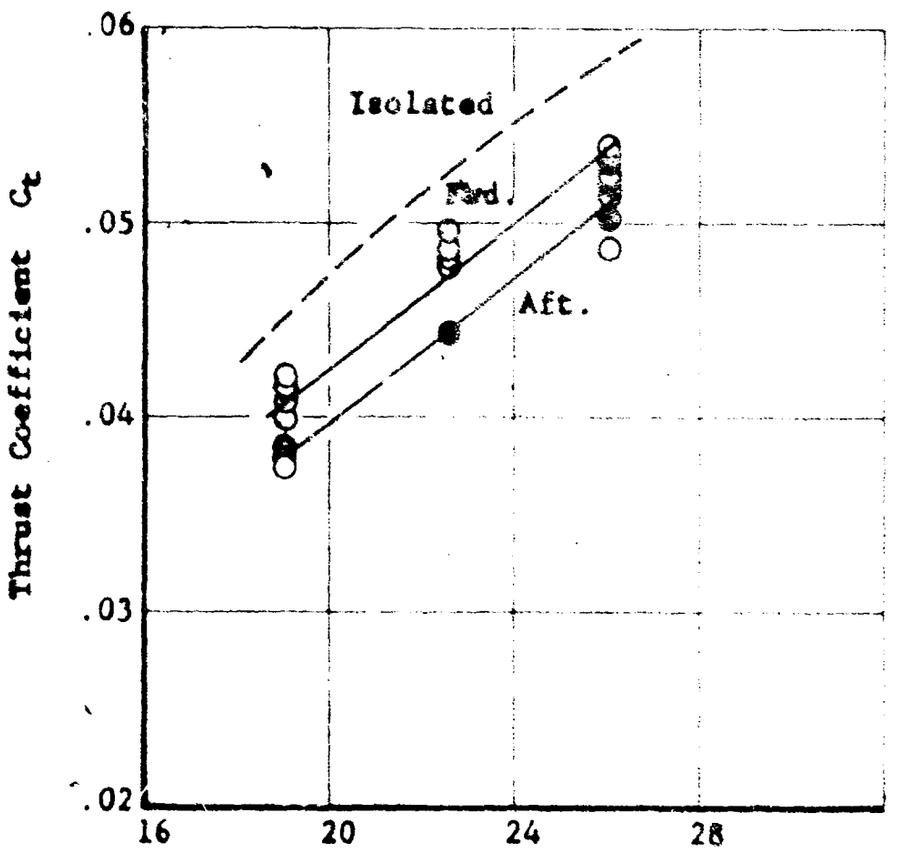

b) Tandem Duct Tests 211, 212, 213, 214 & 215
h/d = 1.5 and 1.0, y/d = 2.375. Ducts staggered 46 inches.

FIGURE 43: THRUST COEFFICIENT VERSUS PROPELLER BLADE ANGLE

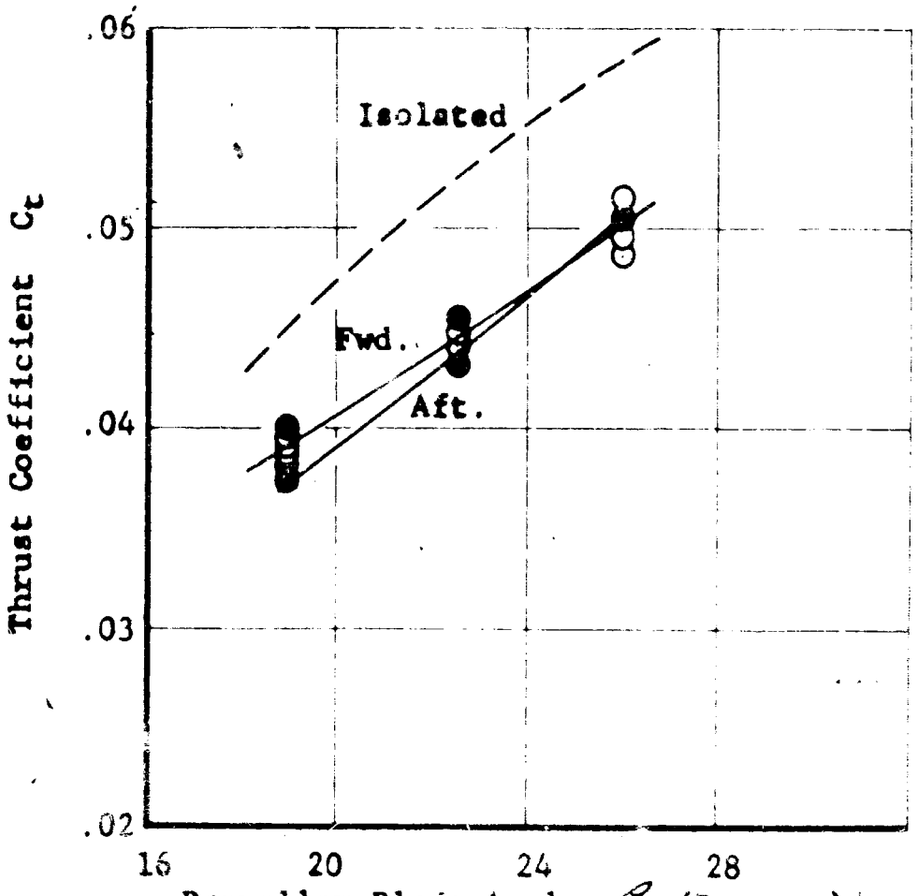

c) Tandem Duct Tests 217, 218 & 219 h/d = 1.0, y/d = 2.0
Ducts staggered 46 inches.

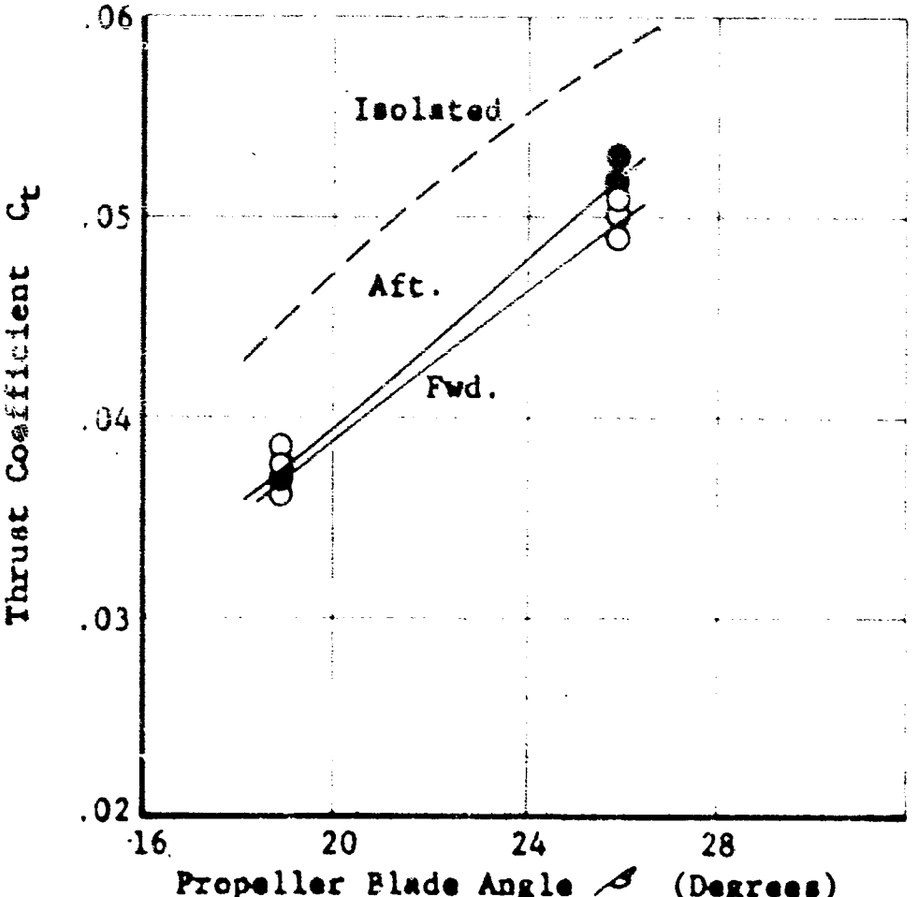

d) Tandem Duct Tests 220 & 222 h/d = 1.0, y/d = 3.0
Ducts staggered 46 inches.

FIGURE 43: THRUST COEFFICIENT VERSUS PROPELLER BLADE ANGLE

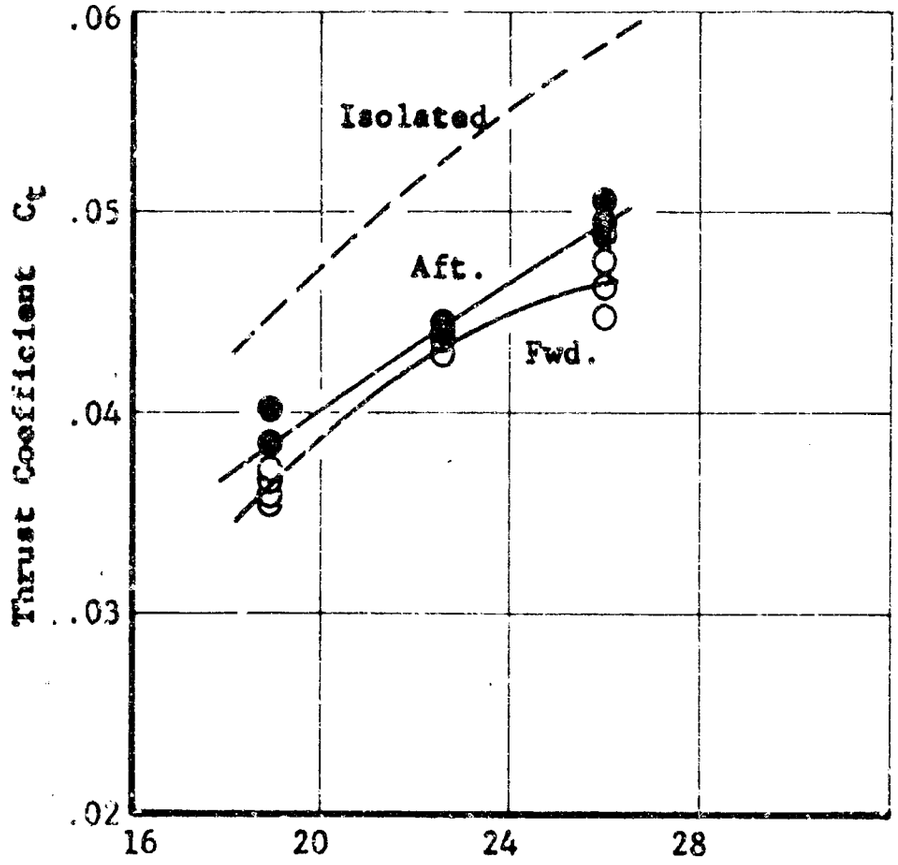

e) Tandem Duct Tests 223, 224 & 225 h/d = 1.0, y/d = 3.0
Ducts in line.

FIGURE 43: THRUST COEFFICIENT VERSUS PROPELLER BLADE ANGLE

1.5 and 1.0 respectively) with runs 211 and 215 (blade angle 26 degrees, duct exit heights 1.5 and 1.0 respectively) as shown in Figure 42. The isolated duct performance characteristics are shown for comparison purposes with all the tandem tests in Figure 42. The major effect is a considerable change in thrust coefficient at the same blade angle due to the presence of recirculation causing an average inflow velocity at the duct as discussed on pages 54 and 55. Figure 43 then presents the change in duct performance due to operation in a tandem configuration. The general effect to be noted here is the loss in thrust coefficient at the same blade angle in all the tandem cases as compared to the isolated duct performance without a corresponding reduction in power coefficient indicating that the figure of merit of the duct is reduced due to the presence of recirculation.

The effect of the longitudinal spacing of the ducts is probably as follows. The recirculation is proportional to the mass flow associated with the upflow between the ducts as shown in Figure 21. When the ducts are very close together (say one-half a diameter or less) this mass flow would be small, as it would be when the ducts are separated by a great distance.

Therefore, there is some spacing at which the recirculation effect is a maximum. From the data presented here, it appears that the maximum recirculation effect for this spacing is approximately three diameters.

It may be noted that the general performance level of the duct is low. It appears from the pressure measurements discussed later that the duct lip is producing considerably less than its theoretical maximum thrust. In addition, the condition of the surface of the propeller blades, due to previous downwash tests with resulting impingement, is not particularly good. This coupled with possible downloads developed by the engine located in the duct, and by pressure distributions on the engine housing, and the fact that the propeller used in these experiments was not designed for ducted propeller operation results in a static efficiency (figure of merit) of about 50 percent.

One additional piece of performance information is of interest and that is the fact that the aft duct generally exhibited a slightly higher thrust than the forward duct at the same propeller blade angle and RPM. The magnitude of this effect is shown in Figure 43. This would indicate that the aft duct, on the average, experiences less recirculation than the forward duct. This seems reasonable from the configuration

where the lateral streamline would be somewhat closer to the forward duct as shown in Figure 39. In addition the shape of the aft end of the fuselage may help to cause some of the wake to leave the area. While this appears somewhat in conflict with Reference 2, where more damage to the rear propeller as a result of recirculation of sand was reported, the general indications from the movies are that there is a greater flow recirculation into the forward duct than into the aft duct.

A typical exit velocity distribution is shown in Figure 44. In order to obtain some idea of the angle of attack distribution we assume, to the first order, that the velocities measured at this location are the same as at the propeller, giving the angle of attack distribution shown in Figure 45. The inboard section of the propeller is operating at nearly constant angle of attack. There is a reduction in angle of attack near the tip. Less twist at the tips would result in an improved angle of attack distribution, as discussed for example, in Reference 10. This effect is probably due to the radial inflow distribution at the duct inlet caused by the presence of the duct as shown also in the above Reference 10.

2. Thrust Variation

The digital readout system reads each channel in series for one half second at a time. In tests 199-204 and 211-216, these one half second thrust readings are the only

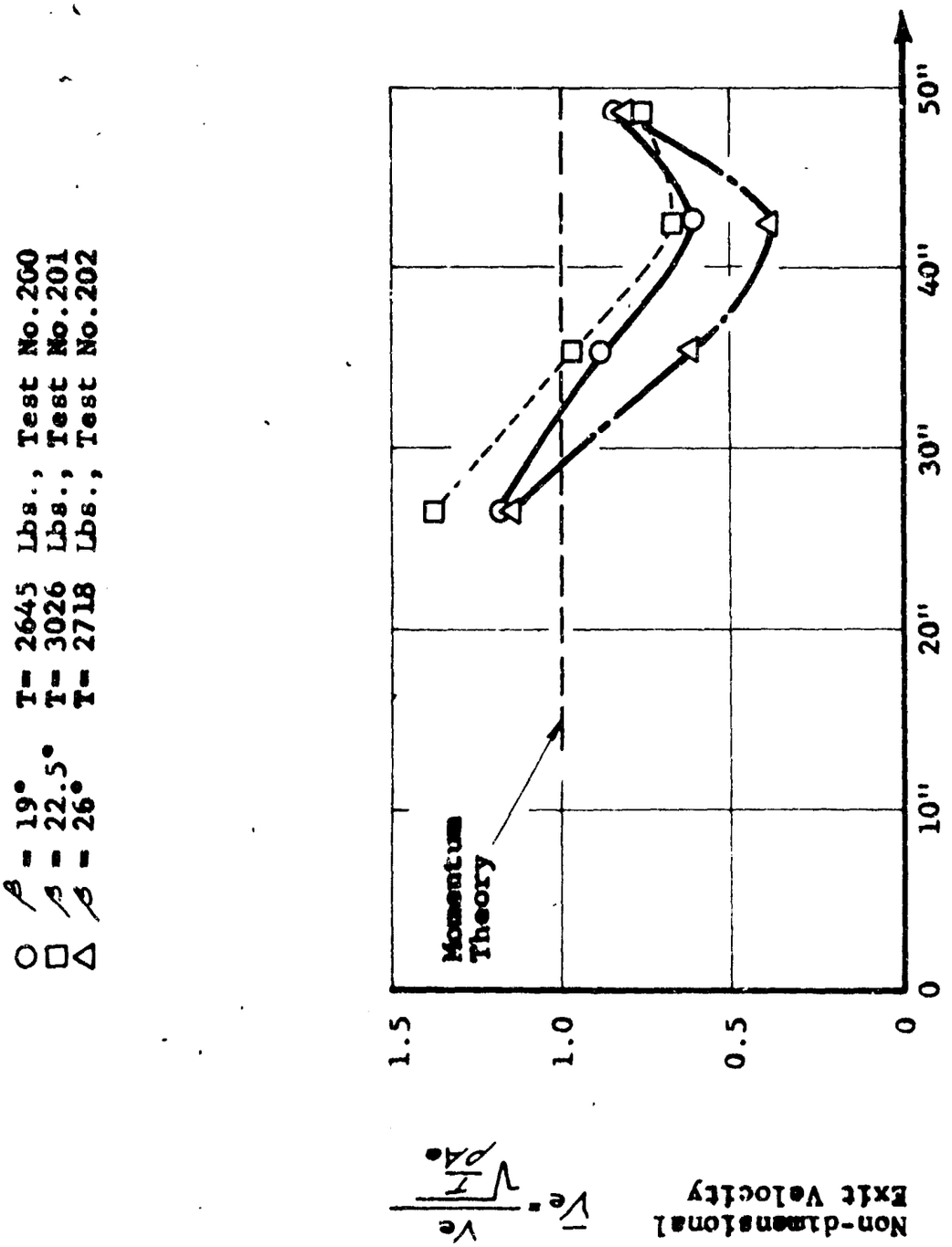

FIGURE 44: EXIT VELOCITY VERSUS RADIUS

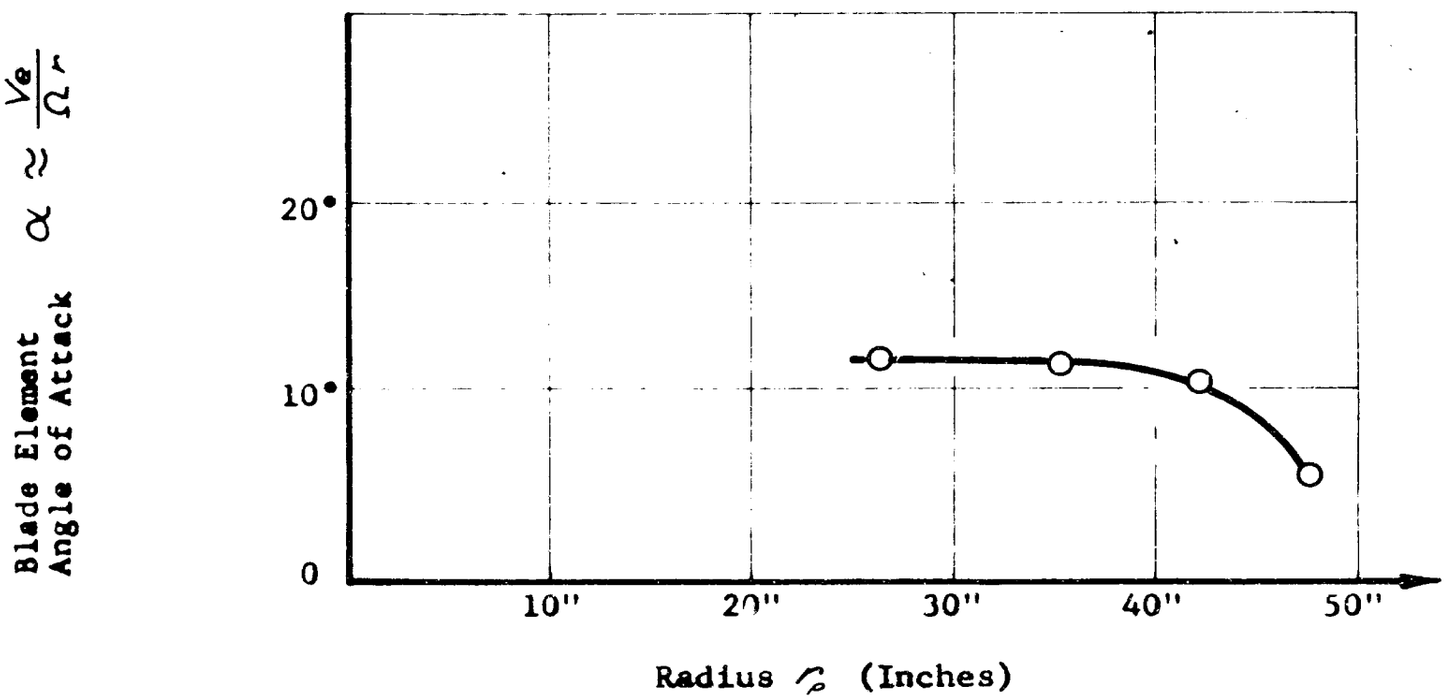

FIGURE 45: PROPELLER BLADE ELEMENT ANGLE OF ATTACK VERSUS RADIUS. (TYPICAL CASE)

runs that were made. However, in tests 199-204 the length of each thrust run was long enough such that three one-half second intervals were present, separated by about 3 seconds, that could be used as a measure of the thrust fluctuation in the isolated case. In order to investigate the long term thrust variations in the series of tests 217 through 225, data were also taken reading only thrust for a period of about six seconds on each duct. These runs were then averaged over half second intervals to give the low frequency thrust variations. Typical runs of these half second averages are shown in Figure 46 and actual time histories of each point 20 milliseconds apart are shown in Figure 29. Again, recall that the high amplitude at about 7-8 cps is a resonance of the structure and does not actually represent the variation in thrust. The fact that the thrust is not fluctuating this greatly was verified by the fact that the exit velocity measurements remain relatively constant. This correspondence was evaluated only at very low thrust levels. At high thrust levels, the sensitivity of the velocity probes is not adequate to read the thrust variation indicated by the load cells. Recall also, that the dynamics of the recording system used in the tests reported in Reference 2, resulted in a considerable attenuation of this resonant frequency.

Table 11 presents the maximum variation of the one-half second averages over the six second interval. There does not appear to be any particular trend with geometry. In fact the only trend evident is a slight increase in the percentage

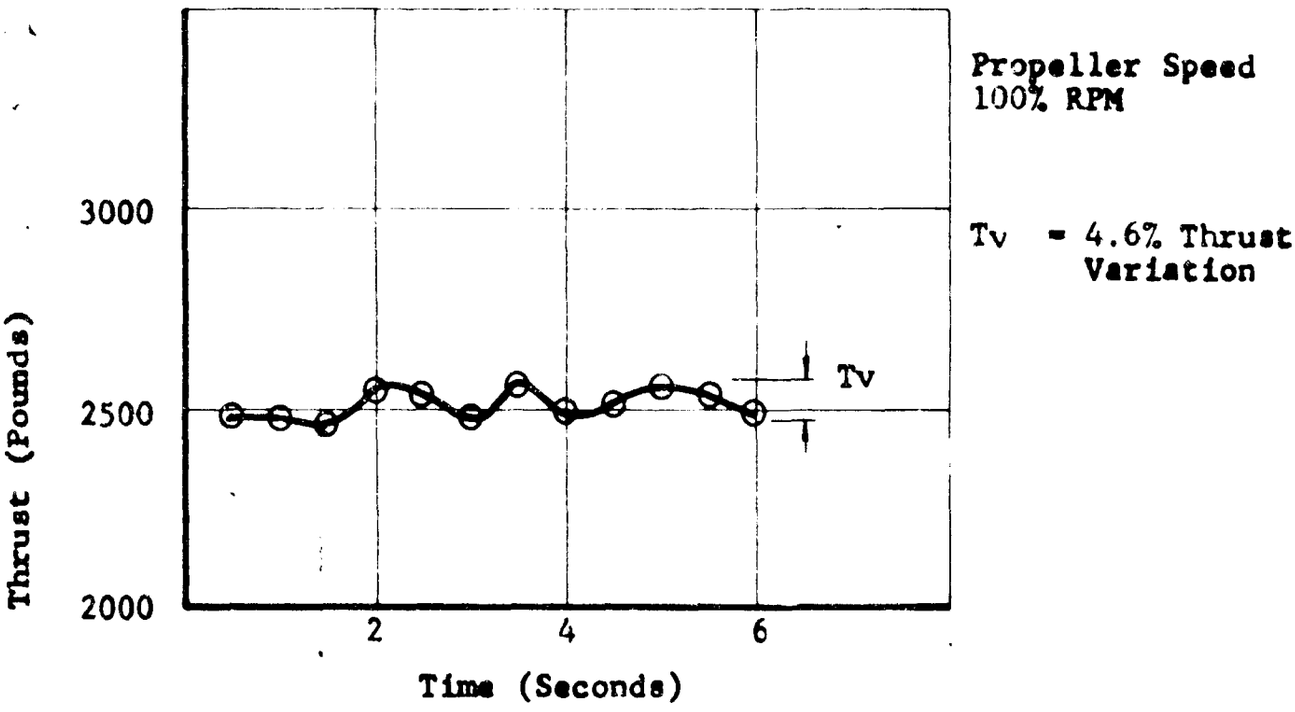

a) Test Number 218 Fwd Duct
(Propeller Pitch Angle * 22½°)

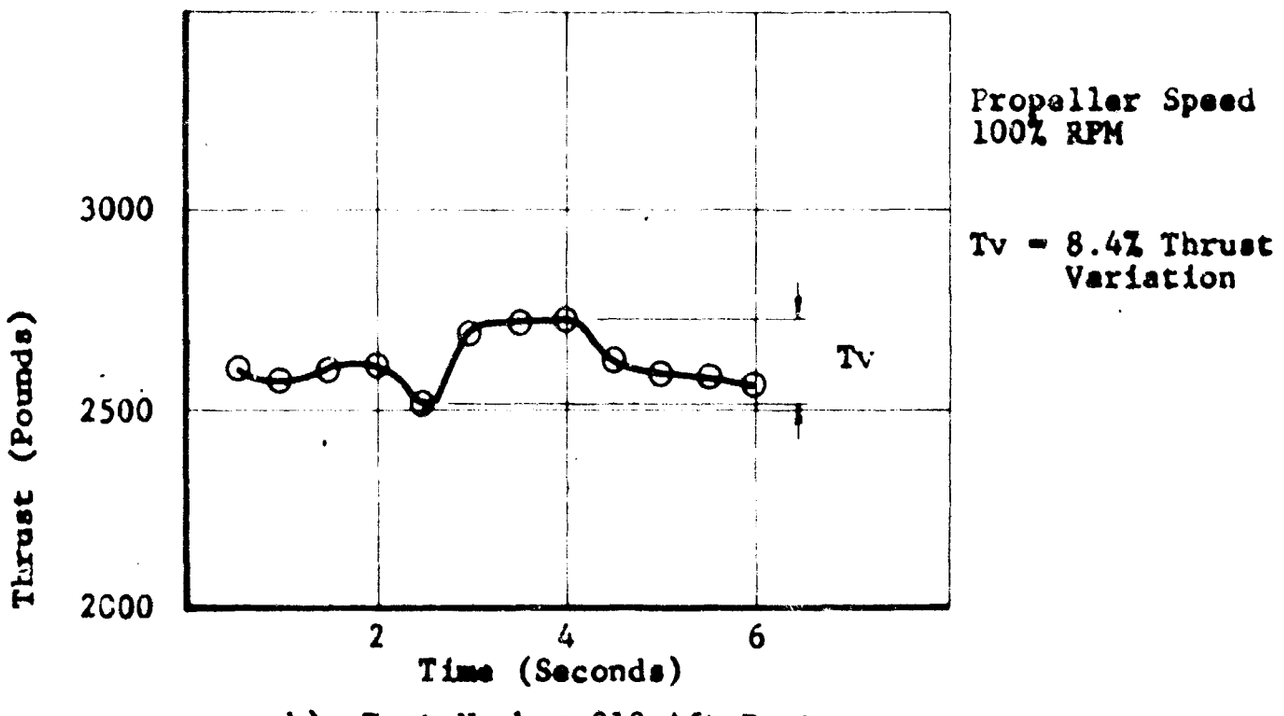

b) Test Number 218 Aft Duct
(Propeller Pitch Angle * 22½°)

FIGURE 46: TYPICAL THRUST VARIATIONS WITH TIME.

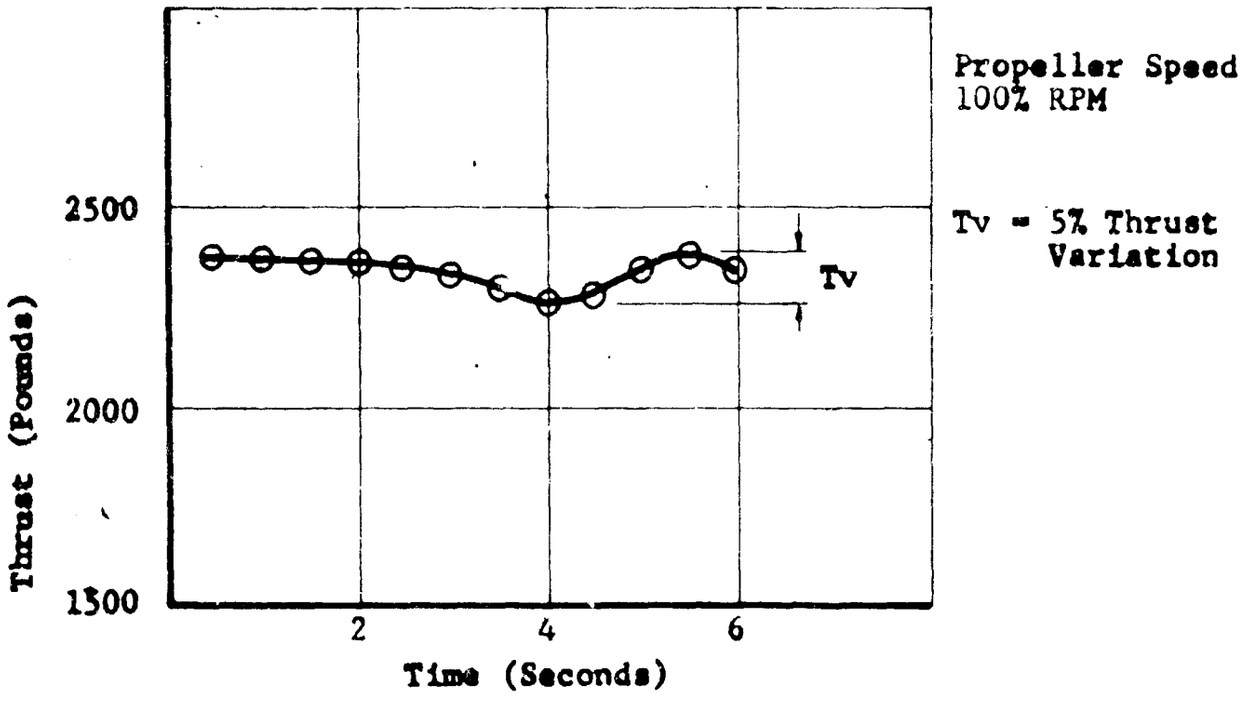

c) Test Number 219 Fwd Duct
(Propeller Pitch Angle * 19°)

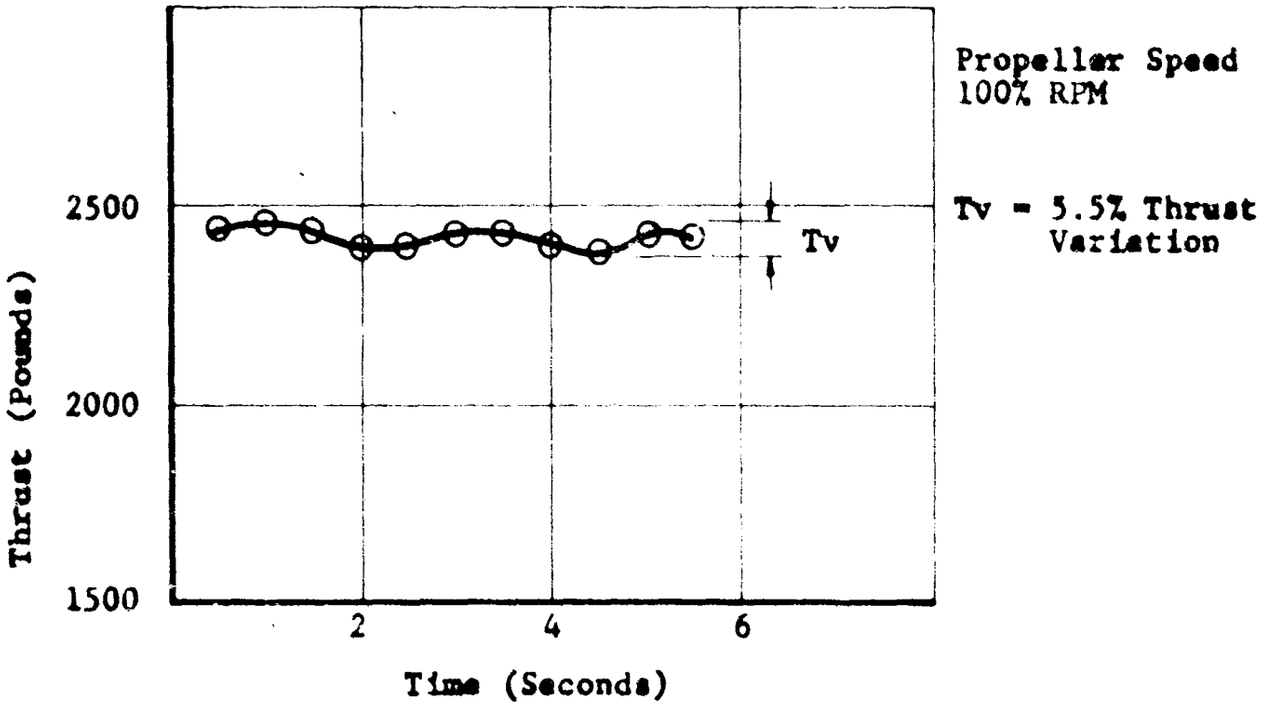

d) Test Number 219 Aft Duct
(Propeller Pitch Angle * 19°)

FIGURE 46: TYPICAL THRUST VARIATIONS WITH TIME.

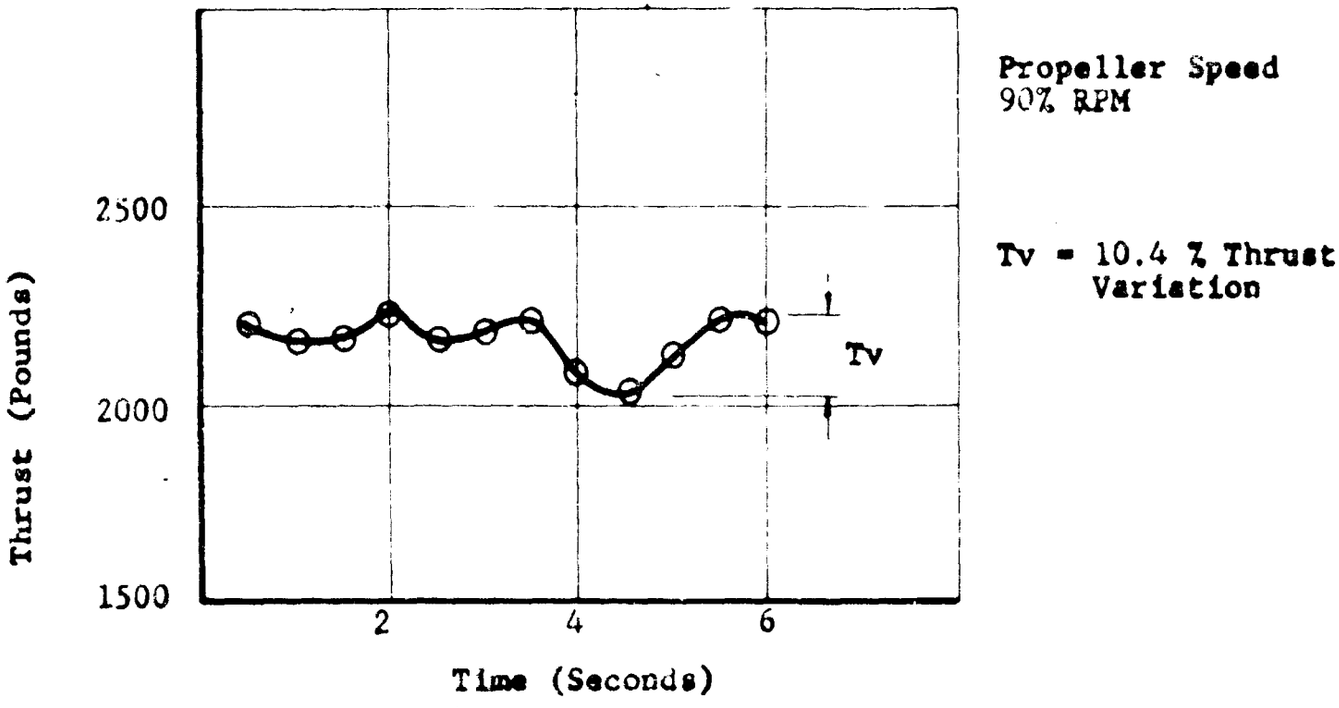

e) Test Number 223 Fwd Duct
(Propeller Pitch Angle * 26°)

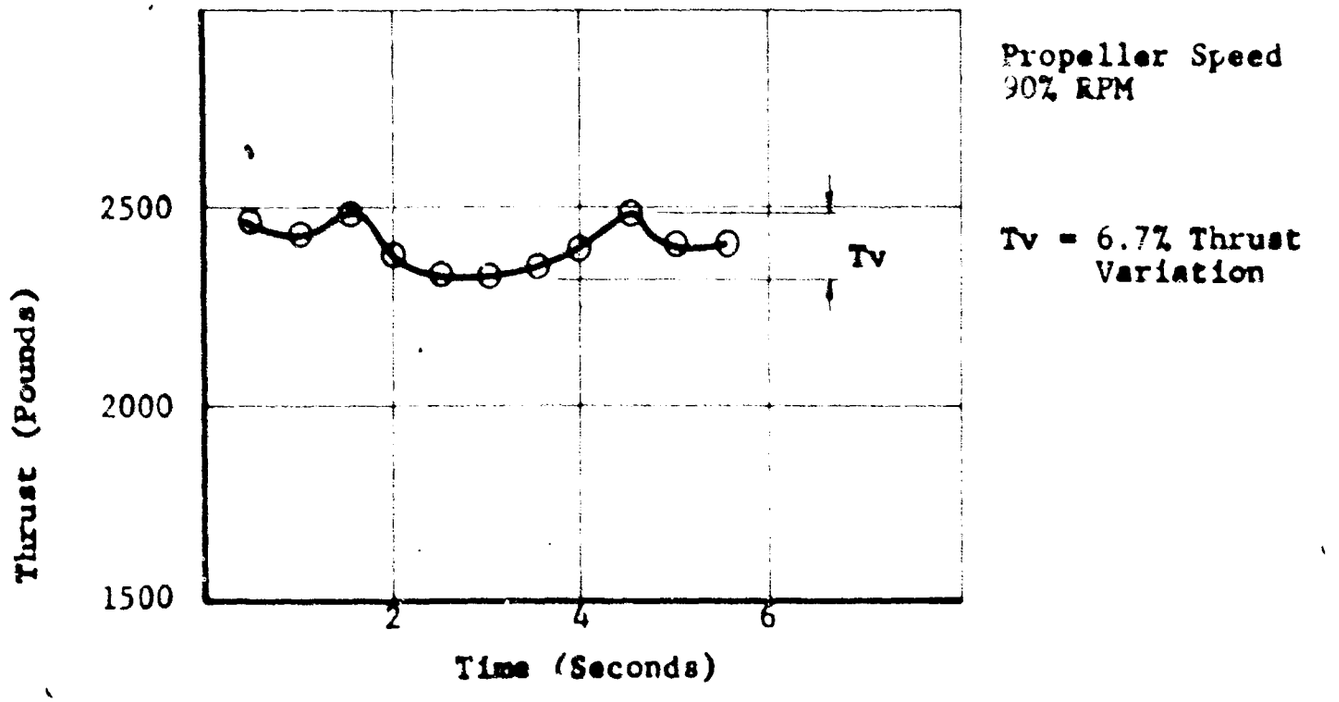

f) Test Number 223 Aft Duct
(Propeller Pitch Angle * 26°)

FIGURE 46: TYPICAL THRUST VARIATIONS WITH TIME.

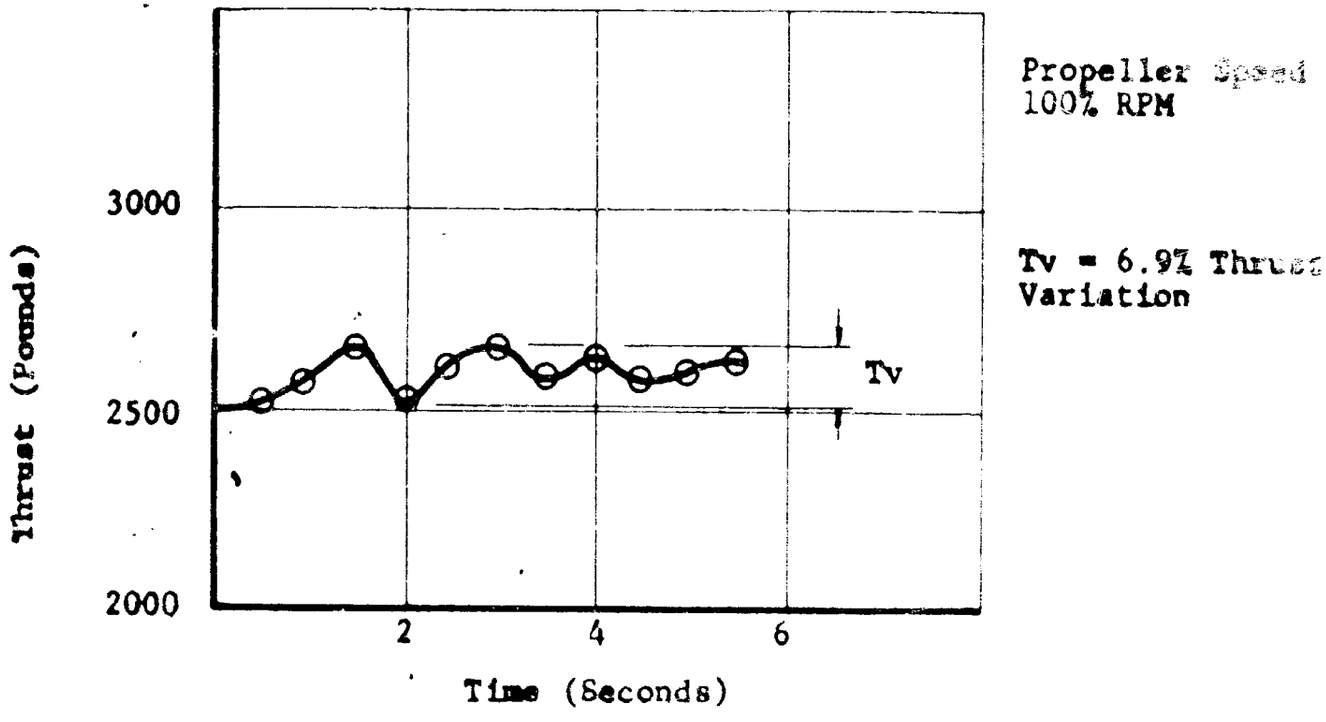

g) Test Number 223 Fwd Duct
(Propeller Pitch Angle * 26°)

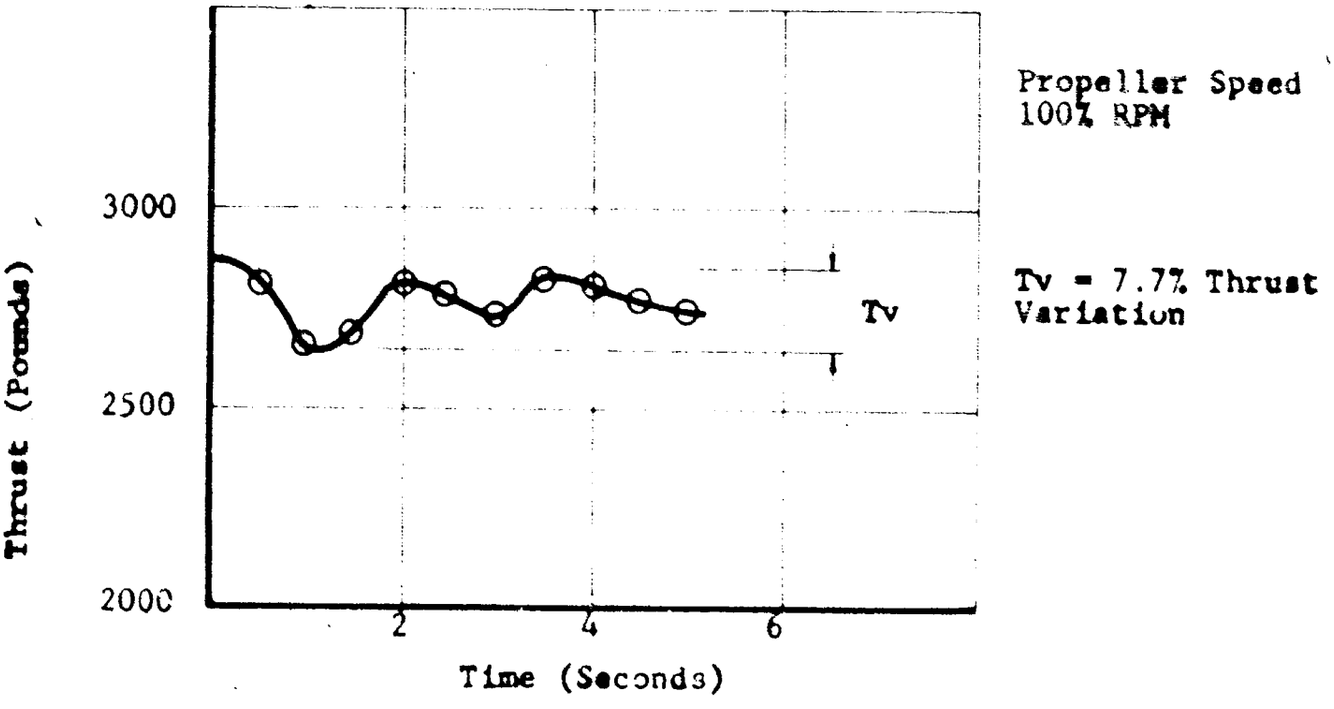

h) Test Number 223 Aft Duct
(Propeller Pitch Angle * 26°)

*Measured at 7/8 Radius

FIGURE 46: TYPICAL THRUST VARIATIONS WITH TIME.

thrust variation with blade angle. The level appears to be essentially independent of thrust (RPM) and is the order of 100 pounds at a propeller blade angle of 19 degrees, rising in some cases to 200 pounds at a blade angle of 26 degrees. At average thrust levels of 2000-2400 pounds, this fluctuation in thrust is of a similar order to the difference in thrust measured in some cases between the forward and aft ducts. The variation in thrust did not appear to contain any predominate frequency, but appeared quite random as indicated by the sample traces shown in Figure 46. From Table 11, it can be seen that in all tandem experiments, the thrust variations were considerably larger than the isolated experiments in which the thrust fluctuation did not exceed 2 percent. The thrust fluctuations in the tandem experiments varied mostly between 5 percent and 10 percent.

In the case of the higher frequency fluctuations, that is, the structural frequency of the duct crane system, again there was no trend apparent with variation in the geometry of the tandem configuration. However, in all cases the amplification of this frequency was considerably higher in the tandem configurations than in the isolated cases as shown in Figure 29. The only cases in which the load cell fluctuations were appreciable in the isolated case were those in which the propeller RPM was near 600, that is, close to the natural frequency of the system.

From the type of tests conducted here it is difficult to obtain any further insight into the precise source of the

ISOLATED PROPELLER DUCT TEST

Test No.	*Propeller Speed 80% RPM	*Propeller Speed 90% RPM	*Propeller Speed 100% RPM
199	2.0	-	-
200	-	2.2	1.7
201	-	0.9	0.7
202	1.0	-	0.2
203	-	-	2.0
204	1.6	1.0	0.9

TANDEM PROPELLER DUCT TEST

	*Propeller Speed 80% RPM		*Propeller Speed 90% RPM		*Propeller Speed 100% RPM	
Test No.	Fwd Duct	Aft Duct	Fwd Duct	Aft Duct	Fwd Duct	Aft Duct
217	12	8.0	5.1	7.5	3.5	7.1
218	6.6	9.7	6.9	9.8	4.6	8.4
219	7.2	9.0	6.5	9.4	5.0	5.5
220	8.5	9.2	7.1	5.1	7.[illegible]	4.4
221	-	8.9	-	7.0	-	5.9
222	10.3	2.7	7.8	9.2	8.6	3.3
223	5.5	5.5	10.4	6.7	6.9	7.7
224	4.4	7.4	5.2	6.7	7.6	4.6
225	4.4	9.0	5.7	6.6	6.6	3.9

*Propeller Speed Percent RPM is Approximate

TABLE 11: THRUST VARIATION PERCENTAGES.

roughness other than the considerations discussed above. That is, it is difficult for example, to decide how much of the thrust fluctuation may be arising from the duct lip pressures varying, and how much comes from the propeller thrust. The duct lip thrust is probably more sensitive to the presence of recirculation and to variations in local wind than the propeller thrust, Reference 10. The measurements made here indicate that this duct has a low static efficiency. Greater fluctuations in thrust may be experienced on a ducted propeller in which the duct carries a greater portion of the total load. That is, it is considered that the thrust fluctuations obtained from these tests may be less than would be expected on a duct with better static performance.

Further insight into the recirculation problem can be gained by conducting transient tests in which the duct is brought rapidly up to operating RPM. The behavior of the thrust and various other quantities as a function of time will show the nature of the establishment of recirculation.

It may be noted from Figure 43 that the average level of the recirculation causes an inflow velocity that is equivalent to a propeller blade change of about 4 degrees. To obtain a rough estimate of the magnitude of the recirculation, we assume for simplicity that this change comes only from a change

in local angle of attack of the propeller blades at 3/4 radius, this change in blade angle corresponds to an average inflow velocity, caused by recirculation, of about 20 percent of the duct exit velocity.

VII CONCLUSIONS

A. Engine Ingestion and Inlet Protection Test Conclusions

Based on this testing, the following conclusions are believed to apply to the dual tandem ducted propeller VTOL aircraft when in vertical flight in close proximity to loose particle covered terrain.

1. Aircraft with disc loadings of 50 psf or greater and with unprotected aft stub wing mounted engines can expect engine ingestion rates in excess of 0.004 pounds of terrain per pound of ingested air when operated over sand. The rate of ingestion will be about one-half as great if the terrain particles are similar to the crushed stone which was tested.
2. The influence of the blocked half screen deflector inlet protection device was to reduce the engine ingestion by one-third at 50 psf with no significant change in the size of the particles ingested. The long and short chord deflectors reduced the engine ingestion by one-half at 50 psf. This protection is believed to be inadequate.
3. For tests over sand, stationary inlet screens which protrude into the upflow region between the propeller ducts should not be used with the dual tandem configuration as they will increase engine ingestion.

4. Analytical interpretations of the data indicate that screens used in conjunction with a properly protected suction device would show potential as a particle trapping device and could be used to alleviate particle ingestion.
5. Ducted propeller ingestion data indicate that when operating over sand, an average of 60 pounds of sand per million cubic feet of air can be expected at 50 psf disc loading.
6. The data obtained in this program substantiate the tests of Reference 2 and indicate that for this configuration, large amounts of terrain can be transported to sensitive areas of the airframe by the effects of downwash.
7. If an aircraft of this configuration is operated at 50 psf disc loading it is unlikely that the environment can be more severe than that which was studied in the testing over crushed stone. Since the test rig could tolerate this environment for a relatively long period it is likely that a practical VTOL aircraft can be developed which can tolerate similar environments for short periods of time.

B. Aerodynamic Test Conclusions

1. Recirculating flow arising from the presence of two ducted propellers running in close proximity, near the ground, with their thrust axes vertical, acts to

reduce the thrust coefficient of each ducted propeller at a given blade angle. This reduction in thrust coefficient is accompanied by a reduction in figure of merit.

2. The recirculation also produces slow variations in the thrust of the ducted propeller varying from 5 percent to 10 percent of the average thrust for the conditions of these tests.
3. Considerable excitation of the predominate structural frequencies of the duct supports also arose from the recirculating flow.

C. Propeller Blade Stress Studies

The Hamilton Standard report on propeller blade stress studies, made during the Aerodynamic Interaction tests, has been included as Appendix A.

REFERENCES

1. Pruyn, R.R. and Goland, L., An Investigation of VTOL Operational Proolems Due to Downwash Effects, Kellett Aircraft Corporation, Report 179T80-2, June 1961. (Also paper presented at American Helicopter Society, 18th Annual Forum, May 1962). (Also published as Report Number AD 264560, Defense Documentation Center, Cameron Station, Alexandria, Virginia)

2. Pruyn, R.R., Effects of Airframe Geometry on Downwash Problems of Tandem Ducted-Propeller VTOL Aircraft, Kellett Aircraft Corporation, Report 179T80-6, January 1964. (Also published as Report Number AD 452792, Defense Documentation Center, Cameron Station, Alexandria, Virginia).

3. Paxia, V.B., and Sing, E.Y., Design Development of a Dual Tandem Ducted Propeller VTOL Aircraft, IAS paper 63-30, January 1963.

4. Anonymous, Model Specification Engine, Aircraft, Turboshaft, General Electric Company T58-GE-8 Engine, Specification E1025, May 1960.

5. Stewart, W., Helicopter Behavior in the Vortex Ring State, Aeronautical Research Council of Great Britain, R and M 3117, 1959.

6. NASA Conference on V/STOL Aircraft, A Compilation of the Papers Presented, Langley Research Center, Langley, Virginia, November 17 and 18, 1960.

7. Mallinckrodt, A.J., Aliasing Errors in Sampling Data Systems, AGARD Flight Test Manual Vol. 4, Instrumentation Systems, Second Edition, Pergamon Press, 1962.

8. Anonymous, First Test Results, Lycoming's "Sand and Dust" Program For the T53 Gas Turbine Engine, Lycoming Report 13 October 1958.

9. Watsen, E., Amount of Dust Re-Circulated By a Hovering Helicopter, Kaman Aircraft Corporation, Report R-169, December 1956.

10. Neal, B., The Design and Testing of Three Six-Foot Diameter Ducted Propellers with Their Rotational Axes Normal to the Free Stream, National Research Council of Canada, Aeronautical Report LR-426, March 1965.

APPENDIX A

HAMILTON STANDARD REPORT HSER 3731

Division of Kellett Aircraft Corporation
Windsor Locks, Connecticut

VIBRATORY STRESS MEASUREMENTS

on a

SHROUDED PROPELLER

in the

KELLETT AIRCRAFT CORPORATION

DOWNWASH TEST FACILITY

October 27, 1965

Kellett Aircraft Corporation
Purchase Order No. 31808

Written by:

Clifford H Bivens — Senior Analytical Engineer

Approved by:

Research Engineer - Vibration

W W Conwell — Head of Applied Mechanics and Mathematics

Samuel E Eytinge — Chief of Technical Staff

No. of Pages: 23

ABSTRACT

This report presents the results of blade vibratory stress measurements on a Hamilton Standard 53C51 / 7563-30 propeller operating in a shroud in the Kellett Aircraft Corporation downwash test facility. This shrouded propeller was tested as an isolated unit and also as an aft installation in a ground test arrangement containing components representative of the Bell X-22 aircraft. These tests were conducted at intervals during the period of April 29 to August 6, 1965 at Willow Grove, Pennsylvania.

TABLE OF CONTENTS

SUMMARY

This program was conducted for the purpose of assessing the influence of adjacent aircraft components and ground effects on aerodynamically excited vibratory stresses in the blades of a shrouded propeller.

Isolated tests of the shrouded propeller were made with the unit in a vertical position at two elevations to assess ground effects separately. With the blade angle set to absorb maximum available power at maximum rotational speed, a 70% increase in blade vibratory stress was obtained when the shroud exit position was reduced from 1.5 to 1.0 propeller diameters above the ground. This increase occurred in the peak stress obtained at a critical speed within the operating range.

The same shrouded propeller was also tested as an aft installation in an arrangement which included a similar forward unit and a half fuselage representative of the Bell X-22. Variations in the spacing between these components produced significant changes in peak stress in the aft propeller blades. In one configuration, vibratory stresses were more than twice those obtained from the isolated unit.

These results indicate that with the shrouded propeller in a vertical position, ground effects and the proximity of the simulated aircraft components had an appreciable influence on aerodynamic excitation of the propeller blades.

CONCLUSIONS

1. Based on tests of an isolated shrouded propeller in a vertical position, aerodynamic excitation of the propeller blades is increased significantly when the shroud exit is lowered to 1 propeller diameter above the ground from the 1-1/2 propeller diameter above the ground position.

2. The relative location of one shrouded propeller to another and to the aircraft fuselage can have a significant effect on blade excitation with the shrouded propellers in a vertical take-off position on the ground.

3. Aerodynamic excitation produced by changes in ground proximity, the relative location of aircraft components, or a combination of both, can produce substantial variations in propeller blade vibratory stress, particularly if there is an important critical speed within the operating speed range.

INTRODUCTION

The Kellett Aircraft Corporation, under Navy contract, has constructed and operated an outdoor test facility for downwash investigations relative to a shrouded propeller driven VTOL aircraft. This static ground test facility consisted of two turbine powered shrouded propellers and a half fuselage mock-up mounted on a vertical reflection plane. These components were representative of those on one side of the Bell X-22 aircraft. The shrouded propeller assemblies were mounted on movable cranes which allowed their positions to be varied with respect to the fixed half fuselage.

The existance of this facility provided an opportunity to investigate vibratory stresses in a shrouded propeller in simulated VTOL aircraft configurations on the ground. While a number of shrouded propeller performance tests have been conducted in the past, principally in wind tunnels, little is known of aerodynamically excited vibratory stresses in shrouded propeller blades. This facility offered the possibility, therefore, of measuring such stresses under the influence of ground effects and adjacent aircraft components, and comparing them with those measured in an isolated unit. Consequently, a test program was proposed by Hamilton Standard Division, which, after a number of revisions was conducted under Kellett Aircraft Corporation Purchase Order No. 31808.

DESCRIPTION OF TESTS

A sketch showing the general arrangement of the ground test facility is shown in Figure 1. Further details may be found in Figure 2 of Kellett Report No. 179T80-12.

Each of the two 8 ft. diameter propellers was driven by a Lycoming YT53-L-3 turbine engine. These 3-way propellers contained solid aluminum blades which were held in fixed pitch during test. Blade angles were changed manually in the adjustable hub between tests. The entire propulsive assembly consisting of propeller, engine, support struts and shroud was mounted through thrust and torque load cells to a structural ring around the shroud. This ring was pivoted at the end of the crane boom to allow the shrouded unit to be rotated between horizontal and vertical positions. Details of the engine-propeller installation and the shroud contour may be obtained from Figures 23 and 24 of Kellett Report No. 179T80-12.

The boom supporting the forward unit passed through the X-22 half fuselage mockup. Since the aft unit was supported free of the fuselage, this unit was more easily moved to vary the spacing between components or to be completely removed for tests as an isolated unit. The blade vibratory stress tests were conducted on the aft shrouded propeller.

The vibratory stress measurements were obtained from strain gages installed on the camber side of the blade and on the blade shank. The radial locations of these gages along the blade centerline are shown in Figure 2. The shank leading edge gage was positioned to measure vibratory bending at a circumferential location aligned with the blade leading edge at the 3/4 radius. The shank 90° gage and the bending gages along the blade centerline were positioned to measure vibratory stresses resulting from flatwise bending modes. The pair of shear gages 12" from the tip were installed to measure vibratory stresses arising from torsional response of the blade. Strain signals from these gages were conducted through a slip ring assembly mounted on the propeller dome, amplified, and recorded on a Miller oscillograph. A 1P (once per revolution) signal was also recorded on the oscillograph simultaneously with the strain measurements.

The isolated shrouded propeller tests were made with the aft unit in both horizontal and vertical positions. In the latter position, tests were made at two elevations above the ground.

In the simulated aircraft configuration, the location of the aft unit was changed to vary the longitudinal spacing, Y, between units and the lateral spacing from the fuselage, X. When variations in elevation, H, were made, both shrouded propellers and the fuselage were changed by the same amount. All of these tests were made with both units vertical.

Blade vibratory stresses were measured at three 42" station blade angles over a propeller speed range of approximately 30% to 100% of maximum available rpm. These blade angles were selected to provide power

variations from approximately 50% to 100% of maximum available power at maximum rotational speed. When blade stresses were measured in the aft unit in the simulated aircraft configuration, both units were operated at essentially the same power and speed conditions.

Thrust and torque measurements were recorded at each test point by Kellett Aircraft. A summary of the tests conducted is shown in Table II.

DISCUSSION OF BLADE STRESS FREQUENCIES AND MODES

A brief discussion of propeller blade vibratory stress frequencies and modes is presented herein to assist in the interpretation of the test results. Figure 3 shows a critical speed diagram for the test propeller blade. The solid lines are lines of constant P (propeller speed) order. The dashed curves are calculated values of natural frequencies in the first flatwise, first edgewise, and second flatwise modes for this blade design. The circled points of intersection, therefore, are critical speeds predicted to occur within the test operating range. The natural frequency calculations assume that the propeller hub is motionless, i.e. the reaction of the vibrating blades on the hub is zero. They do consider, however, the stiffness of the blade retention in the hub. In practice where there is some hub motion, it is usually found that measured critical speeds are slightly higher than those predicted by this method.

The diagram indicates, for example, that the 2P first flatwise ($2P_{1f}$) critical speed was calculated to occur at 1175 rpm. Any twice per revolution excitation of the blade should produce the largest vibratory stress in the first flatwise mode at approximately 1175 rpm, therefore, since the calculated blade natural frequency is in resonance with the excitation frequency at this rotational speed. A calculation of the $2P_{1f}$ mode shape, or stress distribution, showed that the vibratory bending stress is a maximum at the 24" from tip strain gage location. $3P_{1f}$ response of the blade would produce a maximum stress at essentially the same gage location.

Similarly, the diagram shows that critical speeds in the first edgewise vibratory bending mode were predicted to occur in the operating range at higher P orders. In this mode, the maximum vibratory stress is produced at the leading edge shank gage location.

The $6P_{2f}$ critical speed was predicted to occur at the upper limit of the operating range. In this mode, which contains a node outboard in the blade, the maximum vibratory stress was calculated to be at the 12" from tip gage location. Vibratory stresses at P orders greater than 6 are generally of less significance. It should be noted that there is no 1P resonant condition anywhere near the propeller rotational speed range. This is an essential requirement for any normal blade design since appreciable 1P excitation can be obtained in flight simply by inclination of the propeller thrust axis with respect to the approaching airstream.

In a turbine installation, vibratory excitations from the engine are negligible, and any vibratory stresses induced in the propeller blades are almost entirely aerodynamically excited. Any non-uniformity or asymmetry in the flow field at the propeller disk which produces periodic variations in blade loading can induce vibratory blade stresses at integer P orders. Any changes in blade vibratory response in these tests at a given blade angle and rotational speed, therefore, can be attributed to the effect of test configuration changes on the propeller flow field.

DISCUSSION OF RESULTS

Blade vibratory stresses obtained from the isolated shrouded propeller tests were low as shown in Figures 4 and 5. As expected, torsional response of the blades was negligible in these and all subsequent tests since the blade design is such as to be free from stall flutter in either a shrouded or unshrouded condition.

The isolated unit was tested in both the horizontal and vertical positions at an H/D of 1.5 in an attempt to determine if ground effects were present at this elevation. However, test limitations allowed this comparison to be made only over a very small propeller speed and power range and these results, therefore, are inconclusive.

Blade angle variations with the shroud in a vertical position at an H/D of 1.5 resulted in practically no change in stress magnitude with power. Simultaneous measurements 24" from the tip on two blades are in good agreement and indicate the $2P_{1f}$ critical speed to be in the vicinity of 1200-1300 rpm. These and subsequent results also confirm that the highest stress occurred at the 24" from tip gage location in the first flatwise mode.

At a blade angle of 26°, the $2P_{1f}$ critical speed is more evident with the H/D reduced to 1.0. This indicates an increase in excitation to which the blade responded at a resonant condition. Over the remainder of the rotational speed range, changes in blade vibratory stress are less evident. The results in Figure 5 show approximately the same power absorption over the propeller speed range at a given blade angle for both H/D ratios. This indicates little change in the mass flow and average velocity in the shroud. The higher $2P_{1f}$ stress peak at an H/D of 1.0 is probably the result of an increase in turbulence or a change in flow distribution at the propeller disk. Since this is a resonant condition, a small increase in excitation can produce a significant increase in blade response. In both cases, some of this excitation may have arisen from the four equally spaced support struts behind the propeller.

The results of the simulated aircraft configuration tests are shown in Figures 6 through 12. When comparing the data from this series of tests, note should be taken of the wind velocity and relative bearing. Operation of an unshrouded propeller in a crosswind can result in blade response at significant P order critical speeds. Little is known about the effect of crosswind on a shrouded propeller, but it may be possible for an appreciable wind velocity perpendicular to the shroud inlet to produce turbulence at the propeller disk with a resulting effect on blade excitation. The results in Figure 6 at a blade angle of 19° and those in Figure 7 may be influenced by higher wind velocities.

The variation in magnitude of the $2P_{1f}$ stress peaks indicates that significant changes in excitation occurred as the result of changes in configuration and ground proximity. In Figure 6, the $3P_{1f}$ critical speed is also evident at approximately 800 rpm.

DISCUSSION OF RESULTS (continued)

A summary of all of the $2P_{1f}$ peak stresses is contained in Figure 13. This figure illustrates an increase of approximately 70% in blade stress obtained by a reduction in H/D of the isolated duct from 1.5 to 1.0.

Figure 13 also shows that at an X/D of 1.25 and an H/D of 1.5, peak stresses were higher in this simulated aircraft configuration than in the isolated unit. With the above relationships, a Y/D of 2.38, and a blade angle of 19°, the maximum blade stress was more than twice that obtained from the isolated units. With the H/D reduced to 1.0, the spacing between units had some influence on blade stress at the higher blade angles. The highest response was obtained at a blade angle of 19° at a Y/D of 2.38 where the peak stress was probably 2 or 3 times that from the isolated unit. The increase in stress at low blade angle and power at this spacing ratio is somewhat supported by the results obtained at an H/D of 1.5. Operation of the aft unit in closer proximity to the fuselage at an H/D of 1.0 and a Y/D of 3.0 also produced an increase in blade vibratory stress.

The scope of this program did not permit a more complete test configuration variation to establish consistent trends, nor did it allow simultaneous assessments of flow fields around or within the shroud. Visual observations from previous tests in the facility have indicated large distortions in the flow field adjacent to the vertical shrouded propeller and the half fuselage. It is also suspected that this flow field is unsteady which may account for any inconsistencies in the test data. It is evident, however, that the flow distortions produced by ground effects or the influence of other aircraft components, or a combination of both, can result in significant excitation of the propeller blades. If the propeller has a critical speed within its operating speed range, this excitation can develop appreciable blade vibratory stress.

In this test facility, the Bell X-22 aircraft arrangement would be most closely represented by an H/D of .7, a Y/D of 2.3, and an X/D of 1.0. The available data does not allow a reasonable extrapolation to this combination of test variables. It is apparent, however, that adjacent aircraft components in the presence of ground effects will produce aerodynamic excitations of the propeller blades in the vertical take-off condition.

TABLE I

DEFINITION OF SYMBOLS

β_{42}	-	blade angle at 42" radius, degrees
D	-	propeller diameter, ft.
e	-	edgewise bending mode
f	-	flatwise bending mode
H	-	vertical distance from shroud exit to ground, ft.
P	-	propeller rotational speed, rpm
X	-	horizontal distance between shrouded propeller axis and fuselage, ft.
Y	-	horizontal distance between shrouded propeller axes, ft.

TABLE II
SHROUDED PROPELLER TEST CONDITIONS

Kellet Test No.	Shroud Position	X/D	Y/D	H/D	β° 42" Sta.	RPM Range	Test Date
199	Horizontal	Isolated		1.5	19.0	610-1150	4/29/65
200	Vertical	"		"	"	610-1720	"
201	"	"		"	22.5	590-1720	"
202	"	"		"	26.0	530-1730	"
204	"	"		1.0	"	580-1770	4/30/65
211	Vertical	1.25	2.38	1.5	26.0	600-1660	6/29/65
212	"	"	"	"	19.0	720-1700	"
213	"	"	"	1.0	"	650-1700	7/29/65
214	"	"	"	"	22.5	660-1700	"
215	"	"	"	"	26.0	680-1660	"
217	"	"	2.0	"	"	850-1720	8/3/65
218	"	"	"	"	22.5	860-1750	"
219	"	"	"	"	19.0	860-1700	"
220	"	"	3.0	"	"	840-1700	8/4/65
221	"	"	"	"	22.5	830-1690	"
222	"	"	"	"	26.0	840-1590	"
223	"	0.75	"	"	"	840-1640	8/6/65
224	"	"	"	"	22.5	850-1690	"
225	"	"	"	"	19.0	840-1730	"

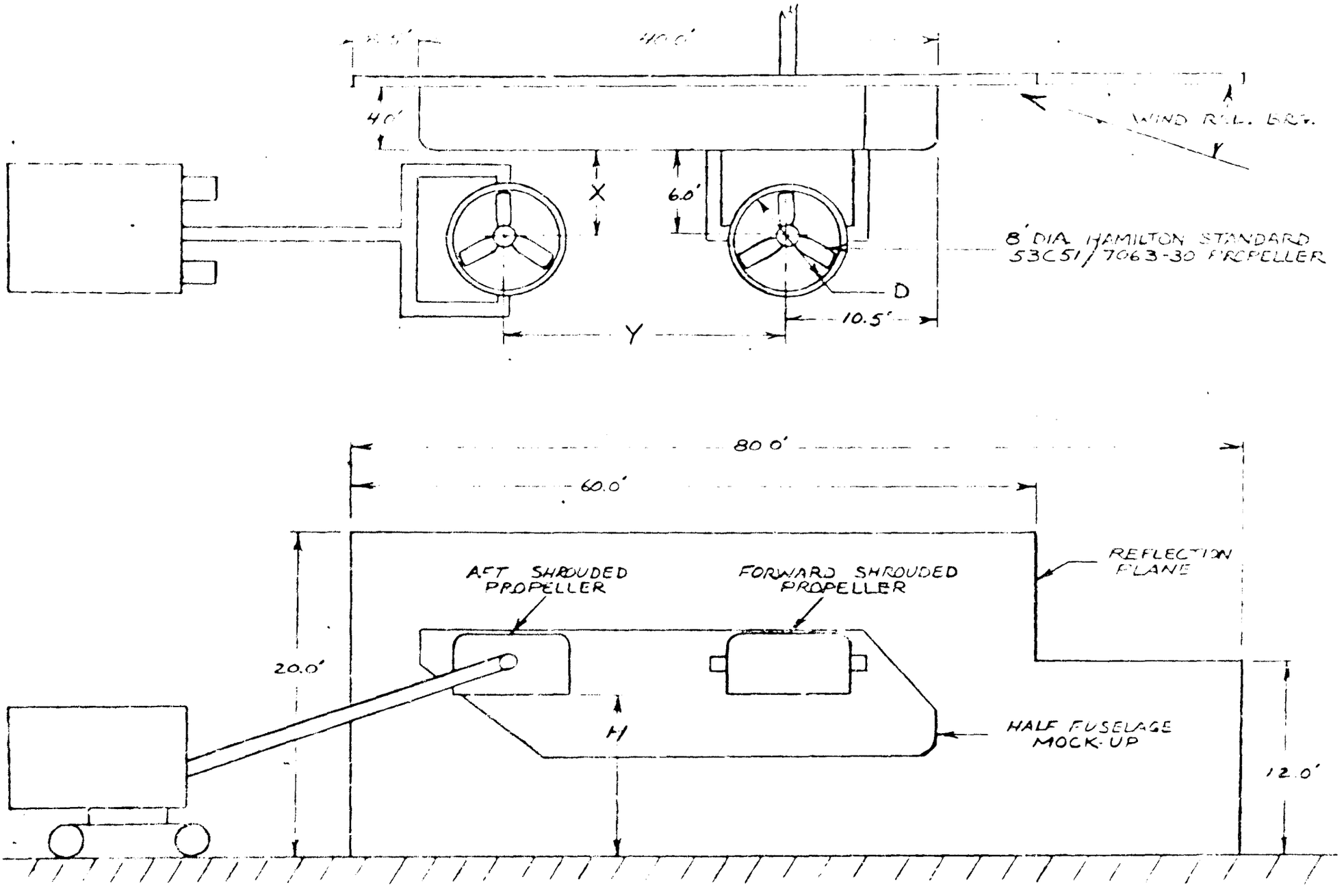

SHROUDED PROPELLER TEST ARRANGEMENT

HSER 3721

7063-30 BLADE STRAIN GAGE INSTALLATION
KELLETT SHROUDED PROPELLER
TEST STAND

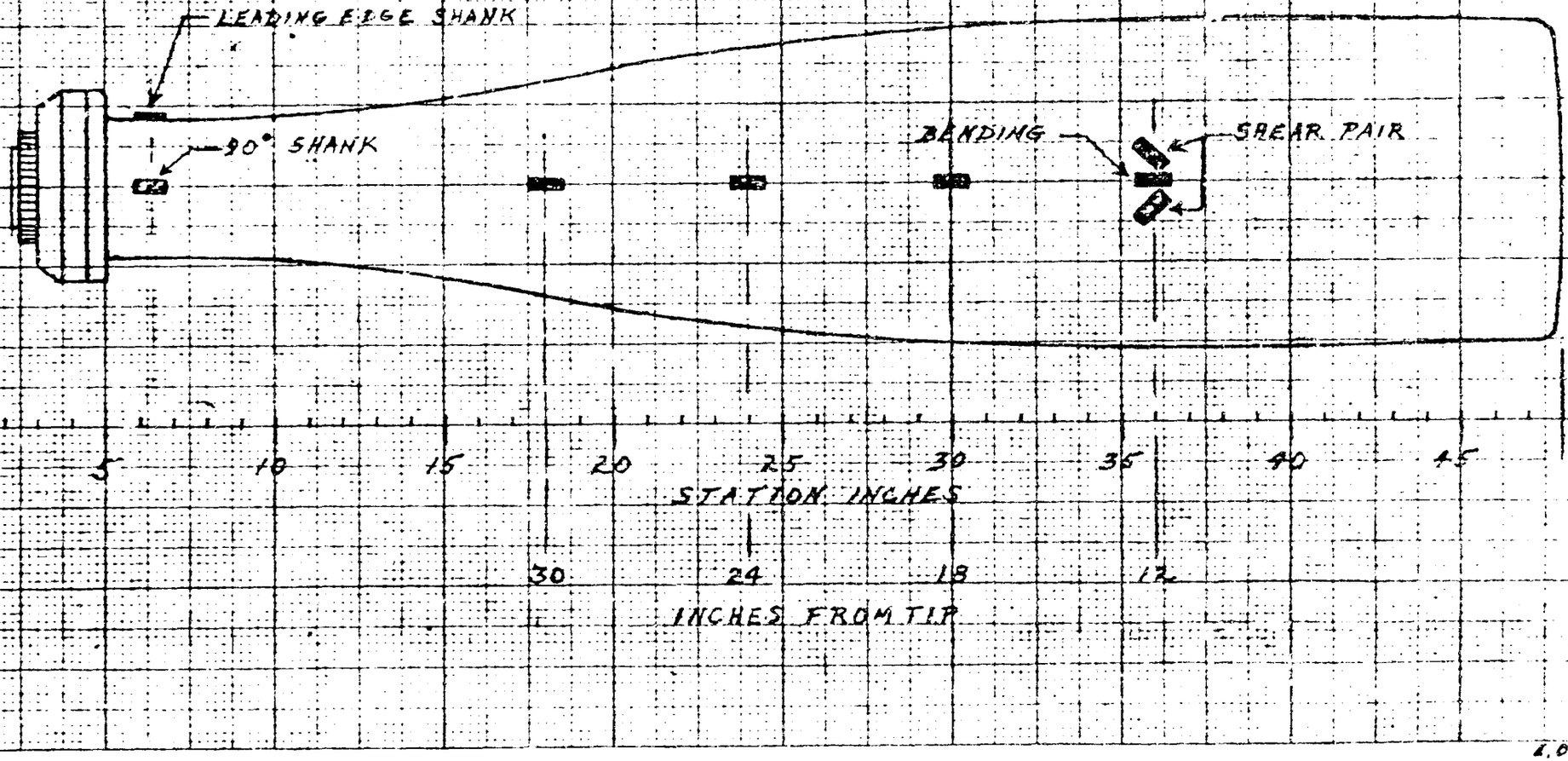

FIG. 2

12

L.O.
12-1-64

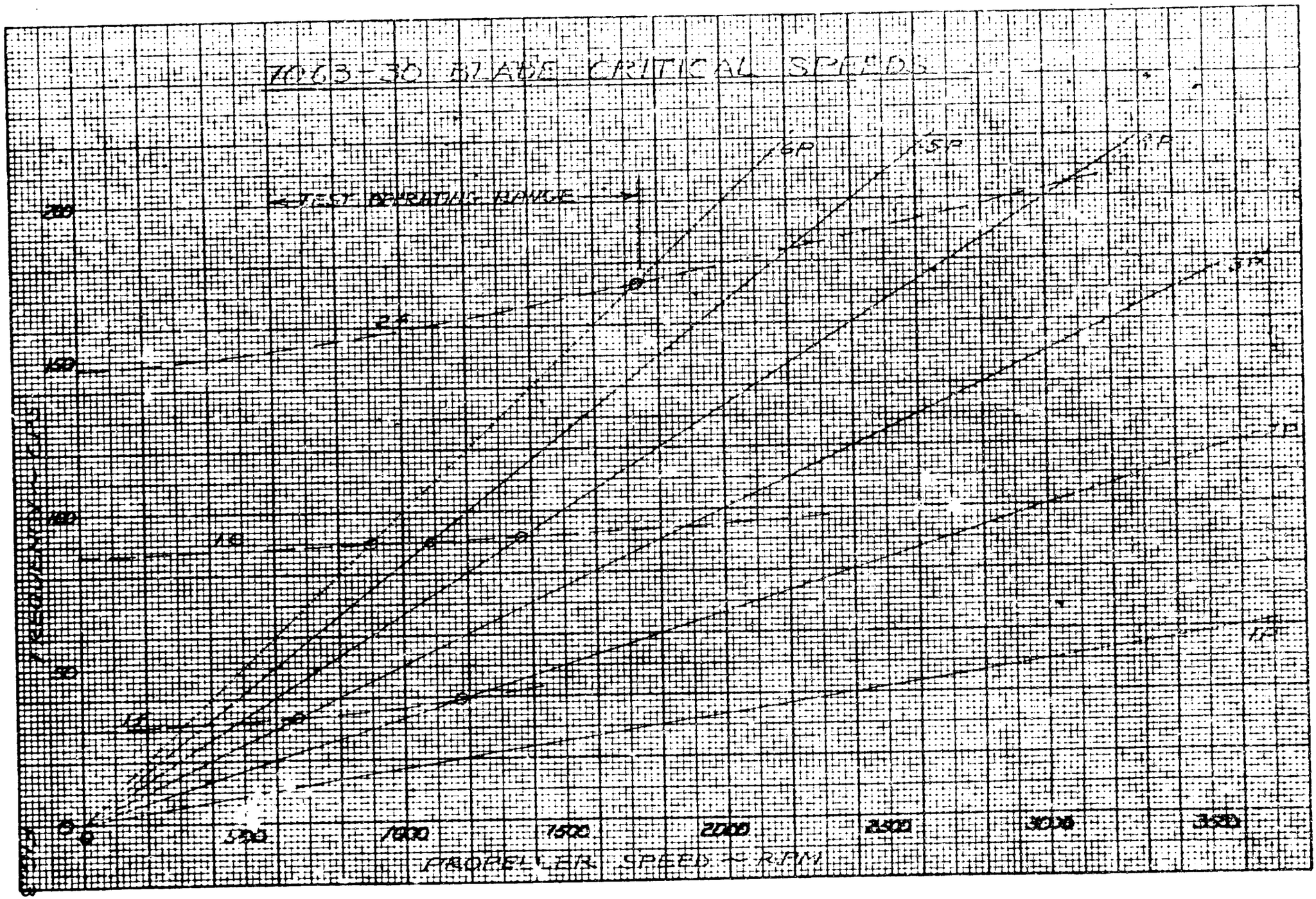

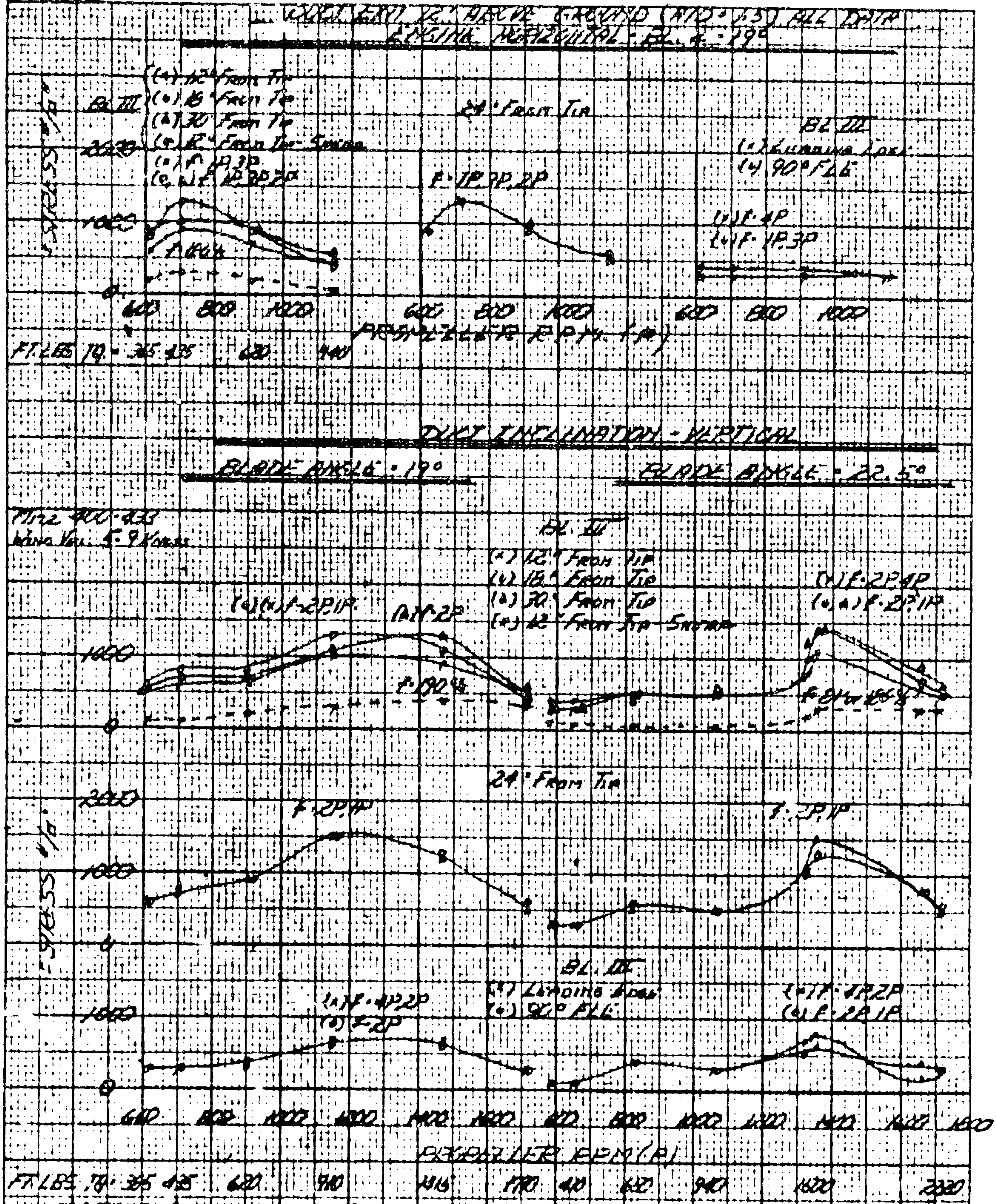

HUB 53C5V-305 ENGINE NO. LE 6B0043 TYPE YT-53L-3 DRIVE 12.46:1

BLADE 7063-70

DIAMETER 8'

AIRPLANE Kellett Aircraft Corp.

STAND Wilson Field

THE BLADE AND SHANK STRESSES ON KELLETT SHROUDED PROP. TEST STAND ISOLATED DUCT TEST

HAMILTON STANDARD
DIVISION OF UNITED AIRCRAFT CORPORATION
WINDSOR LOCKS, CONNECTICUT, U.S.A.

APPROVED

DRAWN BY

DATE

CHART NO. 46205

FIG 4

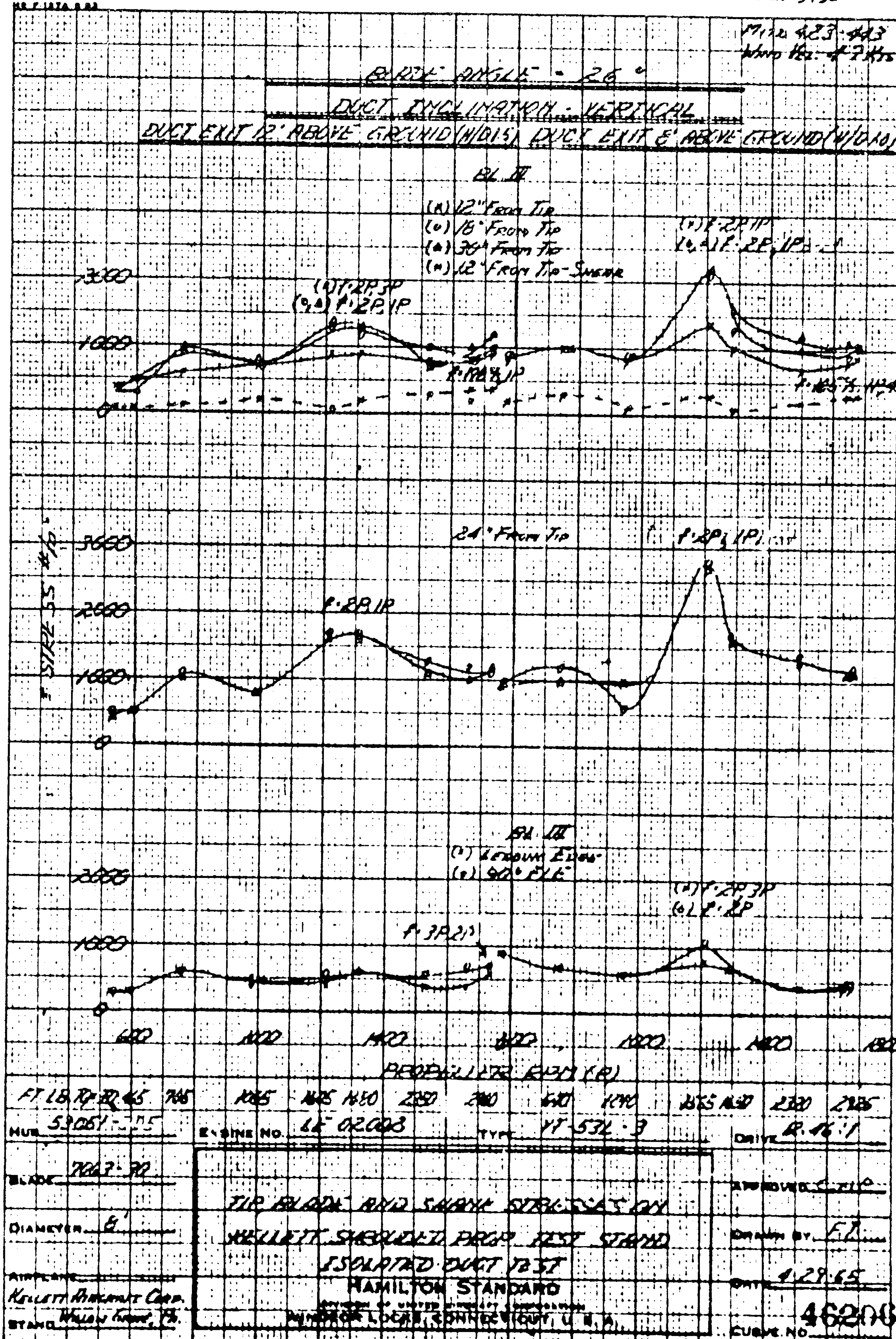
Blade Angle - 26°
Duct Inclination - Vertical
Duct Exit 12' Above Ground (H/D 1.5) Duct Exit 8' Above Ground (H/D 1.0)
Bl. II
(x) 12" From Tip
(o) 18" From Tip
(Δ) 30" From Tip
(□) 12" From Tip - Shank
24" From Tip
Bl. III
(x) Leading Edge
(o) 90° FLE
Stress #/in
Propeller RPM (R)
Hub 53051-
Engine No.
Type YT-53L-3
Blade
Diameter 8'
Airplane Kellett Aircraft Corp.
Stand Willow Grove, Pa.
Tip Blade and Shank Stress on Kellett Shrouded Prop Test Stand
Isolated Duct Test
HAMILTON STANDARD
WINDSOR LOCKS, CONNECTICUT, U.S.A.
Drive
Approved
Drawn By
Date 4-29-65
Curve No. 46206

FIG 5

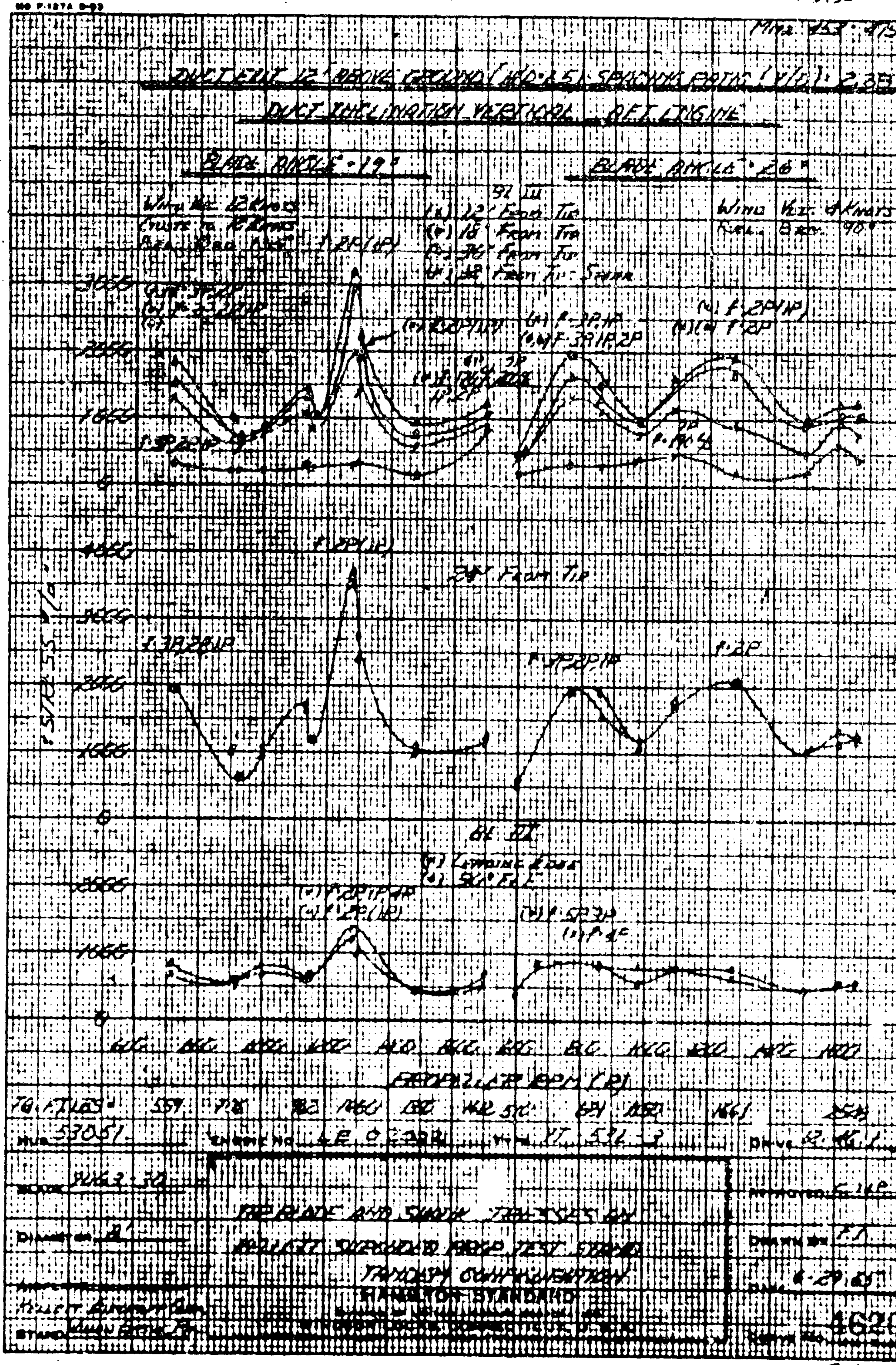

FIG. 6

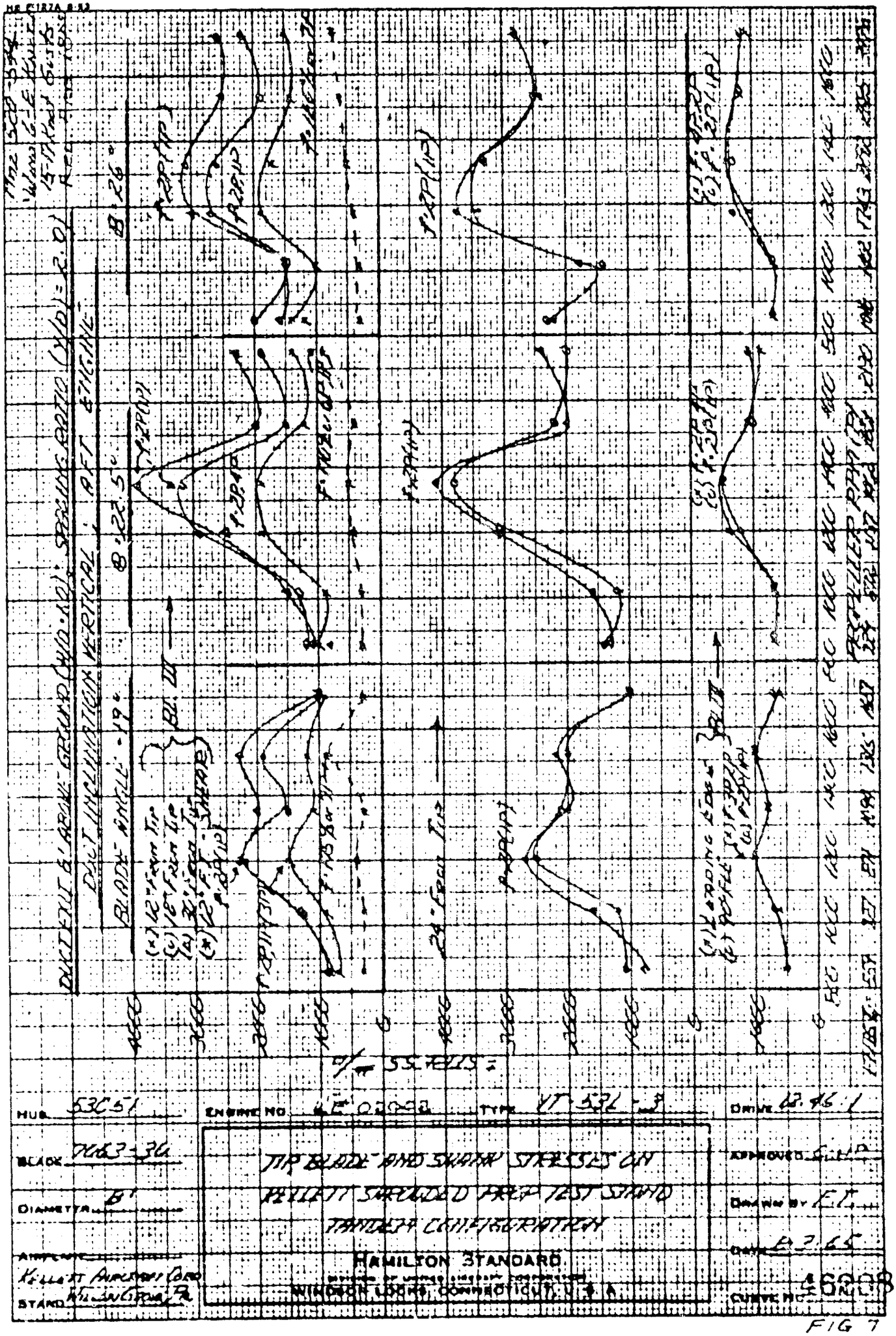
TIP BLADE AND SHANK STRESSES ON
KELLETT SPECIALIZED PROP TEST STAND
TRANSIENT CONDITIONS
HAMILTON STANDARD
WINDSOR LOCKS, CONNECTICUT, U.S.A.
HUB 53C51
BLADE 7663-36
DIAMETER 8'
AIRFRAME
STAND
ENGINE NO
TYPE
DRIVE
APPROVED
DRAWN BY
DATE
CURVE NO

FIG 7

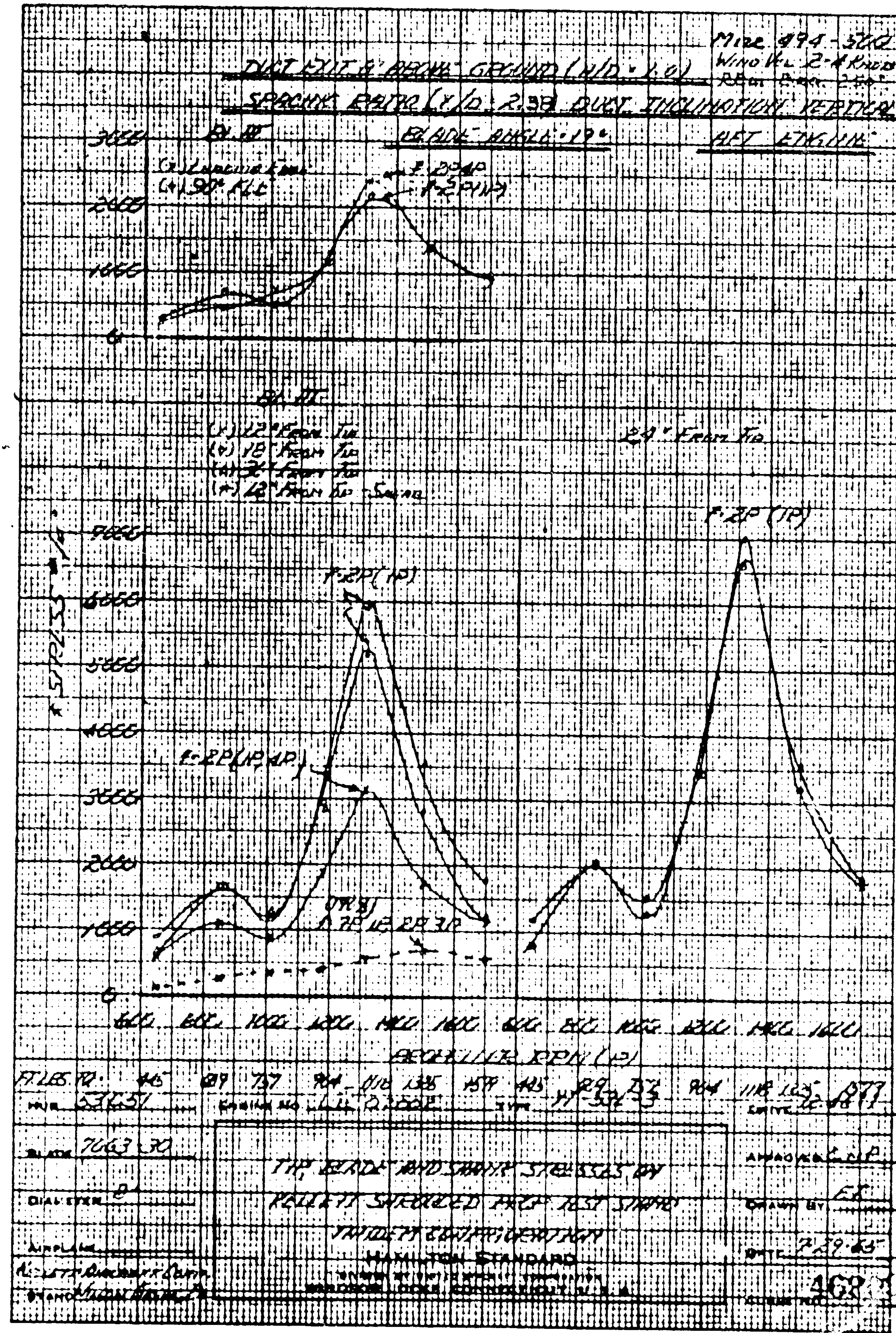
SPACING RATIO
BLADE ANGLE
ALT ENGINE
STRESS
PROPELLER RPM
HAMILTON STANDARD

FIG. 8

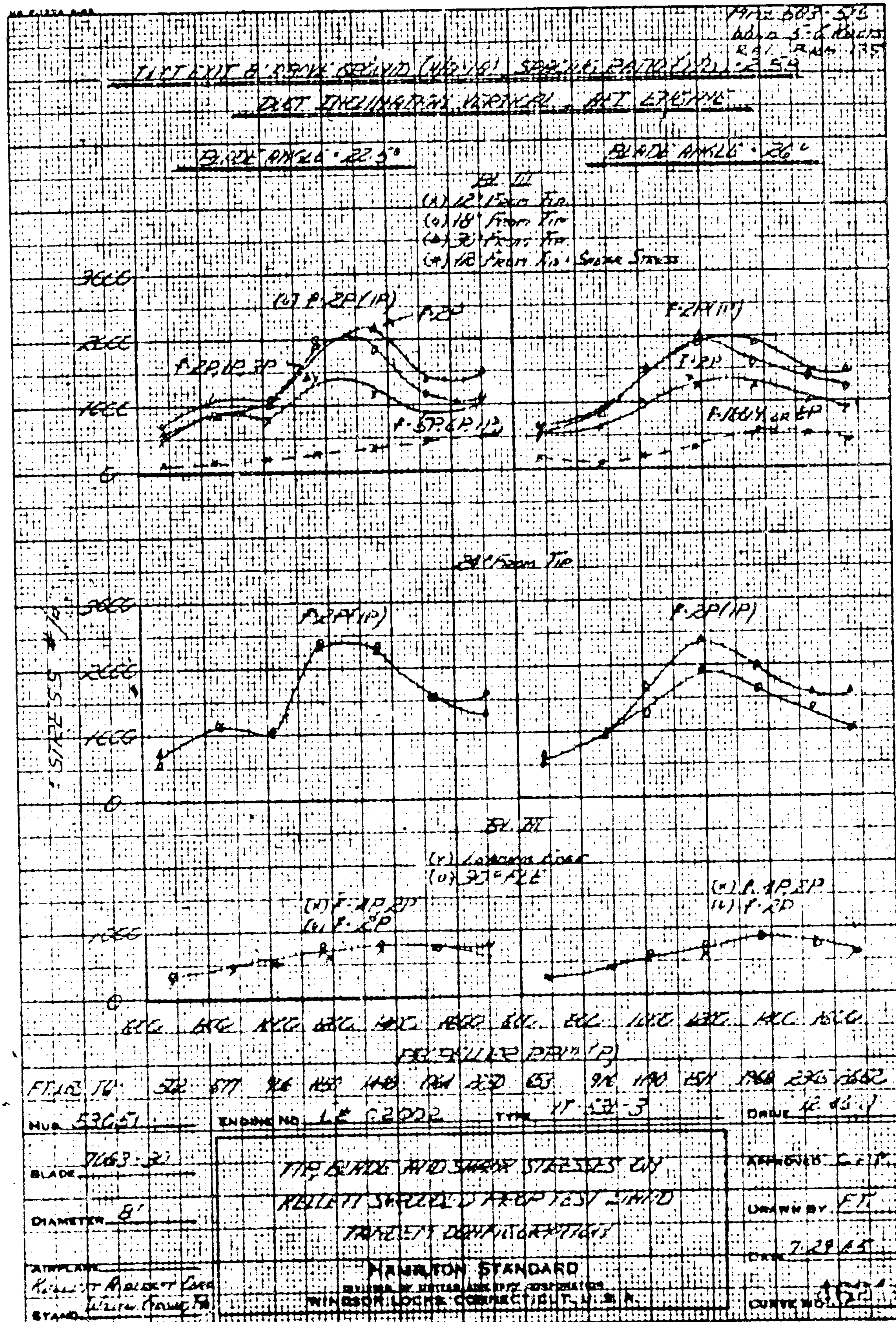
BLADE ANGLE 22.5°
BLADE ANGLE 26°
HUB
ENGINE NO.
TYPE
DRIVE
BLADE
APPROVED
DIAMETER
DRAWN BY
DATE
AIRPLANE
STAND
CURVE NO.
HAMILTON STANDARD
WINDSOR LOCKS, CONNECTICUT, U.S.A.

FIG. 9

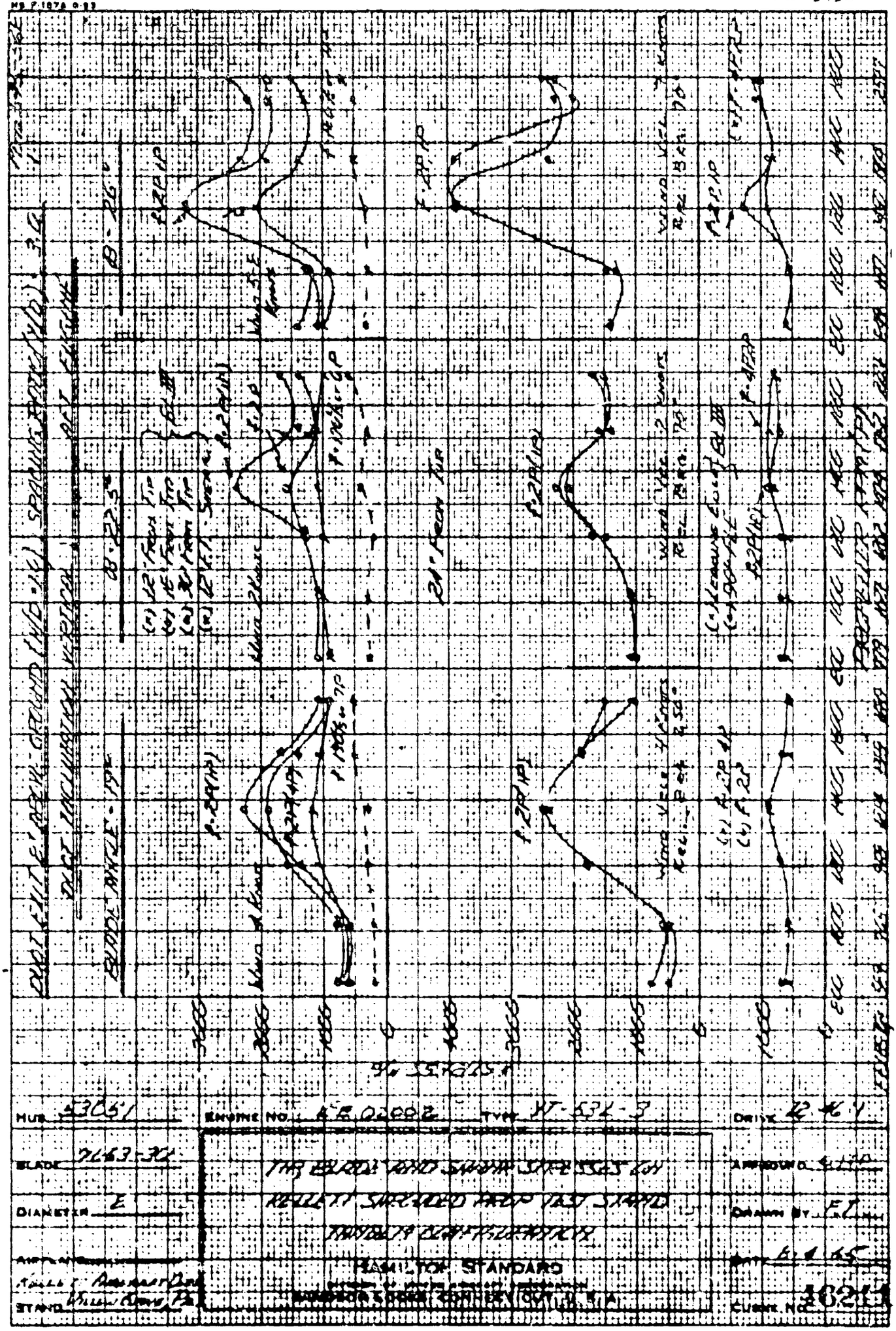
HUB 3061
ENGINE NO. AE 02002
TYPE HT-531-3
DRIVE 42 46 1
BLADE 7663-32
DIAMETER E
HAMILTON STANDARD
DRAWN BY F.E.
DATE 6-1-65
CUSTR. NO. 3621

FIG 10

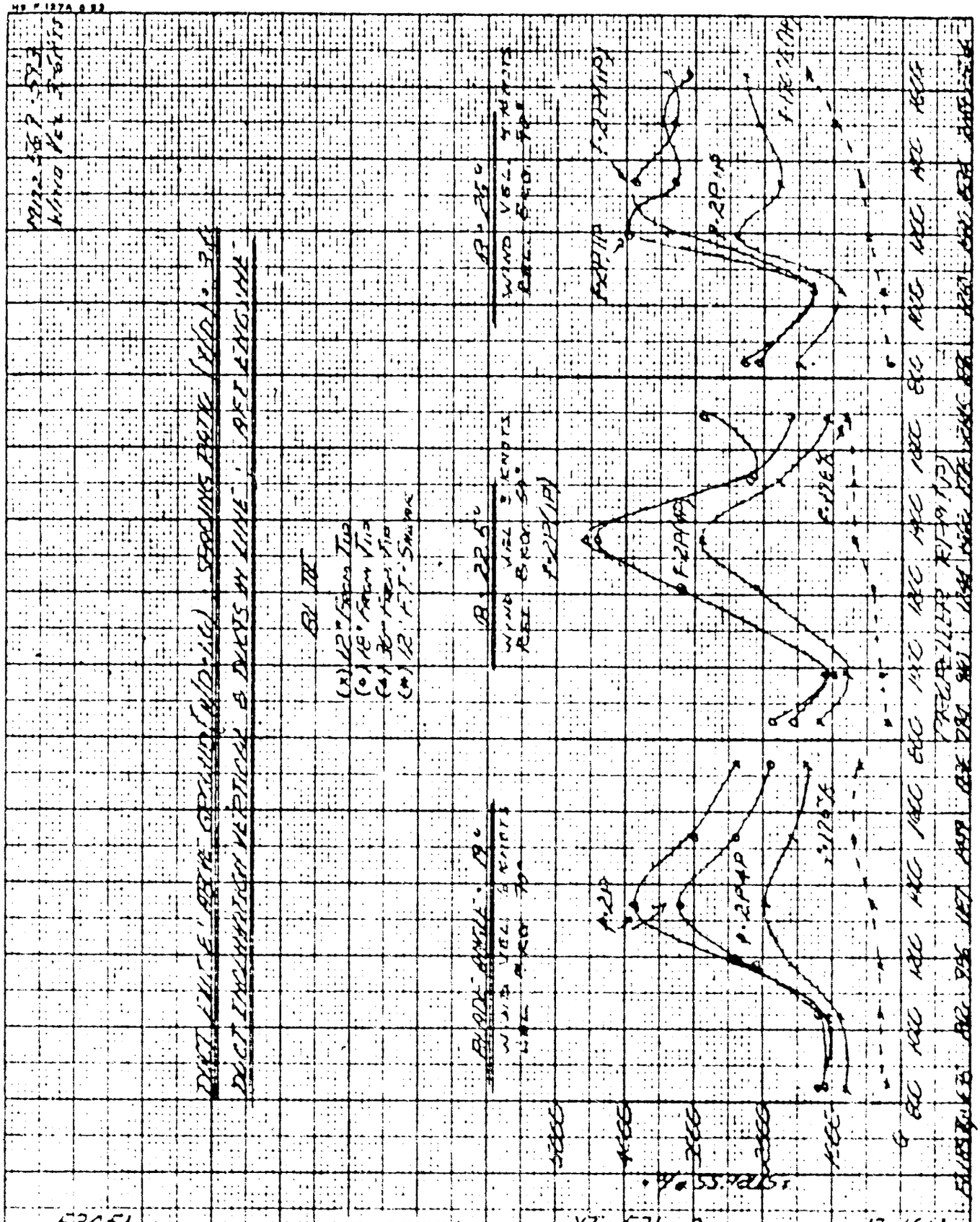
HUB 53C51
ENGINE NO LE 12222
TYP YT-53A-3
DRIVE 42.46.1
BLADE 7663-31
DIAMETER 21
AIRPLANE
STAND
TIP BLADE STA 355.5 CAT ASSY
SUPERCHARGED FIELD TEST STAND
TANDEM CONFIGURATION
HAMILTON STANDARD
WINDSOR LOCKS, CONNECTICUT, U.S.A.
DRAWN BY
DATE
CURVE NO 469

FIG. 11

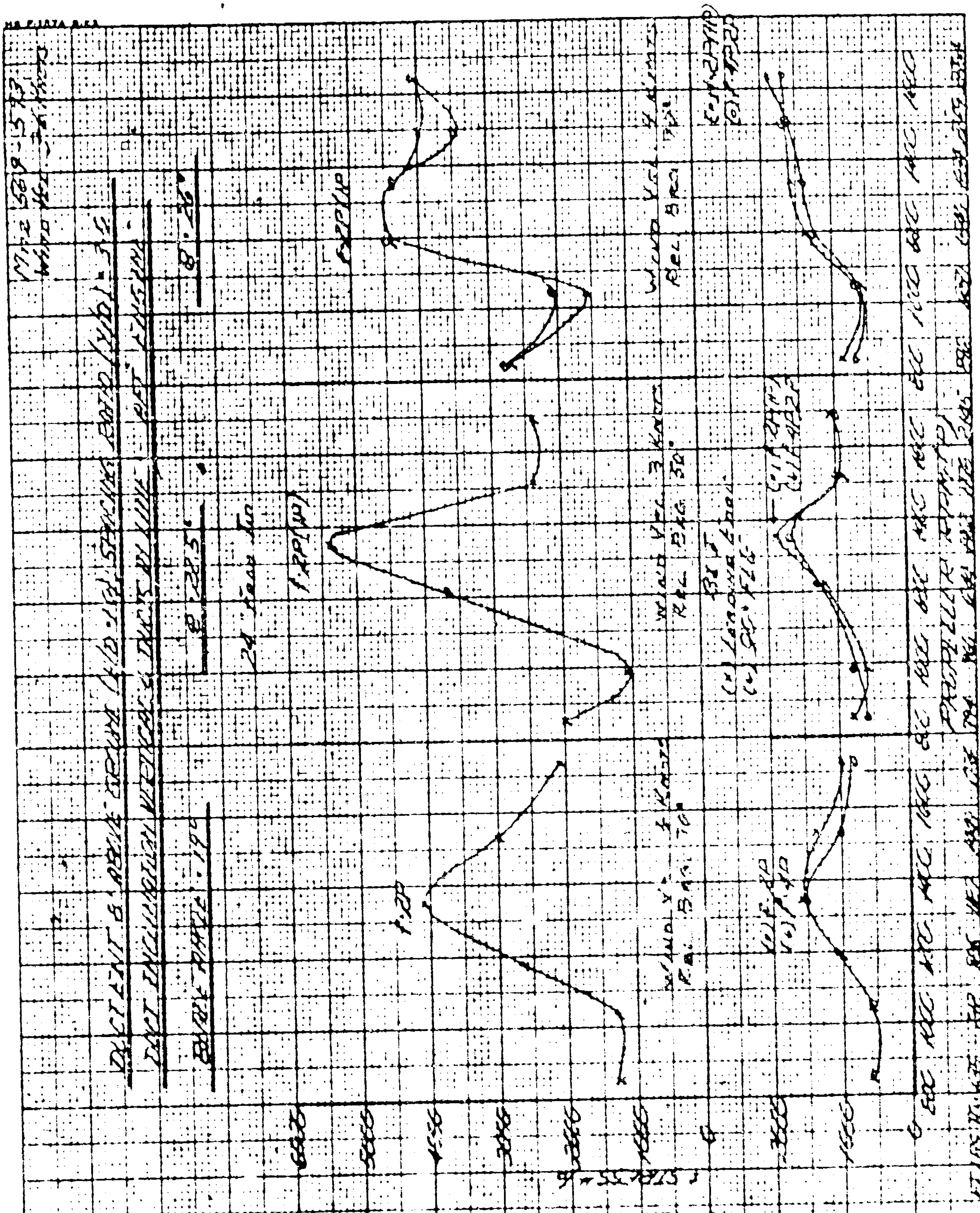

HUB 5?C61 | DESIGN NO. LE-02072 | TYPE YT-532-3 | DRIVE

BLADE 7263-?

BLADE & SHANK STRESSES VS VELOCITY
SHROUDED PROP TEST PROP
TANDEM CONFIGURATION

APPROVED

DIAMETER 8'

DRAWN BY Y.T.

DATE 6-6-65

AIRPLANE

HAMILTON STANDARD
DIVISION OF UNITED AIRCRAFT CORPORATION
WINDSOR LOCKS, CONNECTICUT, U.S.A.

STAND

DWG NO.

FIG 12